

## 7. SITE 814<sup>1</sup>

### Shipboard Scientific Party<sup>2</sup>

#### HOLE 814A

**Date occupied:** 25 August 1990  
**Date departed:** 26 August 1990  
**Time on hole:** 1 day, 5 hr, 15 min  
**Position:** 17°49.985'S, 149°30.831'E  
**Bottom felt (rig floor; m, drill-pipe measurement):** 531.4  
**Distance between rig floor and sea level (m):** 11.08  
**Water depth (drill-pipe measurement from sea level, m):** 520.4  
**Total depth (rig floor; m):** 831.4  
**Penetration (m):** 300.0  
**Number of cores (including cores with no recovery):** 33  
**Total length of cored section (m):** 300.0  
**Total core recovered (m):** 162.42  
**Core recovery (%):** 54.1  
**Oldest sediment recovered:**  
**Depth (mbsf):** 300.0  
**Nature:** dolomite  
**Age:** middle Miocene or older

**Principal results:** Site 814 is located on the southwestern edge of the extensive Tregrosse/Lihou/Coringa Bank complex and is part of a three-site transect, along with Sites 812 and 813, that was intended for studying facies distribution in response to changes in sea level across a platform-slope transition in a pure carbonate system. The site is positioned in front of a carbonate bank and represents the proximal transition between the lagoonal bank (Site 812) and the distal part (Site 813) of an aggradational/progradational sequence.

Drilling penetrated a 300-m-thick sequence of platform-slope sediments (average carbonate content = 96%) that ranged in age from middle Miocene (or older) to Pleistocene. Benthic foraminifers indicate an overall deepening of the depositional environment from a shallow neritic setting (0–100 m) in the middle Miocene to an upper bathyal environment (200–600 m) during the late Pliocene-Pleistocene. The sedimentation rate for the late Pleistocene was 2.5 cm/k.y., whereas it was reduced to about 1.2 cm/k.y. in the late Pliocene to early Pleistocene. The late Miocene to early Pliocene at Site 814 corresponds to a time of reduced sedimentation. A preliminary estimate of middle Miocene sedimentation rates, based on initial data, is approximately 1.4 cm/k.y.

Five major sedimentary units were recovered between the seafloor and 300.0 mbsf. These lithologic units are as follows:

1. *Unit I* (0–56.8 mbsf; Pleistocene to upper Pliocene): Unit I is divided into two subunits on the basis of intercalations near the base of foraminiferal packstones within the predominant lithology, nannofossil foraminiferal ooze.

(1) *Subunit IA* (0–53.4 mbsf; Pleistocene to upper Pliocene): White nannofossil foraminiferal oozes with minor changes to foraminiferal nannofossil oozes comprise this subunit. These

oozes exhibit scattered gray to brown mottled patterns as a result of burrowing and contain minor amounts of lithoclasts and bioclasts, including bivalve shells and echinoid spines. The calcareous nannofossil content decreases downward from about 70% at the top to about 20% near the base. This trend may reflect decreased amounts of pelagic influx and increased supply of bank-derived metastable carbonates in the older sediments, or a change from pelagic to periplatform sedimentation. Benthic foraminiferal assemblages indicate upper bathyal water depths (200–600 m).

(2) *Subunit IB* (53.4–56.8 mbsf; upper Pliocene): Subunit IB consists of white foraminiferal packstones with minor phosphate grains and fish teeth interbedded within nannofossil micritic ooze. Benthic foraminiferal assemblages indicate neritic water depths (0–200 m).

2. *Unit II* (56.8–66.5 mbsf; Pliocene near the lower Pliocene/upper Pliocene contact). Unit II is a well-lithified, yellow-to-white foraminiferal micritic limestone that contains fish teeth and phosphate grains and is capped by a well-developed hardground surface coated with a multilaminated iron-rich crust. The surface has been bored, and these borings are filled in by several generations of cement. Moldic and vuggy porosity occurs, in addition to scattered silt-sized dolomite crystals and grains. Coring recovered only 0.6 m of limestone, but downhole logging suggests that Unit II is approximately 8 m thick, while the degree of induration decreases downward.

3. *Unit III* (66.5–136.0 mbsf; lower Pliocene to upper to middle Miocene): Unit III is divided into two subunits based on a composition change from micritic ooze to bioclastic packstone.

(1) *Subunit IIIA* (66.5–114.0 mbsf; lower Pliocene to (?)upper to middle Miocene): Subunit IIIA contains micritic oozes with nannofossils and foraminifers and foraminiferal nannofossil oozes that show subtle color changes from reddish-brown to white. Abundance of nannofossils is less than 20%. Silt-sized monocrySTALLINE calcite is locally abundant, together with minor amounts of dolomite. Between 96.5 and 98.3 mbsf, unlithified bioclastic floatstones with shelf-derived coarse skeletal grains are intercalated with micritic ooze. These sediments were deposited in outer neritic water depths (100–200 m), which apparently shallowed to middle neritic (30–100 m) near the top of Subunit IIIA (76.0 mbsf). Downhole logging shows that this subunit has a uniformly high porosity.

(2) *Subunit IIIB* (114.0–136.0 mbsf; middle Miocene): Subunit IIIB is characterized by unlithified to partially lithified, white bioclastic packstones. The bioclastic components include bivalve shells, echinoid spines, shark teeth, and solitary corals. Benthic foraminiferal assemblages indicate outer neritic water depths (100–200 m).

4. *Unit IV* (136.0–263.9 mbsf; middle Miocene or older): The occurrence of coarse-grained lithologies at the top and base of this predominately fine-grained interval defines three subunits for Unit IV.

(1) *Subunit IVA* (136.0–150.0 mbsf; middle Miocene): Subunit IVA is a white dolomitized bioclastic packstone. Dolomitization has been so pervasive that only coralline algal fragments—a minor component—are recognizable. Downhole logging distinguishes the top of the subunit and indicates that it is the most indurated interval in Hole 814A.

(2) *Subunit IVB* (150.0–256.1 mbsf; middle Miocene or older): The lithologies of Subunit IVB vary between a calcareous ooze and partially lithified mudstone. Bioclasts are locally abundant (up to 25%). Benthic foraminiferal assemblages indicate middle neritic

<sup>1</sup> Davies, P. J., McKenzie, J. A., Palmer-Julson, A., et al., 1991. *Proc. ODP, Init. Repts.*, 133: College Station, TX (Ocean Drilling Program).

<sup>2</sup> Shipboard Scientific Party is as given in list of participants preceding the contents.

water depths (50–100 m). The mudstones are composed predominantly of silt-sized calcite crystals with euhedral, bipyramidal elongate habits. These are thought to be originally detrital grains with later diagenetic overgrowth. Downhole logging shows this subunit to be relatively uniform in character.

(3) *Subunit IVC* (256.1–263.9 mbsf; middle Miocene or older): The upper part of Subunit IVC (256.1–258.9 mbsf) contains white, partially lithified lithoclastic floatstones, whereas the lower part (258.9–263.9 mbsf) consists of white, unlithified lithoclastic rudstones. Benthic foraminifers are abundant, while lithoclasts are exclusively dolomite.

5. *Unit V* (263.9–300.0 mbsf; middle Miocene or older): Unit V is a yellowish-brown to pale brown dolomitized lithified packstone. The rock is primarily composed of sucrosic dolomite having intergranular porosity. Dolomitization has obliterated any original fabric and texture.

Aragonite concentrations up to 63% were recorded at 0.8 mbsf and progressively decreased downward, disappearing entirely by 32.4 mbsf. Aragonite reappears deeper in Hole 814A and has values up to 34% at 258 mbsf. Interstitial water chemistry for the interval between 0 and 50 mbsf shows an increase in  $\text{Ca}^{2+}$  and  $\text{Sr}^{2+}$  concentrations above seawater values, indicating dissolution of metastable carbonate phases. Over the entire water chemistry profile,  $\text{Mg}^{2+}$  concentration has a perceptible downward decrease, which may be related to *in-situ* dolomitization of the calcareous sediments. Using X-ray diffraction analysis of selected samples, we detected the occurrence of dolomite in two discrete intervals: (1) between 96 and 138 mbsf and (2) below 244 mbsf.

$\text{Ca}^{2+}$  and  $\text{Sr}^{2+}$  concentrations remain fairly constant below 50 mbsf to the bottom of the water profile at 257 mbsf. In particular,  $\text{Sr}^{2+}$  concentration below 50 mbsf resembles that for seawater. Apparently, as at Site 813, two aquifers were penetrated during drilling; however, in the case of Site 814, these are separated by a distinct lithologic boundary, i.e., the limestone hardground of Unit II. Chemistries of the lower aquifers at both Sites 813 and 814 appear to be the same, a possible indication of fluid flow between the two areas. In addition, temperature logs for Hole 814A indicate that warm water (~19.5°C) is flowing upward out of the lowest penetrated portion of the formation. The lower boundary of the upper aquifer at both sites coincides with lithologic changes that correspond to upper Miocene–lower Pliocene condensed sedimentation intervals. Seismic profiles run between both sites indicate that the sediment package comprising the lower aquifer apparently is an aggradational/progradational wedge beneath the condensed surface.

Shipboard paleomagnetic studies revealed a good reversal stratigraphy in the upper part of the section registering the Matuyama/Gauss boundary in Hole 814B at 43 mbsf (2.47 Ma). Based on an initial interpretation of the paleomagnetic data, the sediments directly overlying the hardground (Unit II) were deposited during the Gauss magnetic zone and are probably not older than 3.4 Ma. Below this level, the paleomagnetic reversal signal should be resolvable by shore-based study of discrete samples.

Contents of total organic carbon in the sediments was low—less than 0.30%. Volatile hydrocarbons, with methane concentrations of 2 ppm and no detectable ethane or propane, presented no safety problems.

## BACKGROUND AND SCIENTIFIC OBJECTIVES

Site 814 is one of three sites in close proximity along the southern margin of the Queensland Plateau. For a summary of the background and overall objectives of these sites the reader is referred to the “Background and Scientific Objectives” section of the “Site 812” chapter (this volume).

The location of the site and track maps of the site survey data appear in Figures 1 and 2. The pre-drilling prognosis for Site 814 is shown in Figure 3.

Our objectives for Site 814 were as follows:

1. To determine the age and facies of the periplatform and reef sequences toward the margin of the carbonate platform complex.

2. To determine the late Paleogene to Holocene paleoceanographic and paleoclimatic signal in the reef and periplatform sequences.

3. To analyze the “backstepping” history of the shallow carbonate banks of the Queensland Plateau.

4. To establish the relationship between fluctuations in sea level and bank-derived carbonate facies.

5. To determine the late Cenozoic carbonate saturation history within the region.

6. To determine the diagenetic signal contained within periplatform sediments; in particular, to establish the stability regimes of high-magnesium calcite and aragonite within the platform margin environment.

## OPERATIONS

### Transit to Site 814

The transit from Site 813 (NEA-10A/3) to Site 814 (NEA-10A/2) covered 1.2 nmi in 1.3 hr at 0.9 kt average speed (in dynamic positioning mode). A Datasonics beacon was dropped at 1035L, 25 August (all times in this section are local time, or L) within an optimal global positioning system (GPS) window at the coordinates previously surveyed with GPS.

### Hole 814A

The precision depth recorder (PDR) indicated that the water depth was 520.3 m from sea level at the site, at a position of 17°49.985'S, 149°30.831'E. The bit was positioned at 516.7 m from sea level, and Hole 814A was spudded at 1215L, 25 August. From the mud-line core (Core 133-814A-1H) we recovered 5.86 m of sediment; the mud line was determined to be at a water depth of 520.4 m from sea level. Continuous APC cores (Cores 133-814A-1H to -7H) were taken from 0 to 56.8 mbsf with 56.8 m of sediment cored and 58.61 m recovered (103.19% recovery). Core 133-814A-7H resulted from a partial stroke in hard formation. Core 133-814A-8X was taken from 56.8 to 66.5 mbsf, with 9.7 m cored and 0.57 m recovered (5.88% recovery). Core 133-814A-8X broke through the hard formation back into soft ooze, as happened at Site 812. Therefore, we decided to resume APC coring in hopes of improving recovery. From Cores 133-814A-9H to -16H (76.0–136.0 mbsf), we cored 66.5 m and recovered 71.51 m (102.89% recovery).

Cores 133-814A-17X to -33X were taken from 136.0 to 300.0 mbsf, with 164.0 m cored and 31.77 m recovered (19.37% recovery). Coring ended at our target depth. A 30-bbl-mud sweep was circulated to clean the hole, and a short trip conditioned the hole for logs.

Logs were run as follows:

1. The caliper springs on the induction/density/sonic/caliper/gamma-ray (DITE/HLDT/SDT/MCDG/NGT) logging tool would not go through the 3.80-in. landing sub. The caliper springs were removed and the log was run to 296.1 mbsf (3.9 m of fill was present in the bottom of the hole). The logging tool was in the hole at 0901L, 26 August and was out at 1220L.

2. The formation microscanner/gamma-ray/temperature (FMS/NGT/TCC) logging tool was in the hole at 1450L.

After logging was completed, we recalled the beacon, and the bit was back on deck at 1612L, 26 August.

The coring summary for Site 814 is presented in Table 1.

### SITE GEOPHYSICS

A general description of the design and operation of the combined site-location survey for Sites 812, 813, and 814 is

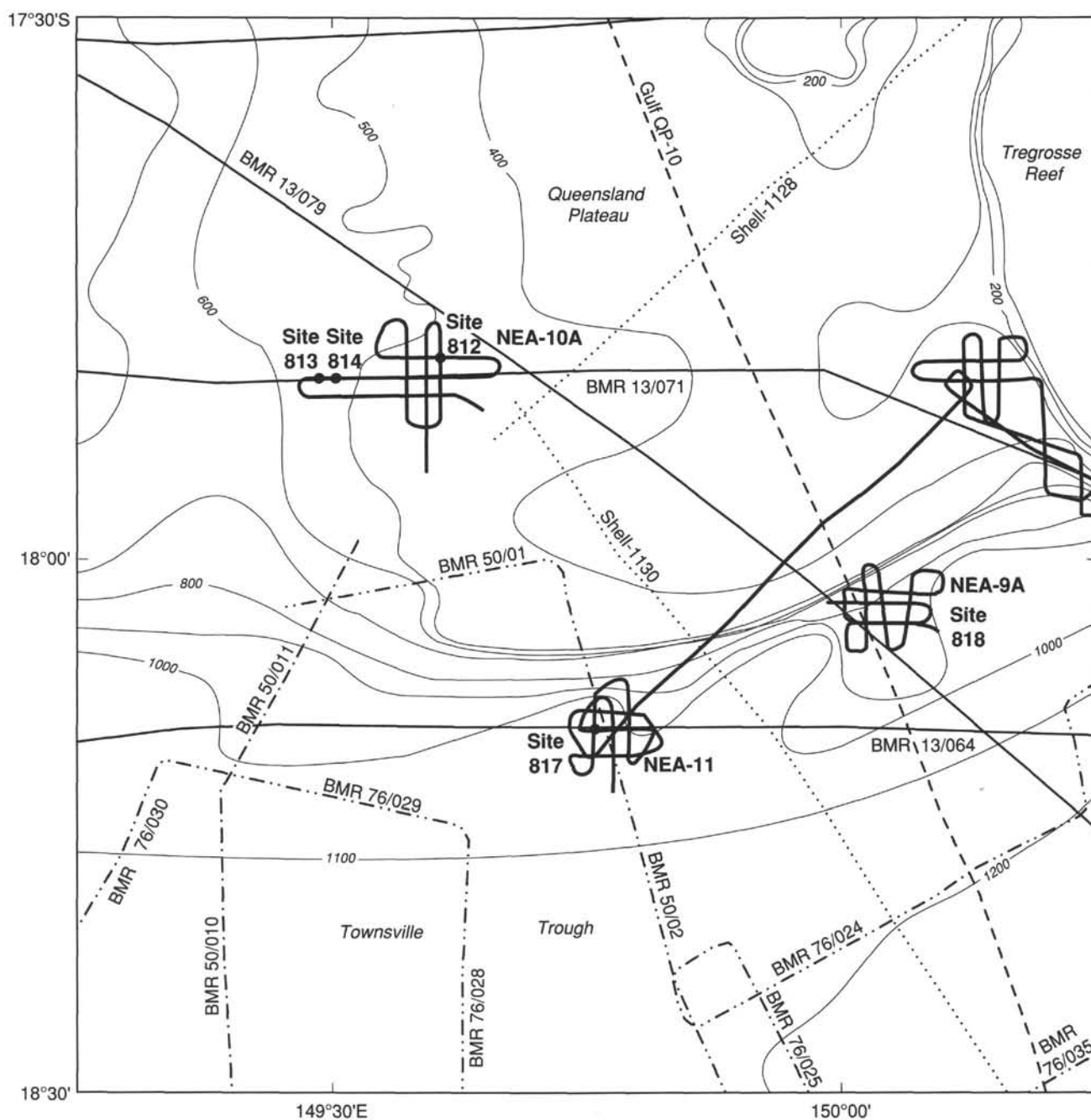


Figure 1. Track chart showing distribution of regional seismic data in the area around Sites 812, 813, and 814. Also shows the locations of Holes 817A and 818A and simplified bathymetry in meters.

included in the "Site Geophysics" section of the "Site 812" chapter (this volume).

#### Site 814

After completion of drilling at Site 813 and separation from the beacon at JD 236/2230UTC on 24 August 1990, the *JOIDES Resolution* slowly moved to the confirmed GPS position of Site 814 in dynamic positioning mode while trailing the drill string. A beacon was dropped at the site at JD 237/0035UTC; the final coordinates of Hole 814A are 17°49.985'S and 149°30.831'E in a water depth of 520.4 m (drill-pipe measurement [DPM] from sea level).

Site 814 is located near the southern margin of Queensland Plateau, between Tregrosse and Flinders reefs, about 65 km

west of the edge of the modern Tregrosse Reef bank (Fig. 1). It is the middle site of a group of three sites (Sites 812, 813, and 814) positioned to examine the factors controlling the development of carbonate platforms on Queensland Plateau. Site 814 represents the proximal part of a prograding platform margin system and lies about 3 km west of the edge of the platform and about 2.5 km east of Site 813 (Figs. 1 and 2).

Good correlation exists at the site between the two intersecting *JOIDES Resolution* single-channel seismic profiles and the *Rig Seismic* multichannel seismic profile (Figs. 1, 2, and 4). Five major seismic sequences can be recognized above the top of a strong band of reflectors about 0.5 s TWT below seafloor. A strong reflector about 1.1 s TWT below the seafloor, visible on both the processed BMR water-gun site

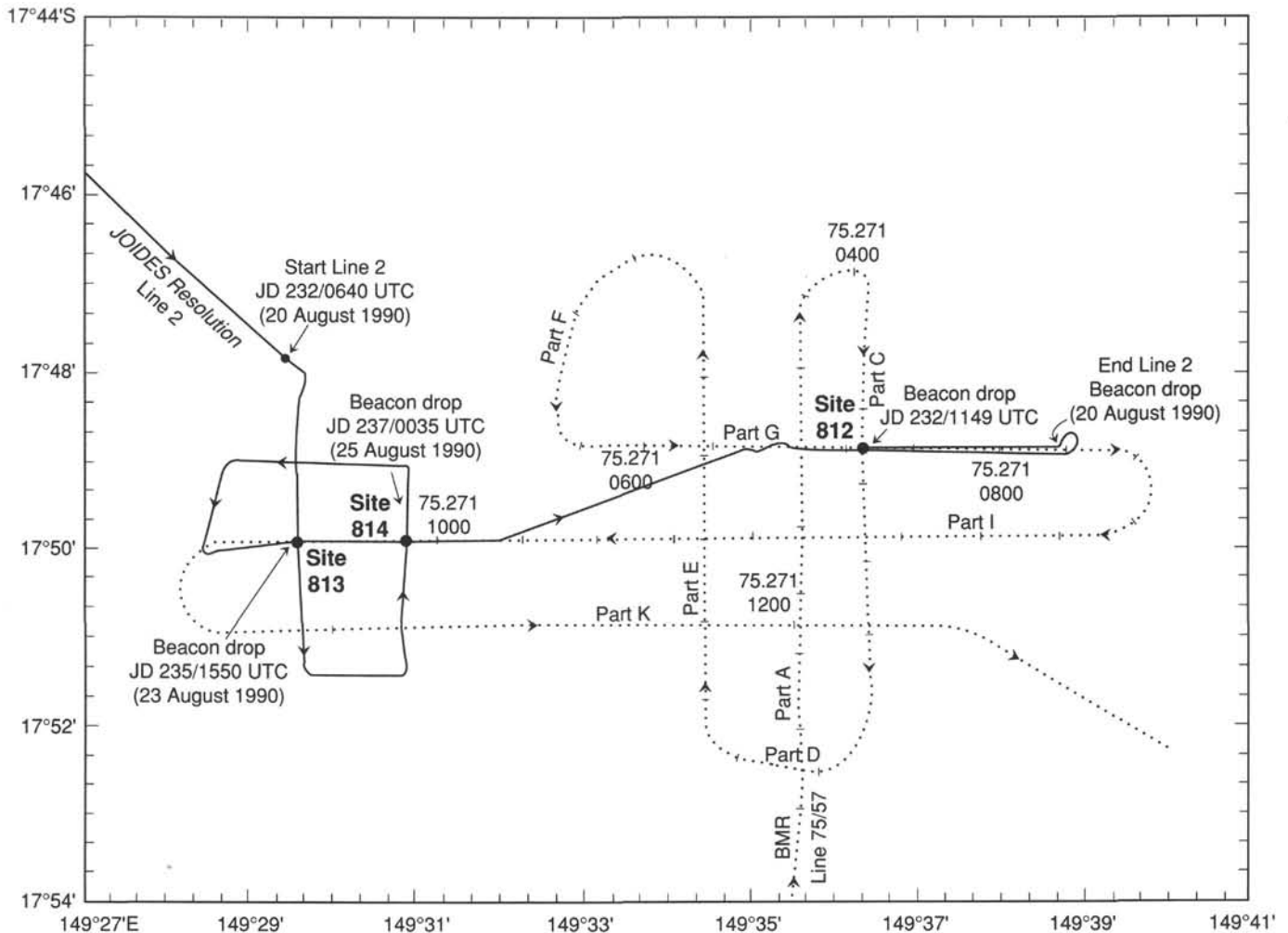


Figure 2. Detail of JOIDES Resolution Leg 133 site-location tracks (solid line) and Rig Seismic 1987 site-survey tracks (dotted line) around Sites 812, 813, and 814.

survey data and other regional data in the area, may mark either the top of basement or the rift-fill section. This reflector probably corresponds to the so-called regional Paleocene break-up unconformity, which is thought to have formed following the start of seafloor spreading in the Coral Sea Basin and consequent thermal sag of the continental margin (Falvey and Mutter, 1981; Symonds et al., 1984).

To provide some predictive capability during the drilling at Site 814, we estimated the reflection time (TWT)/depth relationship below the seafloor using stacking-derived interval velocities from the BMR seismic line across the site (Fig. 5). At depths greater than 100 mbsf, the velocities of the sediments at Site 814 are higher than those for Site 811 and DSDP Site 209 (Andrews, 1973) and are the highest of the Sites 812/813/814 group. This probably reflects the carbonate platform setting of Site 814 proximal to the platform margin facies.

#### LITHOSTRATIGRAPHY

At Site 814, a 300-m-thick carbonate sequence extending from the Pleistocene to the lower Miocene(?) was drilled using the APC and XCB. The sequence consists mostly of fine-grained carbonate sediments (oozes and mudstones) interbedded with minor carbonate sands (packstones/floatstones).

Some sediments have been dolomitized. All of these sediments were deposited at the edge of the Queensland Plateau in a periplatform position in water depths from 20 m below the wave base to several hundreds of meters.

Five lithologic units (I, II, III, IV, and V) can be distinguished at Site 814, several of which are divided into subunits (Fig. 6). The five primary units are separated by surfaces that were interpreted as major unconformities. Units I, III, and IV exhibit a more-or-less complete and, to a certain extent, comparable stratigraphic record, whereas in Unit II, a condensed sequence occurs. In Unit V, only the topmost sediments were drilled and recovered. Most of these units start at their base with neritic, bioclastic carbonate sands that pass vertically to fine-grained, pelagic carbonates, which dominate the sequence and which in turn can be overlain by dolomitized bioclastic sands. The stratigraphic distribution of the different units and subunits is summarized in Figure 6.

*Unit I (Sections 133-814A-1H-1 to -7H-CC, 0-56.8 mbsf; age, Pleistocene to late early Pliocene, 0-3.88 Ma)*

The predominant lithology in this unit is nannofossil foraminifer ooze. At its base, un lithified foraminifer packstones also occur. These marked lithological differences divide the unit into two distinct subunits.

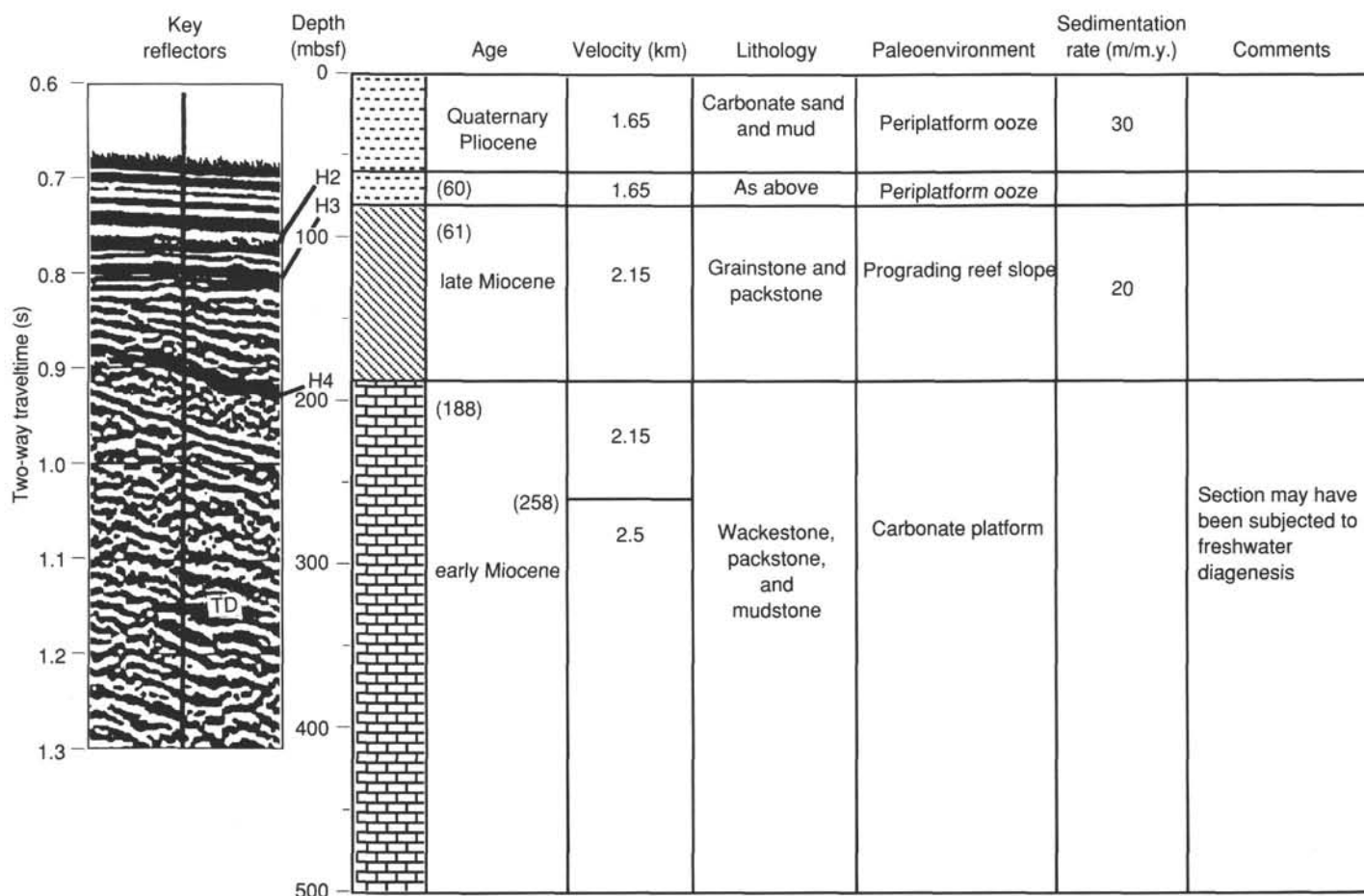


Figure 3. Pre-drilling prognosis for Site 814.

**Subunit IA** (Sections 133-814A-1H-1 to -6H-CC; 0–53.4 mbsf; age, Pleistocene to late Pliocene, 0–3.45 Ma)

The predominant lithology in Subunit IA is white nannofossil foraminifer ooze with minor foraminifer nannofossil ooze. Some conspicuous colored (gray to pale brown) mottling is present, probably produced by burrowing. Lithoclasts (up to 5 cm long) and large bioclasts (bivalve shells, echinoid spines) are also present in minor amounts. Micrite is relatively abundant (up to 30%). Traces of possible detrital dolomite were observed in one smear slide.

**Subunit IB** (Sections 133-814A-7H-1 to -7H-CC, 53.4–56.8 mbsf; age, late Pliocene 3.45–3.88 Ma)

This subunit consists of unlithified, white, foraminifer packstones interbedded with nannofossil micrite ooze. Fish teeth and phosphate grains are minor, but significant, components of the sands (Fig. 7).

**Unit II** (Core 133-814A-8X, 56.8–66.5 mbsf; age, Pliocene [near the early Pliocennellate Pliocene boundary])

This unit consists of well-lithified, yellow-to-white, foraminifer micrite limestone that contains fish teeth and phosphate grains. A well-developed hardground having a crust up to several millimeters thick and containing several generations of brown (iron-rich) cement caps the limestone and has been bored to a certain extent. Moldic (as a result of dissolution of foraminifer tests) and vuggy porosity occurs in

the limestone, as well as a few silt-sized dolomite crystals and grains.

**Unit III** (Sections 133-814A-9H-1 to -16H-CC, 66.5–136.0 mbsf; age, [?]early Pliocene to middle to [?]late Miocene)

The predominant lithology in this unit is a micrite ooze that, at one point, intercalates with bioclastic floatstones. Bioclastic sands are dominant at the base of the unit. The unit has been subdivided into two subunits on the basis of its lithological composition.

**Subunit IIIA** (Sections 133-814A-9H-1 to 133-814A-13H-CC; 66.5–114.0 mbsf; age, [?]early Pliocene to middle to [?]late Miocene)

Micrite oozes with nannofossils and foraminifers and foraminifer nannofossil micrite oozes are the major constituents of the subunit. Subtle differences in color occur from reddish-brown to white. Silt-sized, detrital(?), monocrystalline calcite crystals can be locally abundant (up to 10% or even more), together with minor dolomite (less than 5%). Chalk lumps of partly to firmly lithified sediment also occur.

The most interesting feature in this subunit is the existence in Sections 133-814A-12H-2 and -12H-3 (96.5–98.3 mbsf) of an unlithified bioclastic floatstone horizon with shelf-derived, coarse grains (sand- to pebble-sized) consisting of large benthic foraminifers, bivalve debris, branching bryozoans, and intraclasts embedded in the micrite ooze (Fig. 8).

Table 1. Coring summary for Site 814.

Core no.	Date (Aug. 1990)	Time (UTC)	Depth (mbsf)	Length cored (m)	Length recovered (m)	Recovery (%)
1H	25	0220	.0–5.9	5.9	5.86	99.3
2H	25	0235	5.9–15.4	9.5	9.96	105.0
3H	25	0250	15.4–24.9	9.5	9.81	103.0
4H	25	0310	24.9–34.4	9.5	9.97	105.0
5H	25	0330	34.4–43.9	9.5	10.01	105.3
6H	25	0350	43.9–53.4	9.5	9.64	101.0
7H	25	0415	53.4–56.8	3.4	3.36	98.8
8H	25	0520	56.8–66.5	9.7	0.57	5.9
9H	25	0550	66.5–76.0	9.5	9.77	103.0
10H	25	0605	76.0–85.5	9.5	9.92	104.0
11H	25	0625	85.5–95.0	9.5	9.96	105.0
12H	25	0645	95.0–104.5	9.5	9.74	102.0
13H	25	0700	104.5–114.0	9.5	9.83	103.0
14H	25	0720	114.0–123.5	9.5	9.56	100.0
15H	25	0755	123.5–133.0	9.5	9.69	102.0
16H	25	0835	133.0–136.0	3.0	3.00	100.0
17X	25	0955	136.0–145.7	9.7	0.25	2.6
18X	25	1030	145.7–155.4	9.7	0.10	1.0
19X	25	1055	155.4–165.1	9.7	0.00	0.0
20X	25	1140	165.1–174.8	9.7	0.00	0.0
21X	25	1230	174.8–184.5	9.7	0.00	0.0
22X	25	1325	184.5–197.1	12.6	0.00	0.0
23X	25	1325	197.1–206.8	9.7	3.05	31.4
24X	25	1410	206.8–216.4	9.6	4.34	45.2
25X	25	1425	216.4–225.7	9.3	0.00	0.0
26X	25	1445	225.7–235.3	9.6	6.46	67.3
27X	25	1500	235.3–244.6	9.3	6.85	73.6
28X	25	1520	244.6–254.2	9.6	4.86	50.6
29X	25	1540	254.2–263.9	9.7	5.34	55.0
30X	25	1615	263.9–273.6	9.7	0.00	0.0
31X	25	1705	273.6–283.2	9.6	0.00	0.0
32X	25	1825	283.2–292.9	9.7	0.02	0.2
33X	25	1905	292.9–300.0	7.1	0.50	7.0
Coring totals				300.0	162.42	54.1

Note that times are given in Universal Time Coordinated or UTC, which is 10 hr later than local time, L).

**Subunit IIIB (Sections 133-814A-14H-1 to -16H-CC, 114.0–136.0 mbsf; age, middle Miocene)**

This subunit consists of white, unlithified to partially lithified, bioclastic packstones having a matrix of nannofossil ooze and silt-sized calcite crystals. Planktonic and benthic foraminifers are abundant. Fragments of bivalve shells, echinoid spines, shark teeth, and solitary corals also were noted, although they are not common. Detrital dolomite is locally present in minor amounts.

**Unit IV (Sections 133-814A-17X-1 to -29X-CC, 136.0–263.9 mbsf; age, middle Miocene or older)**

Three distinct lithologies occur in this unit. Whereas mudstones are dominant for most of the section, calcareous sands occur both at the base (lithoclastic floatstones/rudstones) and at the top (dolomitized bioclastic packstones) of the unit. These lithological variations permit differentiation of three subunits.

**Subunit IVA (Sections 133-814A-17H-1 to -18X-1; 136.0–150.0; age, middle Miocene)**

As there was no recovery for most of this subunit, we determined the lower limit from the available logging information. The uppermost limit of this subunit is strongly marked in the logging data as a highly lithified, thin horizon.

This subunit consists of dolomitized, white, highly porous, lithified bioclastic packstones, in which the only visible and recognizable remains of the original limestone are a few sand-sized (medium-to-fine grained) coralline algal fragments (Fig. 9).

**Subunit IVB (Core 133-814A-18X to Section 133-814A-29X-2, 193 cm; 150.0–256.1 mbsf; age, middle Miocene or older)**

In this subunit, lithologies vary from calcareous oozes to partially lithified mudstones, the latter being more dominant. Colors grade from light gray to white. Bioclasts, especially foraminifers (both benthic and planktonic), are locally abundant (up to 25%). Echinoid spines, alcyonarian spicules, sponge spicules, and others also appear in minor quantities.

The presence of silt-sized, calcite crystals having well-marked, euhedral, bipyramidal elongate habits is notable in these mudstones, where they comprise most of the matrix. We postulate that these were originally detrital and developed their overgrowths at a later stage, during diagenesis. The occurrence of some minor detrital dolomite grains and crystals is also noteworthy.

**Subunit IVC (Sections 133-814A-29X-2, 193 cm, to -29X-CC; 256.1–263.9 mbsf; age, middle Miocene or older)**

This subunit is made up of white calcareous sands that occur as partly lithified lithoclastic floatstones in the top 283 cm and as unlithified lithoclastic rudstones in the bottom 58 cm. In these sands, benthic foraminifers are abundant, while the lithoclasts are detrital dolomite.

**Unit V (Sections 133-814A-30X-1 to -33X-1; 263.9–300.0 mbsf; age, middle Miocene or older)**

This unit consists of dolomitized lithified packstones, with colors that range from light yellowish-brown to very pale brown. Because of intense dolomitization, the original fabric and texture cannot be determined. The whole rock now consists of a sucrosic dolomite with abundant intercrystalline, moldic, and vuggy voids and high porosity (30%–40%).

### Interpretation

Five main sedimentary sequences, separated by four major unconformities, can be distinguished at Site 814 (Fig. 6). All lithological units were drilled completely, except the lowermost one, where only the upper part was reached. Recovery was good for the upper three units and poor for the lower two.

The first sequence is Pliocene–Pleistocene in age and extends from 0 to 56.8 m. It corresponds to Unit I above and consists of neritic calcareous sands at the base, overlain by pelagic carbonate oozes. Benthic foraminifers indicate paleowater depths of 0 to 200 m for the sands and 200 to 600 m (upper bathyal) for the oozes. The sequence as a whole shows a rapid upward-deepening with fine-grained pelagic nannofossil oozes clearly dominant on top. The sequence also indicates a substantial drowning of the Queensland Plateau throughout the Pliocene–Pleistocene and supports the contention that the Queensland Plateau underwent subsidence during the Pliocene (Davies et al., 1989).

The second sequence is of Pliocene age, probably from near the early Pliocene/late Pliocene boundary. Although recovery was only 0.57 m, the unit probably extends from 56.8 to 66.5 mbsf on the basis of logging data. This unit is a condensed sequence of well-lithified calcareous sands that exhibits dissolution features (partial leaching of foraminifer tests) and is capped by a hardground. All evidence points to extremely low sedimentation rates and a final cessation of sedimentation, which allowed marine diagenetic processes (dissolution, cementation, phosphatization, etc.) to prevail and form the hardground. The deposition environment of this unit, inferred from the benthic foraminifers, is an outer neritic shelf (100–200 m). Thus, it may be that during the middle Pliocene this zone was mainly a bypass area, starved of sediments for most of the time.

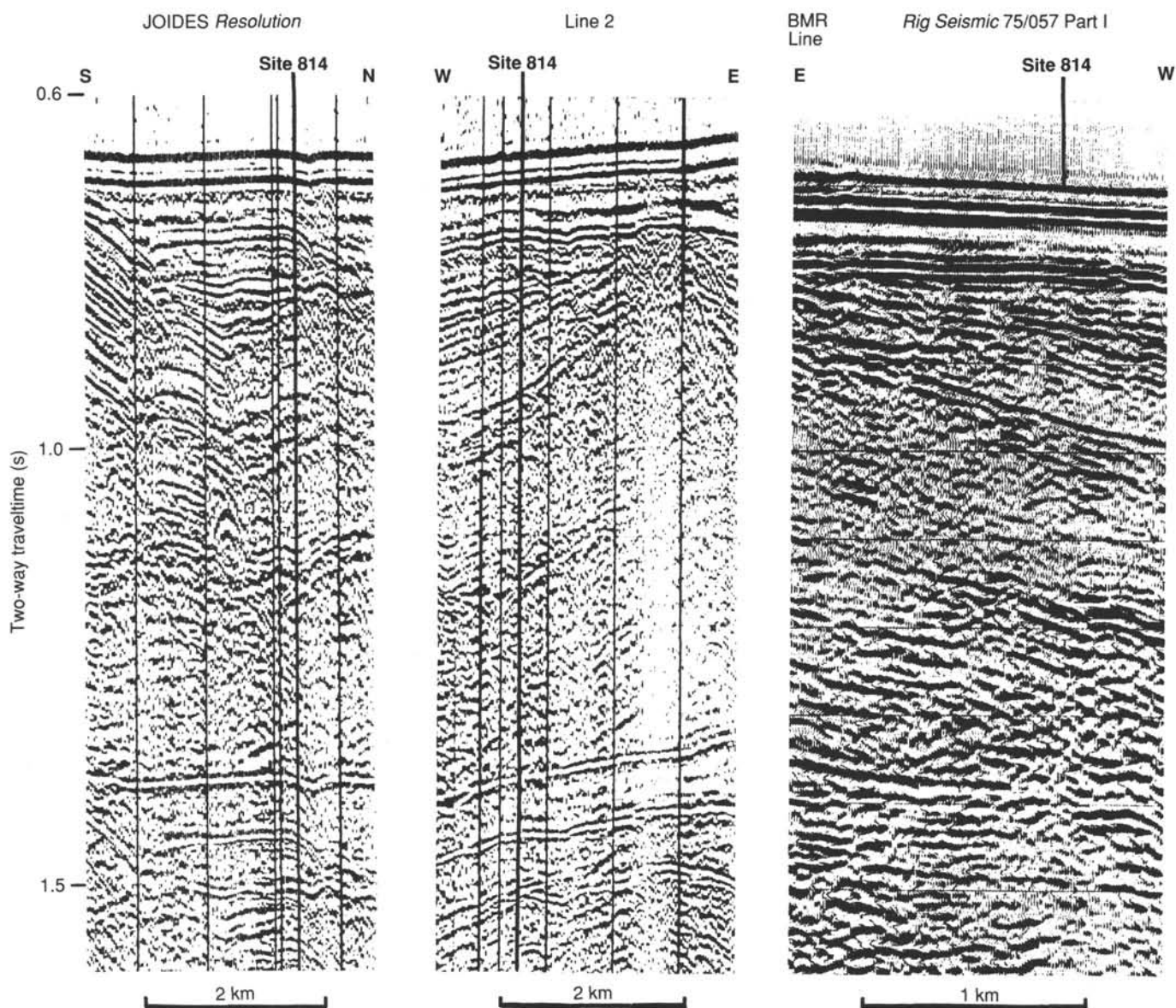


Figure 4. Comparison of *JOIDES Resolution* and *Rig Seismic* 80-in.<sup>3</sup> water-gun seismic profiles across Site 814.

The third sequence, corresponding to Unit III, is middle Miocene in age at its base and extends up into probable upper Miocene and lower Pliocene sediments. The sequence has neritic sands at the base and fine-grained pelagic sediments at the top. Topmost of the sequence (Core 133-814A-9H), the sediments and benthic foraminifers suggest a sudden return to a shallower marine (neritic) situation (see Fig. 10). An unlithified bioclastic floatstone horizon, having shelf-derived coarse grains (benthic foraminifers, bivalves, bryozoans, and intracasts) mixed with pelagic micrite oozes, occurs in the middle of Core 133-814A-12H. This was interpreted as a sediment gravity-flow (debris-flow) deposit. Again, the vertical evolution of the sequence suggests an upward deepening environment for most of its duration, with a slight shallowing at the very top.

The fourth sequence, which corresponds to Unit IV, is of presumed middle Miocene or older age. It consists of calcareous sands at the base, which are overlain by fine-grained carbonates having dolomitized carbonate sands at the top. Benthic foraminifers indicate that the sands at the base of the

unit are neritic, shallow-water deposits. The fine-grained carbonates in the middle of the unit also are neritic, but presumably were deposited below wave base. The abundance of silt-sized, detrital calcite crystals in these fine-grained carbonates is an argument for a low-energy depositional environment that was nevertheless near an elevated shelf area, from which presumably these were derived. These fine-grained sediments thus have been interpreted as having been deposited on a gentle distal slope or ramp. The overlying calcareous sands (now dolomitized) are fine-grained sands that contain small coralline debris. Such sediments may have been deposited in the middle of a slope or ramp. The vertical evolution of this sequence again deepens upward for the most part, except for the top, where it reverses to an upward-shallowing situation. In this succession, the basal sands may represent the low-sea-level sediment wedge. The pelagic sediments should represent high-sea-level deposition, and the neritic sands on top may be part of the prograding shelf-slope sediments that represent the initial stages of a decline in sea level. These last sediments may have been dolomitized when

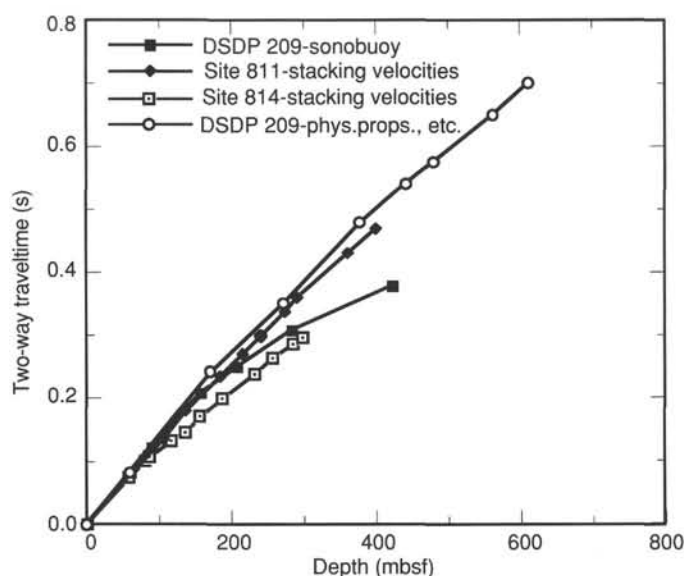


Figure 5. Comparison of TWT-depth curve estimated for Site 814 with those for Sites 811 and DSDP 209 on the Queensland Plateau.

the shelf and slopes were subaerially exposed and then partially eroded as sea level continued to fall.

In the fifth sequence, which corresponds to Unit V, only the topmost sediments (dolomitized calcareous sands) are represented. These sediments seem to be comparable in their depositional environment to the uppermost layers of Unit IV.

The studied section was deposited on a slope adjacent to the Queensland Plateau, but at some distance (several hundreds of meters to a few kilometers) from the shelf area. This distance seems to have increased progressively since early Miocene(?) time. In the lowermost complete sequence drilled (Unit IV), the vertical evolution is from shallow neritic (0–20 m) to distal slope or ramp (20–100 m) and then to a middle-slope (or ramp) position. The next sequence started in a neritic environment (outer shelf; 100–200 m), after which it became pelagic (periplatform? upper bathyal?) and, finally, again neritic (20–100 m). At the time of deposition of the following sequence (Unit II), the area remained in a fixed, outer-shelf position, serving mainly as a bypass zone having an extremely low sedimentation rate. Under these conditions, only a condensed sequence with a hardground cap formed. The upper sequence (Unit I) began with outer-shelf deposits (100–200 m) and evolved quickly to a pelagic environment (upper bathyal; 200–600 m).

## BIOSTRATIGRAPHY

### Biostratigraphy and Paleoenvironment Summary

Calcareous nannofossils, and planktonic, benthic, and larger benthic foraminifers were extracted from core-catcher samples at Hole 814A. Biostratigraphic results are shown in Figure 11. Planktonic fossils are abundant and well preserved in the uppermost part of the section (Samples 133-814A-1H-CC through -7H-CC). Benthic foraminiferal associations point to an upper bathyal depositional setting for the upper interval (Cores 133-814A-1H-CC through -5H-CC) of the succession.

In contrast, below Core 133-814A-7H, planktonic microfossils are rare and are only poorly preserved. The faunas are

dominated by neritic benthic foraminifers in and below Sample 133-814A-6H-CC.

### Calcareous Nannofossils

Calcareous nannofossils were recovered at Site 814 from the seafloor (Cores 133-814A-1H-1, 0 cm) to Sample 133-814A-27X-CC. An overview of the preliminary biostratigraphy is given in Figure 11. Preservation is excellent at the sediment/water interface, but deteriorates in the section, and below Core 133-814A-12H, nannofossils were recovered in only trace amounts—much less than 1% of the sediment. From Cores 133-814A-17H through -22X, we recovered no sediment, nor were sediments recovered in Core 133-814A-30X through Section 133-814A-32X-1, which rendered the corresponding intervals undatable.

The core-catcher sample of Core 133-814A-1H contains abundant *Gephyrocapsa caribbeanica*, but no *Pseudoemiliania lacunosa* and no *Emiliania huxleyi*, hence has been assigned an age of 275 to 465 k.y. The next lower sample (133-814A-2H-CC) contains *Pseudoemiliania lacunosa* along with a large species of *Gephyrocapsa* (*Gephyrocapsa caribbeanica* morphotypes); this sample was assigned an age of 465 to 930 k.y. Sample 133-814A-3H-CC contains abundant minute *Gephyrocapsa* and modest numbers of intermediate size species of that genus (cf. *Gephyrocapsa muelleri*, but constructed like *Gephyrocapsa caribbeanica*), common-to-abundant *Pseudoemiliania lacunosa*, but no *Helicosphaera sellii* or *Calcidiscus tropicus*. The age of this sample is 0.93 to 1.27 Ma. Next below, Sample 133-814A-4H-CC yielded *Discoaster brouweri* and *Discoaster triradiatus*, but no *Discoaster pentaradiatus*, which indicates an age of 1.88 to 2.29 Ma for this level and places the Pliocene/Pleistocene contact within Core 133-814A-4H. The late Pliocene record is represented by Core 133-814A-8X, in which was recovered only a few pieces of limestone. Ages of core-catcher samples become progressively older: 2.42 to 2.60 Ma in Sample 133-814A-5H-CC; 2.6 to 3.45 Ma in Sample 133-814A-6H-CC; and 3.51 to 3.88 Ma in Sample 133-814A-7H-CC. In Core 133-814A-8X, we recovered only a few fragments of rock. Sediment scraped off one of these rock fragments is of late Pliocene age (<3.45 Ma), which is incompatible with the younger age of the overlying Sample 133-814A-7H-CC. Most probably, the ooze adhering to the rock sample is contamination that was picked up during drilling.

The core-catcher sample of Core 133-814A-8X and the next three core-catcher samples (133-814A-9H-CC, -10H-CC, and -11H-CC) contain abundant calcareous nannofossils, but none of the recognized upper Miocene to lower Pliocene marker species are present. Rather, the assemblages consist of generalized species one might associate with a marginal environment, or possibly with relatively cool surface water. The latter alternative seems more attractive than the former simply because the volume of coccoliths (pelagic sediment) is difficult to reconcile with a lagoonal setting.

Sample 133-814A-12H-CC yielded a similar nannofossil assemblage as in the upper three samples, but also contains *Calcidiscus premacintyreii*, which in the absence of *Sphenolithus heteromorphus* indicates an age range of 12.2 to 13.2 Ma for this sample. *Sphenolithus heteromorphus* was recorded from the next lower sample (133-814A-13H-CC) and also from Samples 133-814A-15H-CC and -16H-CC. On the basis of this record of *Sphenolithus heteromorphus*, the core-catcher sample of Core 133-814A-26X was assigned an age no greater than 17.1 Ma, with a minimum possible age of 13.2 Ma.

No datable nannofossils were recorded below Core 133-814A-26X.

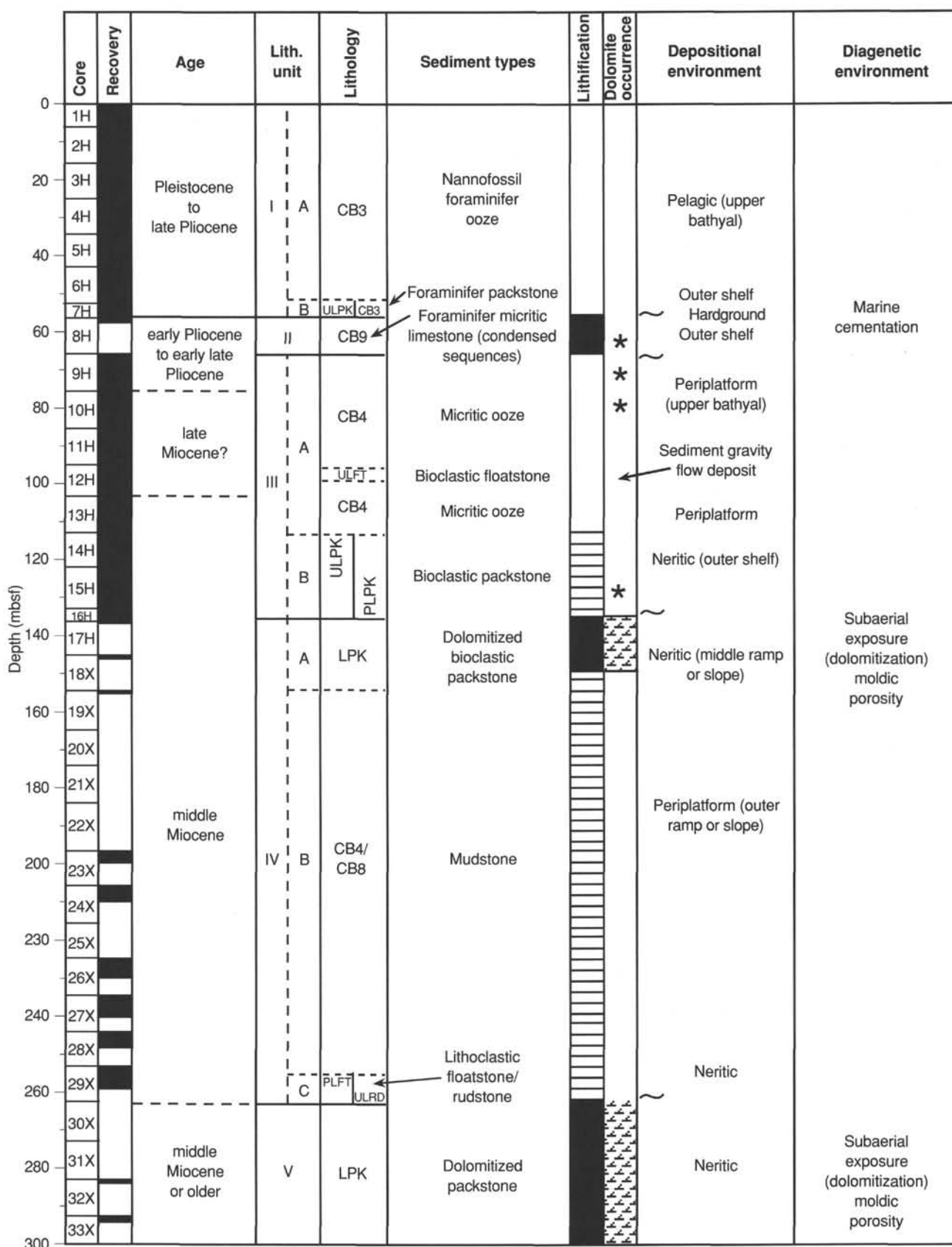


Figure 6. Stratigraphic section of Site 814 showing the lithologies, ages, degree of lithification (solid = lithified; striped = partially lithified; white = unlithified), dolomite occurrence (asterisk = less than 15%; pattern = >15%; white = no dolomite present), and inferred depositional and diagenetic environments.



Figure 7. Subunit IB, Section 133-814A-7H-CC, 9–14 cm. Close-up of un lithified foraminifer packstones with a fish tooth visible in the middle.

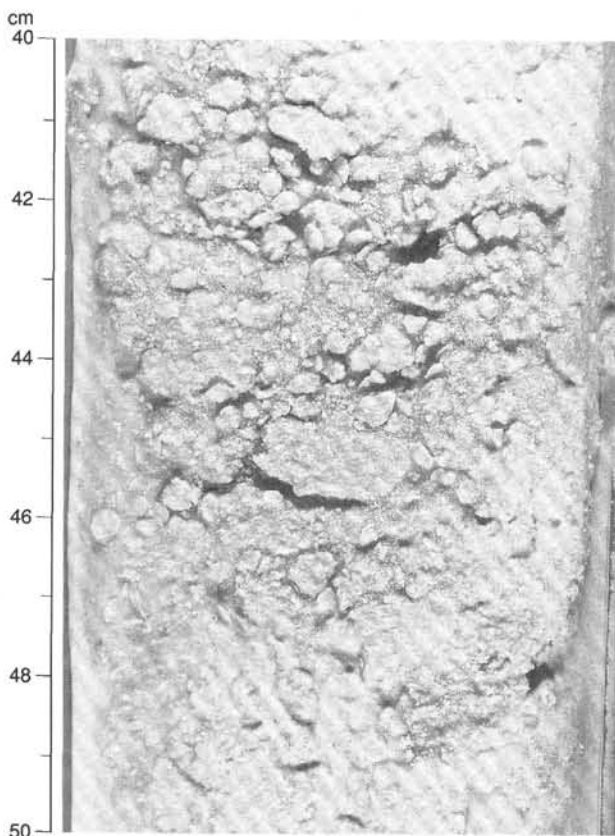


Figure 8. Subunit IIIA, Section 133-814A-12H-2, 40–50 cm. Un lithified bioclastic floatstone with shelf-derived coarse grains (mostly large benthic foraminifers and intraclasts), possibly a debris-flow deposit.

### Planktonic Foraminifers

All core-catcher samples of Hole 814A were examined for contents of planktonic foraminifers. The upper part of the hole (5.9–56.8 mbsf) contains well-preserved foraminiferal assemblages. From this level (56.8 mbsf) to the bottom of the hole, planktonic foraminifers are sparse and preservation of specimens is poor.



Figure 9. Subunit IVA, Section 133-814A-17H-1, 13–17 cm; dolomitized bioclastic packstones. Coralline-algal fragments (dense, white spots) are the only clearly recognizable elements of the original limestone components. The rock is highly porous. Most voids are presumed to be molds of former skeletal grains that were dissolved during dolomitization.

The last occurrences of *Globigerinoides obliquus* (1.8 Ma) and *Globigerinoides fistulosus* (1.6 Ma) are in Sample 133-814A-4H-CC, which indicates the lowermost Pleistocene. The lower limit of Zone N22-N23, defined by the first occurrence of *Globorotalia truncatulinoides*, was found in Sample 133-814A-5H-CC. One sample below this level contains the first occurrence of *Globorotalia tosaensis* (3.1 Ma), which indicates the zonal boundary between Zones N21 and N18-N19. In the same core, we found the first occurrence of *G. fistulosus* (2.9 Ma) and the first occurrence of *Sphaeroidinellopsis seminulina* (3.0 Ma); all these dates refer to the mid-Pliocene.

In Sample 133-814A-7H-CC, *Globorotalia tumida tumida* was found, while *Globigerinoides nepenthes* was not present, which constrains the age of this sample between 2.9 and 3.9 Ma.

In Sample 133-814A-8X-CC, no planktonic foraminifers are present. Samples 133-814A-9H-CC through -11H-CC contain sparse *Neogloboquadrina acostaensis* specimens, while *Globorotalia tumida tumida* is absent, which indicates an age range of 5.2 to 10.2 Ma.

### Benthic Foraminifers

Preservation of benthic foraminifers is poor to moderate in and below Core 133-814A-7H; above this core, preservation is excellent. Transported reefal benthic foraminifers (such as *Amphistegina* spp. and *Asterigerina* spp.) are mixed with *in-situ* benthic foraminiferal assemblages in and below Core 133-814A-7H. Core-catcher samples above this core contain rare transported benthic foraminifer specimens. All core-catcher samples examined in and below Core 133-814A-7H contain neritic benthic foraminiferal assemblages (0–200 m). Core-catcher samples from Cores 133-814A-1H through -5H contain upper bathyal benthic foraminiferal assemblages (200–600 m).

All the neritic core-catcher samples contained abundant *Elphidium* spp. except Sample 133-814A-7H-CC. Other faunal components varied from sample to sample. We defined tenta-

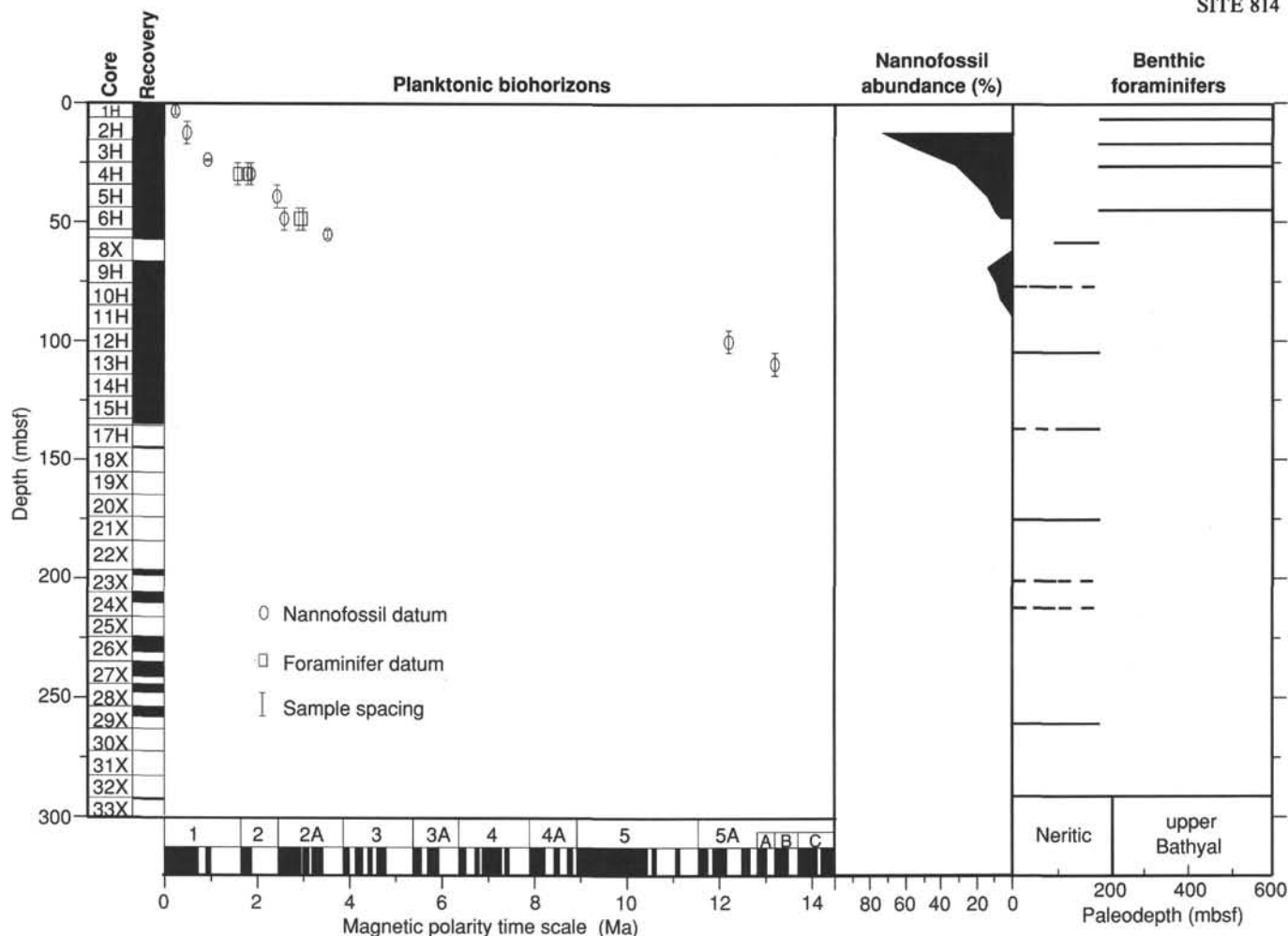


Figure 10. Plot of age vs. depth for Site 814; also shown are contents of calcareous nannofossils and paleobathymetry.

tive subdivisions within the neritic zone for some of the core-catcher samples that we examined. Samples 133-814A-23H-CC and 24H-CC contain *Hyalinea balthica*, but lack the outer neritic to bathyal benthic foraminifers identified in overlying samples (van Morkhoven et al., 1986). This suggests a paleodepth of approximately 50 to 100 m for these samples. Sample 133-814A-16H-CC contains *Cibicidoides dutemplei*, *C. subhaidingerii*, and *Hyalinea balthica*, which suggest an outer neritic paleodepth (100–200 m). The presence of *Sphaeroidina bulloides* in the neritic assemblage of Sample 133-814A-9H-CC and the absence of diagnostic outer neritic to bathyal benthic foraminifers that were found in other neritic samples suggest a middle neritic paleodepth (30–100 m). Sample 133-814A-16H-CC contains *Bulimina marginata* and *B. mexicana*, while no other typically bathyal foraminifers were found in overlying bathyal assemblages, suggesting an outer neritic paleodepth for this sample.

Samples 133-814A-1H-CC, -2H-CC, -3H-CC, and -5H-CC contain upper bathyal benthic foraminiferal assemblages, including the depth-diagnostic species associations of *Bulimina marginata*, *B. mexicana*, *Cibicidoides mundulus*, *Hanzawaia mantaensis*, *Hoeglundina elegans*, *Sigmoilopsis schlumbergeri*, and *Uvigerina proboscidea*.

#### Larger Benthic Foraminifers

We examined core-catcher samples from Hole 814A for larger benthic foraminifers. Larger benthic foraminifers occur in Samples 133-814A-9H-CC, -12H-CC through -24X-CC, -28X-CC, and -29X-CC. The samples contain rare-to-frequent

*Cycloclpeus*, rare-to-frequent *Nephrolepidina*, rare-to-frequent amphisteginids and rare *Operculina*. In addition, in Sample 133-814A-6H-CC *Biarritzina* and encrusting foraminifers associated with encrusting bryozoans (grown on extraclasts) occur. The *Nephrolepidina*–*Cycloclpeus* association is indicative of an inner neritic environment with seagrass (0–30 m).

#### PALEOMAGNETISM

As with Sites 812 and 813, Site 814 recorded a weak, but legible, magnetic reversal stratigraphy in the upper part of the core. After shipboard AF demagnetization at 15 mT, poorly defined polarity zones were evident that allowed us to identify approximate reversal boundaries. Biostratigraphic tie-points permitted correlation of the reversal stratigraphy to the geomagnetic polarity time scale. These shipboard data will be followed by shore-based study to confirm, refine, and expand downward the magnetic reversal stratigraphy.

A tentative magnetostratigraphy, constrained by biostratigraphic tie-points, was developed for the top 55 m of the core above the cemented unit in Core 133-814A-8X. Below the cemented layer (unconformity?), no reliable reversal stratigraphy could be delineated from the shipboard data.

Although at this point reversal boundaries are poorly defined, we propose the following estimates (Fig. 12). From 0 to 14.3 mbsf, a normal polarity zone does correlate with the Brunhes Chron. Biostratigraphic markers in the core-catcher sample of Core 133-814A-2H give an age range of 0.465 to 0.93 Ma. Below the Brunhes/Matuyama boundary (0.73 Ma), a

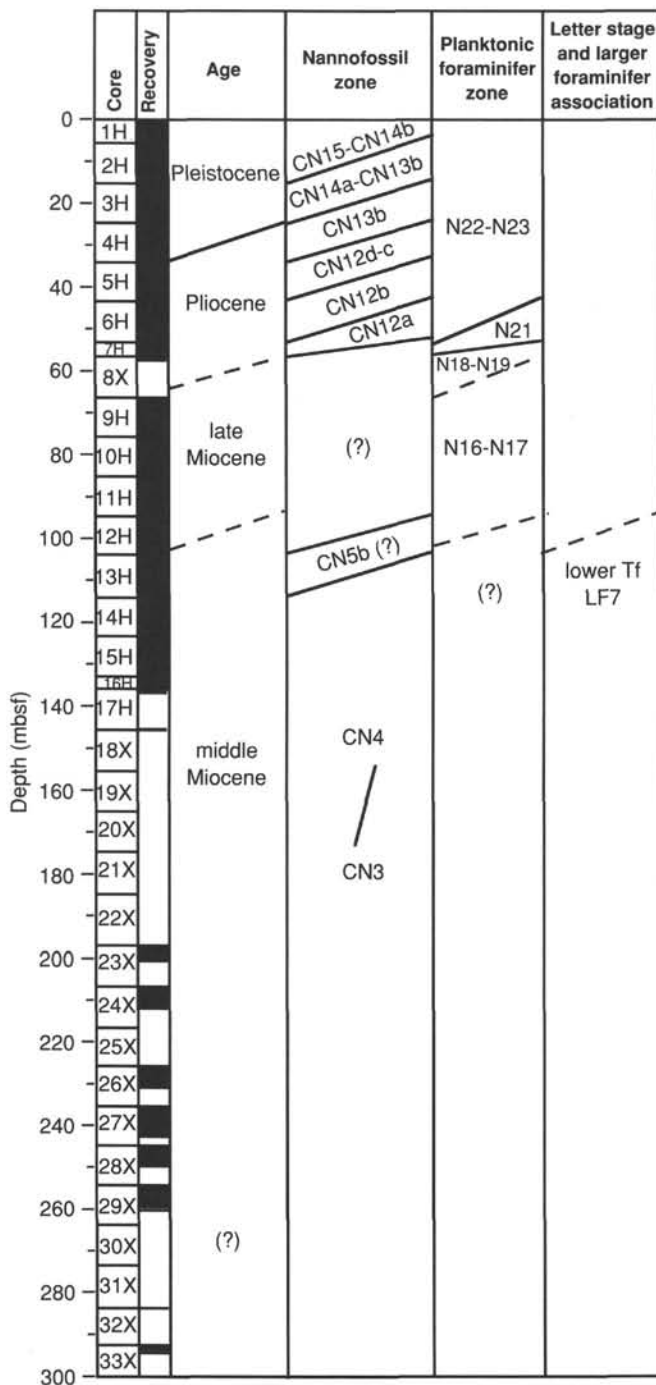


Figure 11. Overview of preliminary biostratigraphy at Site 814.

short normal polarity zone from about 15.5 to 17.3 mbsf may represent the Jaramillo Subchron (0.91–0.98 Ma). From 17.3 to 28.4 mbsf, the inclination record is scattered, with both normal and reversed polarity data points. However, this scattered zone does shift toward reversed polarity after AF demagnetization to 15 mT and at this time does correlate with the upper reversed zone of the Matuyama. A 4-m-thick normal polarity interval between 28.3 and 32.3 mbsf was tentatively correlated to the Olduvai Subchron, and thus ranges in age from 1.66 to 1.88 Ma. From 32.3 to 43 mbsf, a scattered inclination zone, moving progressively toward reversed polarity after AF demagnetization, is thought to represent the lower part of the Matuyama Chron. Shipboard

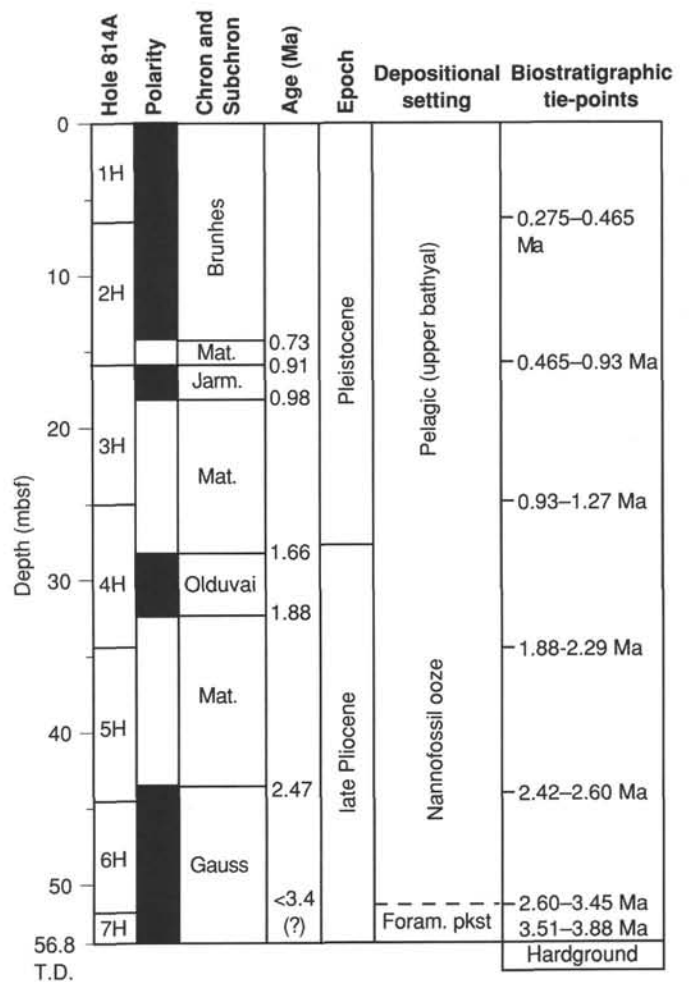


Figure 12. Preliminary shipboard magnetostratigraphy at Hole 814A.

nannofossil age determinations in the core-catcher sample of Core 133-814A-4H (34.4 mbsf) support this correlation, with an age range of 1.88 to 2.29 Ma. Below 43 mbsf, a normal polarity zone is present after the AF 15 mT step. This normal zone does correlate, with biostratigraphic constraints, to the top of the Gauss normal Chron and has an upper boundary age of 2.47 Ma. Normal polarity continues through Cores 133-814A-6H and -7H, the lowermost sediment recovered above the cemented unit in Core 133-814A-8X. Thus, magnetostratigraphic dating of sediments above the hardground constrains the age of this surface to younger than 3.4 Ma, but older than 2.47 Ma. If one assumes a uniform rate of sedimentation in these pelagic sediments (16.3 m/m.y. between the Brunhes/Matuyama and Matuyama/Gauss boundaries), the base of Core 133-814A-7H should be about 3.3 to 3.4 Ma old. This normal polarity through Core 133-814A-7H (younger than 3.4 Ma) conflicts slightly with the nannofossil age of 3.51 to 3.88 Ma (see "Biostratigraphy" section, this chapter).

A total of 211 7-cm<sup>3</sup> discrete samples were collected for preliminary refinement of the reversal stratigraphy throughout the 29 cores. Because these sediments have a weak magnetic intensity (10<sup>-1</sup> mA/m), sample analysis will be completed at a properly shielded laboratory.

Volume magnetic susceptibility data for Hole 814A were collected continuously from the MST between Cores 133-814A-1H and 16H and intermittently between Cores 133-814A-18X and 33X as a result of lower recovery. The downward susceptibility record (Fig. 13) is similar to that in Sites

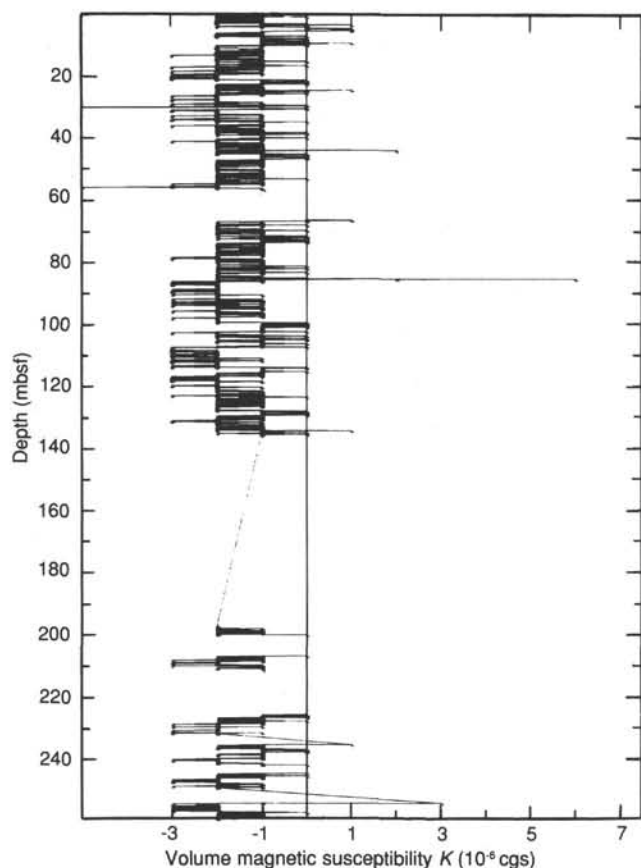


Figure 13. Summary of volume magnetic susceptibility at Hole 814A. Weak susceptibility indicates a low concentration of ferrimagnetic grains in the predominantly carbonate core.

812 and 813, with a weak (zero or negative) susceptibility throughout most of the recovered section. A slight positive susceptibility was recorded in the upper 10 m that corresponds to a slightly higher net magnetic intensity (see Fig. 14). These peaks may represent a change in the influx of ferrimagnetic material or perhaps a progressive diagenetic destruction of magnetite. The occasional abrupt positive excursion in the susceptibility log probably results from contamination, as each peak matches the core's top depth.

#### SEDIMENTATION RATES

This discussion of sedimentation rates at Site 814 is restricted to the upper 114 m, from which datable planktonic microfossils were recovered. An age-vs.-depth plot for this site using calcareous nannofossil and planktonic foraminifer biohorizons is presented in Figure 10. From the Holocene to the middle Pleistocene, sediments accumulated at a rate of 2.49 cm/k.y. During the early Pleistocene and late Pliocene, the rate decreased to 1.2 cm/k.y., and the middle Miocene accumulation rate was 1.4 cm/k.y. This last value is only an approximation, because only two planktonic biohorizons were found within this interval and because the depositional environment was neritic (discontinuous sedimentation, multiple hiatuses, etc.).

The abundance of nannofossils in the sediment indicates predominantly pelagic conditions for the middle and late Pleistocene. The benthic foraminiferal association for this time interval points toward an upper bathyal depositional setting. Below Section 133-815A-5H-CC (43.9 mbsf; late

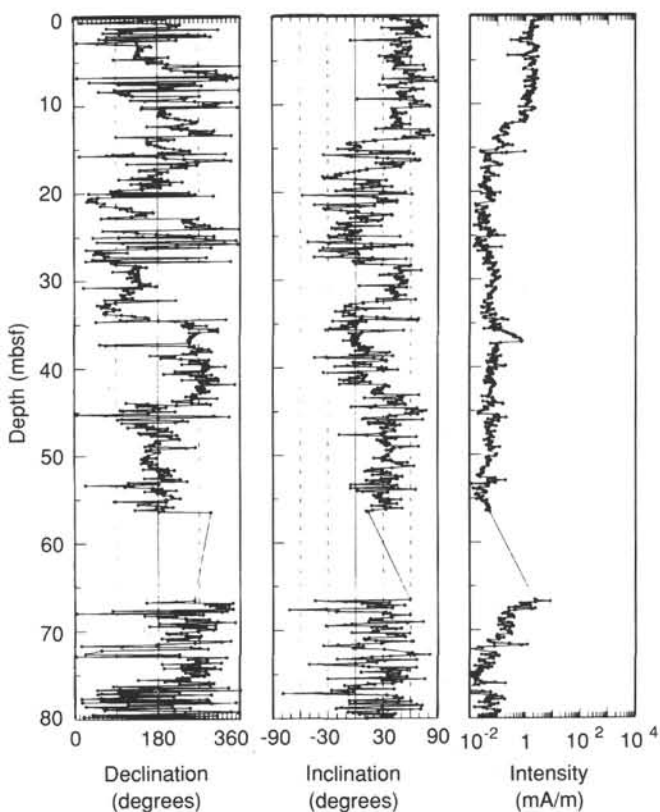


Figure 14. Summary of declination, inclination, and magnetic intensity for Hole 814A. Weak intensity after AF demagnetization contributes to scattered inclination and declination values.

Pliocene), the sedimentary environment changed from upper bathyal to neritic. The occurrence of larger benthic foraminifers below this level suggests inner neritic conditions in parts of the succession.

## INORGANIC GEOCHEMISTRY

### Interstitial Waters

#### Calcium, Magnesium, and Strontium

Interstitial water samples were taken from Cores 133-814A-1H-7H, -9H, -10H, -13H, -23H, -24H, -26H, -28H, and -29H. Samples were squeezed and analyzed according to the methods outlined in the "Explanatory Notes" chapter (this volume).

Concentrations of  $\text{Ca}^{2+}$  increase over the upper 50 m of Hole 814A from seawater values of 10.34 mM in Core 133-814A-6H-5 (Table 2 and Fig. 15) to 11.88 mM at 51.38 mbsf. Below this interval, a small decrease in  $\text{Ca}^{2+}$  concentration occurs, followed by values of approximately 11.90 mM over the rest of the core. The concentrations of  $\text{Sr}^{2+}$  increase rapidly from seawater values of 96 to 181  $\mu\text{M}$  in Core 133-814A-2H-5. Below these maxima, values decrease to near seawater values at 43 mbsf and remain constant over the remainder of the sampled interval (Table 2 and Fig. 15). The concentration of  $\text{Mg}^{2+}$  decreases with increasing depth from seawater values of 54.34 mM to a minimum of 51.94 mM in Core 133-814A-28X (Table 2 and Fig. 15). Magnesium concentrations in the top 100 mbsf of the site show greater variability than those in the lower cores.

Table 2. Interstitial water data for Site 814.

Sample	Depth (mbsf)	pH	Alkalinity (mM)	Salinity (g/kg)	Calcium (mM)	Magnesium (mM)	Chloride (mM)	Silica ( $\mu\text{M}$ )	Strontium ( $\mu\text{M}$ )	Sulfate (mM)
Seawater	0.00			36.2	10.34	54.34	539.90	7	96	28.16
133-814A-										
1H-3 145-150	4.45	7.47	3.90	35.5	10.35	53.62	519.25	81	168	29.08
2H-5 145-150	13.37	7.31	3.26	35.0	10.78	53.42	543.84	85	181	28.37
3H-5 145-150	22.87	7.18	3.20	35.2	11.02	53.83	538.92	96	167	29.25
4H-5 145-150	32.37	7.20	3.13	35.5	11.44	53.60	547.77	87	141	28.40
5H-5 145-150	41.87	7.16	3.12	35.5	11.83	53.14	545.80	71	125	28.70
6H-5 145-150	51.37	7.14	2.88	35.5	11.88	52.96	559.57	52	108	29.29
7H-2 145-150	56.30	7.33	3.04	35.0	11.72	53.28	553.67	39	100	29.18
9H-5 145-150	73.97	7.52	3.14	35.2	11.51	53.09	537.94	28	95	28.59
10H-5 145-150	83.47	7.52	3.20	35.5	11.60	52.84	558.59	31	101	29.74
3H-5 145-150	111.97	7.64	2.56	35.5	11.87	53.05	548.75	33	97	28.25
23H-1 145-150	200.10	7.73	2.77	35.2	11.95	52.26	550.72	35	92	28.13
24H-2 145-150	209.80	7.37	2.78	35.2	12.06	52.15	572.36	33	93	28.46
26H-3 145-150	230.20	7.27	2.61	34.0	11.87	52.34	551.70	33	92	28.25
28H-2 145-150	247.60	7.35	2.755	35.5	11.94	51.94	566.45	26	92	29.09
29H-2 145-150	257.20	7.38	3.209	35.5	11.89	52.71	545.80	31	93	26.97

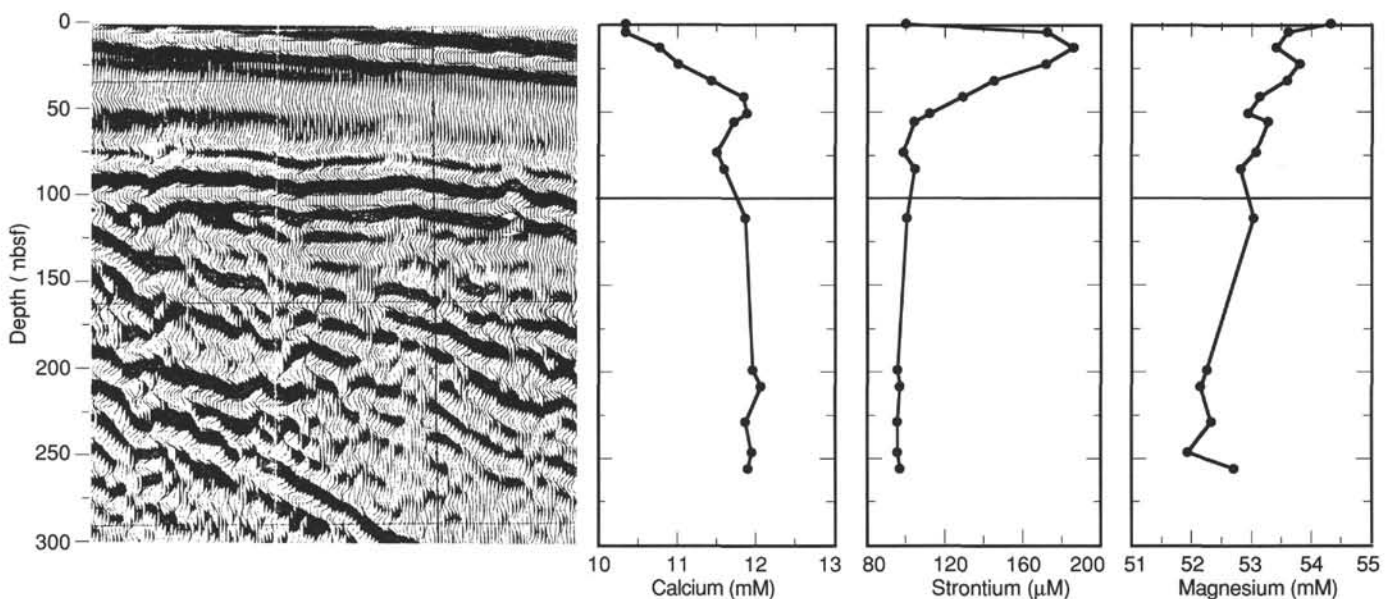


Figure 15. Calcium, strontium, and magnesium data as a function of depth for Hole 814A. The relevant seismic section showing site location also shown. Chemical composition of fluids in the lower seismic unit is similar to the waters in equivalent section at Site 813.

The higher  $\text{Sr}^{2+}$  and  $\text{Ca}^{2+}$  concentrations in the upper cores at Site 814 probably resulted from dissolution of aragonite, which is present at the top of the hole.

Concentrations of  $\text{Sr}^{2+}$ ,  $\text{Ca}^{2+}$ , and  $\text{Mg}^{2+}$  below 56.3 mbsf at Hole 814A correlate to data below 107.4 mbsf at Hole 813A (see "Inorganic Geochemistry" section, "Site 813" chapter, this volume). The top of this interval at both sites correlates to the Unit II/Unit III contact (Fig. 15). The similarity of data from Holes 813A and 814A may be an indication of horizontal fluid flow between these two sites within this interval (see discussion at the end of this section).

#### Chloride

Chloride concentrations remain nearly constant downcore at approximately 545 mM, which is only slightly lower than modern-day seawater values (Table 2).

#### Alkalinity, Sulfate, and pH

Alkalinity at Site 814 decreases from 3.90 mM in Core 133-814A-1H to approximately 3.2 mM by 112 mbsf (Fig. 16A

and Table 2). Below this depth, the alkalinity decreases to 2.7 mM over the next 118 m. From 230 mbsf to the end of the sampled interval, alkalinity increases to 3.21 mM. The decrease in alkalinity between 112 and 230 mbsf is similar to that seen in Unit III of Site 813. Sulfate values remain nearly constant with depth, indicating negligible sulfate reduction and organic matter diagenesis (Fig. 16A and Table 2). The absence of organic carbon remineralization in these sediments is evidenced by the low concentrations of organic carbon present (see "Organic Geochemistry" section, this chapter).

#### Silica

Concentrations of silica increase sharply within the first three cores of Hole 814A from a seawater value of 7 to 96  $\mu\text{M}$  in Section 133-814A-3H-5 (Table 2 and Fig. 16B). Below this depth, concentrations decrease to a value of approximately 30  $\mu\text{M}$ , where they remain constant for the remainder of the cored interval. The increase in the concentration of silica near the top of Hole 814A probably results from the dissolution of siliceous microfossils and quartz in the top 56 m of Hole 814A.

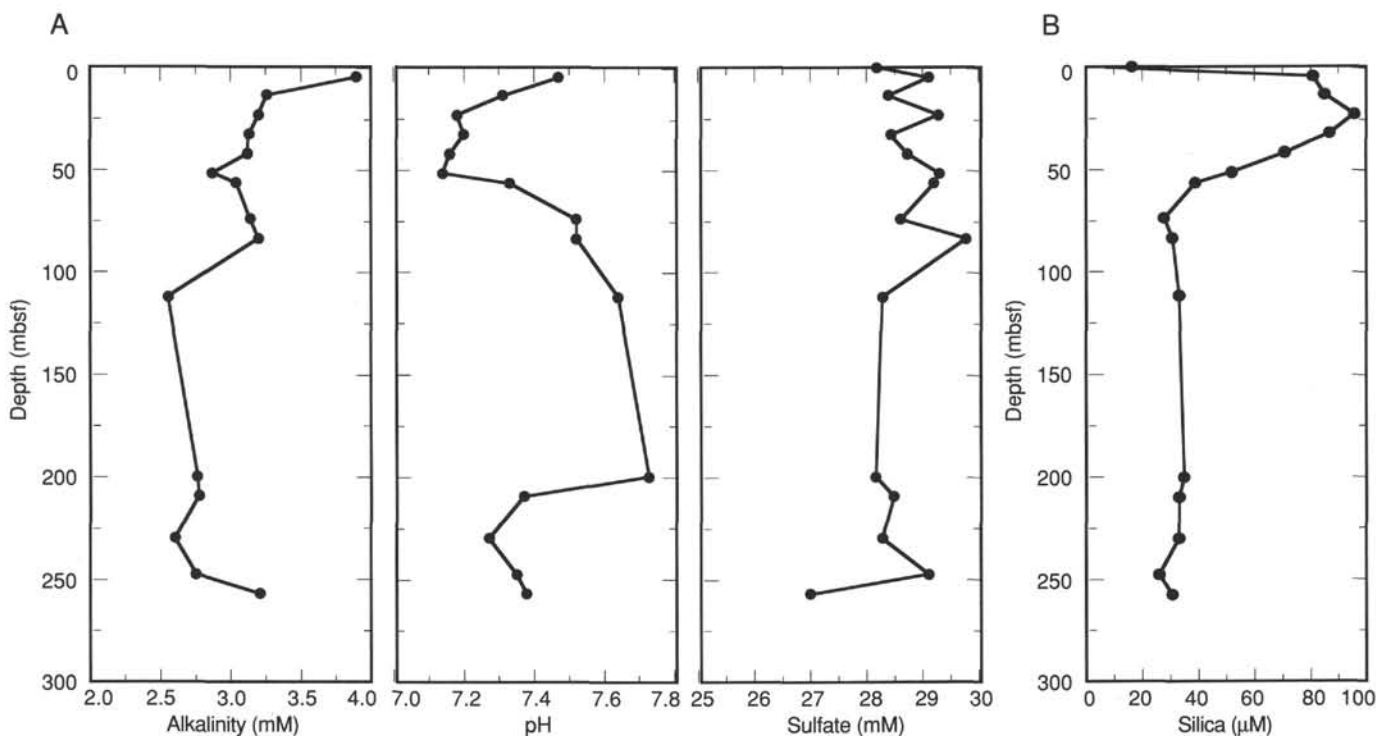


Figure 16. A. Alkalinity, pH, and sulfate data as a function of depth for Hole 814A. B. Interstitial silica data for Site 814.

### Carbonate Content and X-Ray Diffraction Data

Samples for X-ray diffraction (XRD) analyses were taken from interstitial water squeezed from sediments and physical property samples.

Aragonite concentrations decrease with depth from a value of 63% in Sample 133-814A-1H-1, 80–82 cm, to 0% below 22.87 mbsf. As discussed previously, the disappearance of aragonite coincides with an increase in pore-water strontium concentrations, indicating carbonate dissolution and remineralization. Aragonite is scattered with increasing depth, but concentrations are almost always less than 7%. One exception is Sample 133-814A-29X-2, 50–52 cm, near the bottom of the hole, which contains 35% aragonite (Fig. 17 and Table 3).

The concentrations of quartz measured relative to calcite vary from 0% to 7% with depth, although most samples have values below 1%. The absence of quartz from Hole 814A indicates low terrigenous influxes at this site (Fig. 17 and Table 3).

The main fluctuations in mineralogy occur in the calcite and dolomite fractions of the sediment. Calcite dominates throughout most of the hole and has concentrations between 27% and 100%. Dolomite-rich sediments occur in the interval from 96 to 138 mbsf and below 244 mbsf. In these intervals, dolomite is present in concentrations up to 64% (Fig. 17 and Table 3).

Carbonate values were measured in interstitial water and physical properties samples. Carbonate values for the top 22 mbsf of Hole 814A have values that average 96%. Between 22 and 95 mbsf, a sharp increase occurs in carbonate content to values averaging 98% (Fig. 18 and Table 4). This increase corresponds to the boundary between Units I and II. Below 95 mbsf, values increase above 100% carbonate because of the difference in molecular weight between calcite and dolomite, as discussed in the "Inorganic Geochemistry" section, "Site 812" chapter (this volume).

### Fluid Flow at Sites 812, 813, and 814

Sites 812, 813, and 814 are characterized by an influx of substantial quantities of admixtures of bank-derived aragonite, high-Mg calcite (HMC), and pelagic low-Mg calcite (LMC). Previous ODP sites in the Bahamas (Leg 101) and the Maldives (Leg 115), where such periplatform sediments have been cored (Swart and Guzikowski, 1988; Swart and Burns, 1990), were characterized by relatively high concentrations of  $\text{Sr}^{2+}$  in their interstitial pore fluids that resulted from the recrystallization of aragonite and HMC to LMC and the consequent release of  $\text{Sr}^{2+}$ . Therefore, perhaps the most surprising feature concerning the pore-water chemistry at Sites 812, 813, and 814 is the absence of such large increases in  $\text{Sr}^{2+}$ . This is despite the fact that aragonite disappears relatively quickly with increasing sub-bottom depth. In fact, all three sites exhibit an initial small increase in  $\text{Sr}^{2+}$ , followed by a return to concentrations near that of seawater throughout the remainder of the holes (Fig. 19A).

Various scientists have proposed (Mullins et al., 1984; Simms, 1984) that fluid flow through carbonate platforms may be a mechanism whereby normal or slightly modified seawater provides the necessary chemical constituents for diagenetic reactions. Such reactions include the stabilization of metastable minerals, such as HMC and aragonite to LMC, and the formation of dolomite. However, in previous ODP sites (Legs 101 and 115) adjacent to carbonate platforms, strong interstitial pore-water  $\text{Sr}^{2+}$  gradients were measured. The presence of such gradients combined with observation about the mineralogy of the sediments have precluded the existence of large-scale significant fluid flow. For example, Swart and Guzikowski (1988) concluded that to maintain the observed  $\text{Sr}^{2+}$  gradient of 6  $\mu\text{M}/\text{m}$ , typical of that seen at Sites 631, 632, and 633 in the Bahamas, a recrystallization rate of aragonite to calcite of 2.56% per 1000 yr would be necessary if water movement occurred at the rate of 1 m/yr. At such a rate, total recrystallization of the

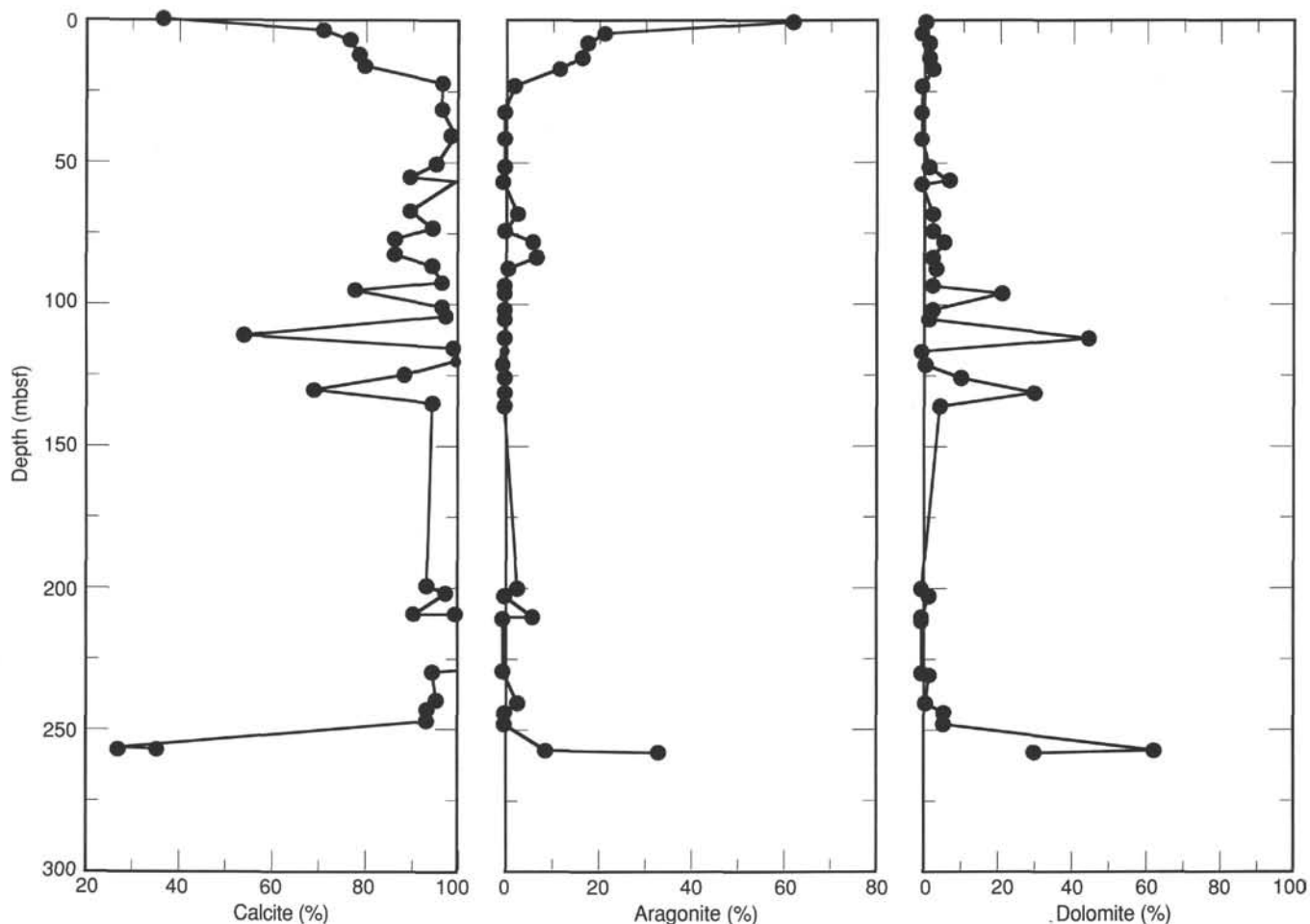


Figure 17. X-ray diffraction data as a function of depth for Hole 814A.

sediments should occur within 39,000 yr. Mineralogical data from these sites show that aragonite is still present at concentrations of up to 50% in sediments as old as 5 Ma, and therefore the sediments cannot have been recrystallized at the rate necessary to support fluid flow. By contrast, the absence of significant changes in the concentrations of pore-water  $\text{Sr}^{2+}$  at Sites 812 to 814, in spite of the disappearance of aragonite, is strong evidence for water flow at these sites.

Of further relevance is the nature of the  $\text{Ca}^{2+}$ ,  $\text{Mg}^{2+}$ , and  $\text{Cl}^-$  gradients at the Leg 133 sites. Sites 813 and 814 are characterized by steep  $\text{Ca}^{2+}$  gradients near the sediment/water interface, but relatively constant  $\text{Ca}^{2+}$  concentrations with increasing sub-bottom depth (Fig. 19B). By contrast, Site 812 exhibits a constant concentration of  $\text{Ca}^{2+}$  with increasing depth and a relative sudden increase in  $\text{Ca}^{2+}$  concentration from 74.97 to 112.97 mbsf. Normally, we would consider the types of geochemical gradients observed at Sites 813 and 814 as indicative either of fluid movement out of the sediments or as horizontal flow parallel to the seafloor. In contrast, the gradients at Site 812 are associated with the movement of normal seawater into the formation.

Our interpretation of fluid movement is further supported by the measurement of temperature gradients at Sites 812 and 814 (see "Downhole Logging" section, "Site 812" chapter and this chapter). Site 812 shows a relatively constant temperature of approximately  $10^\circ\text{C}$  to a depth of 225 mbsf and then an abrupt rise to  $17.6^\circ\text{C}$  at 300 mbsf. Although the geothermal gradient measured at Site 812 reflects that present in the hole during logging and may be partly an artifact

resulting from drilling, it does suggest an under-pressured zone that is drawing fluids through the sediments, which is consistent with the geochemical interpretation. In contrast, Site 814 exhibits a sharp geothermal gradient near the sediment/seawater interface from bottom-water temperatures of  $10^\circ$  to  $18^\circ\text{C}$  at 30 mbsf. This supports the hypothesis that water is moving out of the sediments at these sites.

In summary, the existence of fluid flow at Sites 812 to 814 can be supported on the basis of three independent lines of evidence. First, the rapid removal of Sr-rich aragonite from the sediments through dissolution imparts a strong  $\text{Sr}^{2+}$  signal on the pore fluids, yet this signature is absent and the pore waters have essentially seawater values below the upper one or two cores. Such signals are in contrast to other ODP sites where periplatform sediments have been drilled. Second, the convex nature of the  $\text{Ca}^{2+}$  gradient at Site 812 suggests the movement of normal seawater down through the sediments, whereas the concave nature of the  $\text{Ca}^{2+}$  gradients at Sites 813 and 814 indicates movement of fluids out of the formation. Third, the measured geothermal gradients at Site 812 show a temperature similar to bottom water to a depth of 200 mbsf, followed by a sharp increase to  $18^\circ\text{C}$ , indicating that an underpressured zone is drawing water into the formation. At Site 814, the same temperature change occurs near the sediment/seawater interface.

#### ORGANIC GEOCHEMISTRY

In addition to safety monitoring for hydrocarbons, the main purpose of shipboard organic geochemistry studies at Site 814

Table 3. X-ray diffraction data for Site 814.

Core, section, interval (cm)	Depth (mbsf)	Calcite (%)	Aragonite (%)	Quartz (%)	Dolomite (%)
133-814A-					
1H-1, 80-82	0.82	36.00	63.00	0.00	1.00
1H-3, 145-150	4.45	71.00	22.00	7.00	0.00
2H-2, 70-72	8.10	77.00	18.00	3.00	1.00
2H-5, 145-150	13.37	79.00	17.00	2.00	2.00
3H-2, 100-102	16.90	80.00	12.00	5.00	3.00
3H-5, 145-150	22.87	97.00	2.00	1.00	0.00
4H-5, 145-150	32.37	97.00	0.00	3.00	0.00
5H-5, 145-150	41.87	100.00	0.00	0.00	0.00
6H-5, 145-150	51.37	96.00	0.00	2.00	2.00
7H-2, 145-150	56.30	90.00	0.00	3.00	6.00
8H-1, 57-58	57.37	100.00	0.00	0.00	0.00
9H-2, 75-76	68.17	90.00	3.00	4.00	3.00
9H-5, 145-150	73.97	95.00	0.00	2.00	3.00
10H-2, 102-103	77.97	87.00	6.00	1.00	5.00
10H-5, 145-150	83.47	87.00	7.00	3.00	3.00
11H-2, 102-103	87.47	95.00	1.00	0.00	3.00
11H-5, 102-103	93.47	97.00	0.00	0.00	3.00
12H-2, 101-103	95.97	78.00	0.00	0.00	22.00
12H-5, 101-103	101.97	97.00	0.00	0.00	3.00
13X-1, 77-78	105.50	98.00	0.00	0.00	2.00
13X-5, 145-150	111.97	54.00	0.00	0.00	46.00
14X-2, 103-105	116.80	100.00	0.00	0.00	0.00
14X-5, 101-103	121.30	99.00	0.00	0.00	1.00
15X-2, 63-65	125.80	89.00	0.00	0.00	11.00
15X-5, 101-103	130.80	69.00	0.00	0.00	31.00
16X-2, 101-103	135.80	95.00	0.00	0.00	5.00
23X-3, 90-92	202.50	98.00	0.00	0.00	2.00
23X-1, 145-150	200.10	94.00	3.00	3.00	0.00
24X-2, 20-22	210.00	100.00	0.00	0.00	0.00
24X-2, 145-150	209.80	91.00	6.00	3.00	0.00
24X-3, 20-23	211.50	100.00	0.00	0.00	0.00
26X-2, 80-82	229.50	100.00	0.00	0.00	0.00
26X-3, 145-150	230.20	95.00	0.00	3.00	2.00
27X-3, 70-72	240.50	96.00	3.00	0.00	1.00
27X-5, 70-72	243.50	94.00	0.00	0.00	6.00
28X-2, 145-150	247.60	94.00	0.00	0.00	6.00
29X-2, 50-52	257.70	35.00	34.00	0.00	31.00
29X-2, 145-150	257.00	27.00	9.00	0.00	64.00

was to assess the amount and type of organic matter preserved in the Pleistocene to middle Miocene sediments of the Queensland Plateau.

We determined the total nitrogen, sulfur, and carbon contents and the total organic carbon contents of 22 additional samples collected for chromatographic analyses of volatile hydrocarbons (headspace samples) using an NA 1500 Carlo Erba NCS analyzer. Detailed descriptions of methods are outlined in our "Explanatory Notes" chapter (this volume).

#### Volatile Hydrocarbons

Light hydrocarbon gases ( $C_1$ - $C_3$ ) in sediments were analyzed routinely as part of ODP's safety and pollution-prevention monitoring program, using the headspace technique and the Carle gas chromatograph. The results of 23 analyses from Hole 814A are presented in Table 5.

The sediments at Site 814 contained low concentrations of hydrocarbon gases. Concentrations of methane in headspace gas were approximately 2 ppm, while ethane or propane were not detected.

#### Organic Carbon Contents

Total organic carbon (TOC) contents recorded in Hole 814A are presented in Table 6. We observed very low to low TOC values in the calcium carbonate- or dolomite-rich sediments encountered at Site 814. These values ranged below 0.30%, and total nitrogen and sulfur concentrations were below the detection limits of the NCS analyzer.

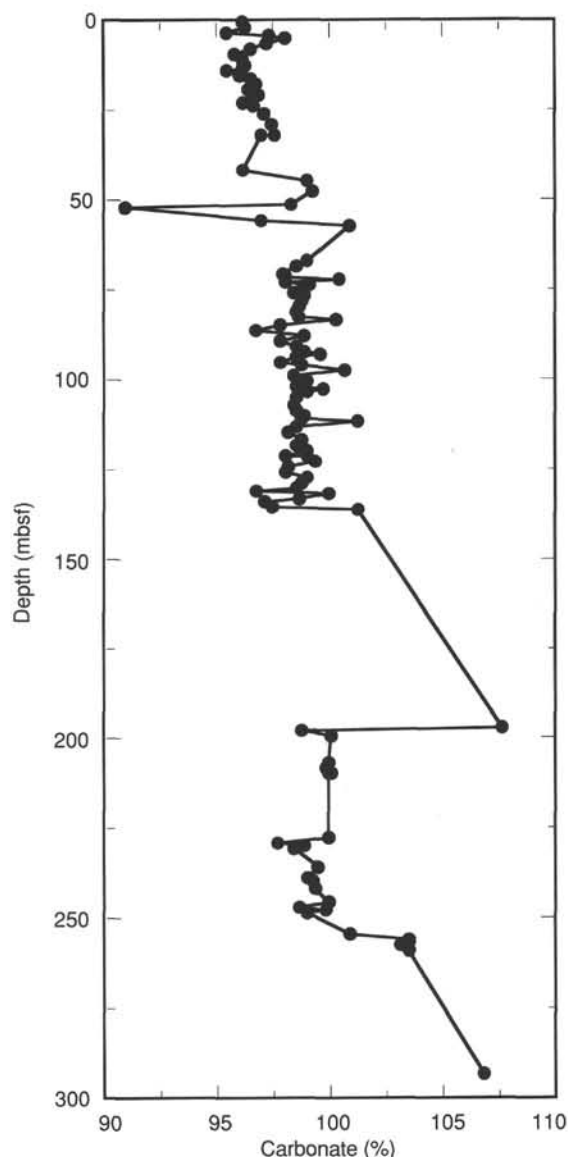


Figure 18. Carbonate data as a function of depth for Hole 814A.

As a consequence of the low organic contents, we were unable to conduct detailed geochemical characterization of kerogen types using the Rock-Eval pyrolysis method, as originally planned.

#### PHYSICAL PROPERTIES

Physical properties analyzed in cores from this site included bulk density,  $P$ -wave velocity, and magnetic susceptibility for unsplit cores and  $P$ -wave velocity, electrical-resistivity formation factor, shear strength, and index properties (including bulk density, grain density, water content, porosity, and void ratio) for split cores. The methods used are described in detail in the "Explanatory Notes" chapter (this volume). Generally poor recovery below 136 mbsf accounts for sparse data in the lower part of the hole.

#### Bulk Density

Bulk densities for Site 814 were determined by measuring volumes and mass on discrete core samples and from gamma-ray absorption of whole-round cores (Figs. 20A and 21A; Table 7).

Table 4. Carbonate data for Site 814.

Core, section, interval (cm)	Depth (mbsf)	Sample type	Carbon (%)	Calcium carbonate (%)
133-814A-				
1H-1, 80-83	0.80	PP	11.55	96.20
1H-2, 80-83	2.30	PP	11.56	96.30
1H-3, 80-83	3.80	PP	11.46	95.50
1H-3, 145-146	4.45	HS	11.68	97.29
1H-4, 80-83	5.30	PP	11.77	98.00
2H-1, 70-73	6.60	PP	11.67	97.20
2H-2, 70-73	8.10	PP	11.59	96.50
2H-3, 70-73	9.60	PP	11.50	95.80
2H-4, 70-73	11.10	PP	11.55	96.20
2H-5, 70-73	12.60	PP	11.56	96.30
2H-5, 145-146	13.35	HS	11.55	96.21
2H-6, 70-73	14.10	PP	11.45	95.40
2H-7, 70-73	15.60	PP	11.53	96.00
3H-1, 105-108	16.45	PP	11.58	96.50
3H-2, 100-103	17.90	PP	11.61	96.70
3H-3, 100-103	19.40	PP	11.57	96.40
3H-4, 100-103	20.90	PP	11.63	96.90
3H-5, 100-103	22.40	PP	11.58	96.50
3H-5, 145-146	22.85	HS	11.55	96.21
3H-6, 100-103	23.90	PP	11.60	96.60
4H-1, 97-100	25.87	PP	11.66	97.10
4H-3, 97-100	28.87	PP	11.69	97.40
4H-5, 97-100	31.87	PP	11.72	97.60
4H-5, 145-146	32.35	HS	11.64	96.96
5H-5, 145-146	41.85	HS	11.54	96.13
6H-1, 96-99	44.86	PP	11.88	99.00
6H-3, 96-99	47.86	PP	11.91	99.20
6H-5, 145-146	51.35	HS	11.80	98.29
6H-6, 97-100	52.37	PP	10.92	91.00
7H-2, 145-146	55.48	HS	11.64	96.96
8X-1, 57-60	57.37	PP	12.11	100.88
9H-1, 82-84	67.32	PP	11.88	99.00
9H-2, 75-76	68.75	PP	11.82	98.50
9H-3, 101-103	70.51	PP	11.75	97.90
9H-4, 56-58	71.56	PP	11.78	98.10
9H-4, 93-94	71.93	JPC	12.06	100.46
9H-5, 63-65	73.13	PP	11.77	98.00
9H-5, 145-146	73.95	HS	11.90	99.13
9H-6, 102-104	75.02	PP	11.85	98.70
9H-7, 44-46	75.94	PP	11.81	98.40
10H-1, 102-104	77.02	PP	11.87	98.90
10H-2, 102-104	78.52	PP	11.86	98.80
10H-3, 81-84	79.81	PP	11.84	98.60
10H-4, 80-83	81.30	PP	11.82	98.50
10H-5, 100-103	83.00	PP	11.84	98.60
10H-5, 145-146	83.45	HS	12.04	100.29
10H-6, 102-105	84.52	PP	11.74	97.80
11H-1, 102-105	86.52	PP	11.62	96.80
11H-2, 102-105	88.02	PP	11.87	98.90
11H-3, 102-105	89.52	PP	11.74	97.80
11H-4, 102-105	91.02	PP	11.83	98.50
11H-5, 102-105	92.52	PP	11.87	98.90
11H-5, 149-150	92.99	HS	11.96	99.63
11H-6, 102-105	94.02	PP	11.83	98.50
11H-7, 51-54	95.01	PP	11.74	97.80
12H-1, 101-104	96.01	PP	11.86	98.80
12H-2, 101-104	97.51	PP	12.08	100.63
12H-3, 101-104	99.01	PP	11.81	98.40
12H-4, 101-104	100.51	PP	11.89	99.00
12H-5, 101-104	102.01	PP	11.83	98.50
12H-5, 149-150	102.49	HS	11.97	99.71
12H-6, 101-104	103.51	PP	11.88	99.00
13H-1, 77-79	105.27	PP	11.82	98.50
13H-2, 102-104	107.02	PP	11.81	98.40
13H-3, 102-104	108.52	PP	11.82	98.50
13H-4, 102-104	110.02	PP	11.87	98.90
13H-5, 72-74	111.22	PP	11.86	98.80
13H-5, 145-146	111.95	HS	12.16	101.29
13H-6, 102-104	113.02	PP	11.82	98.50
14H-1, 101-103	115.01	PP	11.79	98.20
14H-2, 101-103	116.51	PP	11.85	98.70
14H-3, 101-103	118.01	PP	11.82	98.50
14H-4, 101-103	119.51	PP	11.88	99.00
14H-5, 101-103	121.01	PP	11.78	98.10
14H-5, 149-150	121.49	HS	11.89	99.04

Table 4 (continued).

Core, section, interval (cm)	Depth (mbsf)	Sample type	Carbon (%)	Calcium carbonate (%)
14H-6, 101-103	122.51	PP	11.93	99.40
15H-1, 101-103	124.51	PP	11.79	98.20
15H-2, 63-65	125.63	PP	11.76	98.00
15H-3, 101-103	127.51	PP	11.89	99.00
15H-4, 101-103	129.01	PP	11.86	98.80
15H-5, 101-103	130.51	PP	11.83	98.50
15H-5, 149-150	130.99	HS	11.61	96.71
15H-6, 101-103	132.01	PP	12.00	100.00
16H-1, 0-2	133.00	HS	11.84	98.63
16H-1, 101-103	134.01	PP	11.66	97.10
16H-2, 101-103	135.51	SED	11.69	97.40
17X-1, 0-2	136.00	HS	12.15	101.21
23X-1, 5-7	197.15	PP	12.92	107.62
23X-1, 90-93	198.00	PP	11.85	98.70
23X-2, 90-93	199.50	PP	12.02	100.10
24X-1, 20-23	207.00	PP	12.01	100.00
24X-2, 20-23	208.50	PP	11.98	99.80
24X-2, 149-150	209.79	HS	12.01	100.04
24X-3, 20-23	210.00	PP	11.99	99.90
26X-2, 80-83	228.00	PP	12.00	100.00
26X-3, 80-83	229.50	PP	11.73	97.70
26X-3, 149-150	230.19	HS	11.87	98.88
26X-4, 80-83	231.00	PP	11.81	98.40
27X-1, 70-73	236.00	PP	11.95	99.50
27X-3, 70-73	239.00	PP	11.88	99.00
27X-3, 149-150	239.70	HS	11.91	99.21
27X-5, 70-73	242.00	PP	11.92	99.30
28X-1, 70-73	245.30	PP	12.00	100.00
28X-2, 70-73	246.80	PP	11.84	98.60
28X-2, 149-150	247.59	HS	11.98	99.79
28X-3, 70-73	248.30	PP	11.88	99.00
29X-1, 50-53	254.70	PP	12.11	100.90
29X-2, 50-53	256.20	PP	12.42	103.50
29X-2, 149-150	257.19	HS	12.42	103.46
29X-3, 50-53	257.70	PP	12.38	103.10
29X-4, 50-53	259.20	PP	12.42	103.50
33X-1, 49-50	293.39	HS	12.82	106.79

PP = physical property; HS = headdress sample.

### P-Wave Velocity

P-wave velocities were measured for whole-round cores using the multisensor track (MST) and for discrete core samples using the Hamilton Frame (Table 8 and Figs. 20B and 21C). A comparison of velocities among Sites 812, 813, and 814 suggests some similarities of the velocity structure among the three sites (Fig. 22). This figure also shows that at Site 812, a strong correlation exists between sonic velocity and carbonate content. This correlation may be related to dolomitization. In turn, dolomitization may be responsible for increased bulk and shear moduli (which lead to higher velocity values), although the higher density results in reduced porosity.

### Porosity

Porosity was one of the index properties determined from discrete core samples using mass balance and the pycnometer (Table 7). A graph of porosity vs. depth is shown in Figure 23, along with variations in the percentage of carbonate. Comparison of porosity to percentage of carbonate shows a first-order inverse relationship—as porosity decreases in the first 70 m, the percentage of carbonate increases. The apparent general increase in carbonate down-hole is mostly a result of increased dolomitization. With recrystallization of CaCO<sub>3</sub> to dolomite, there is a loss of porosity. However, on a finer scale some variations in porosity are the inverse of variations in carbonate, whereas

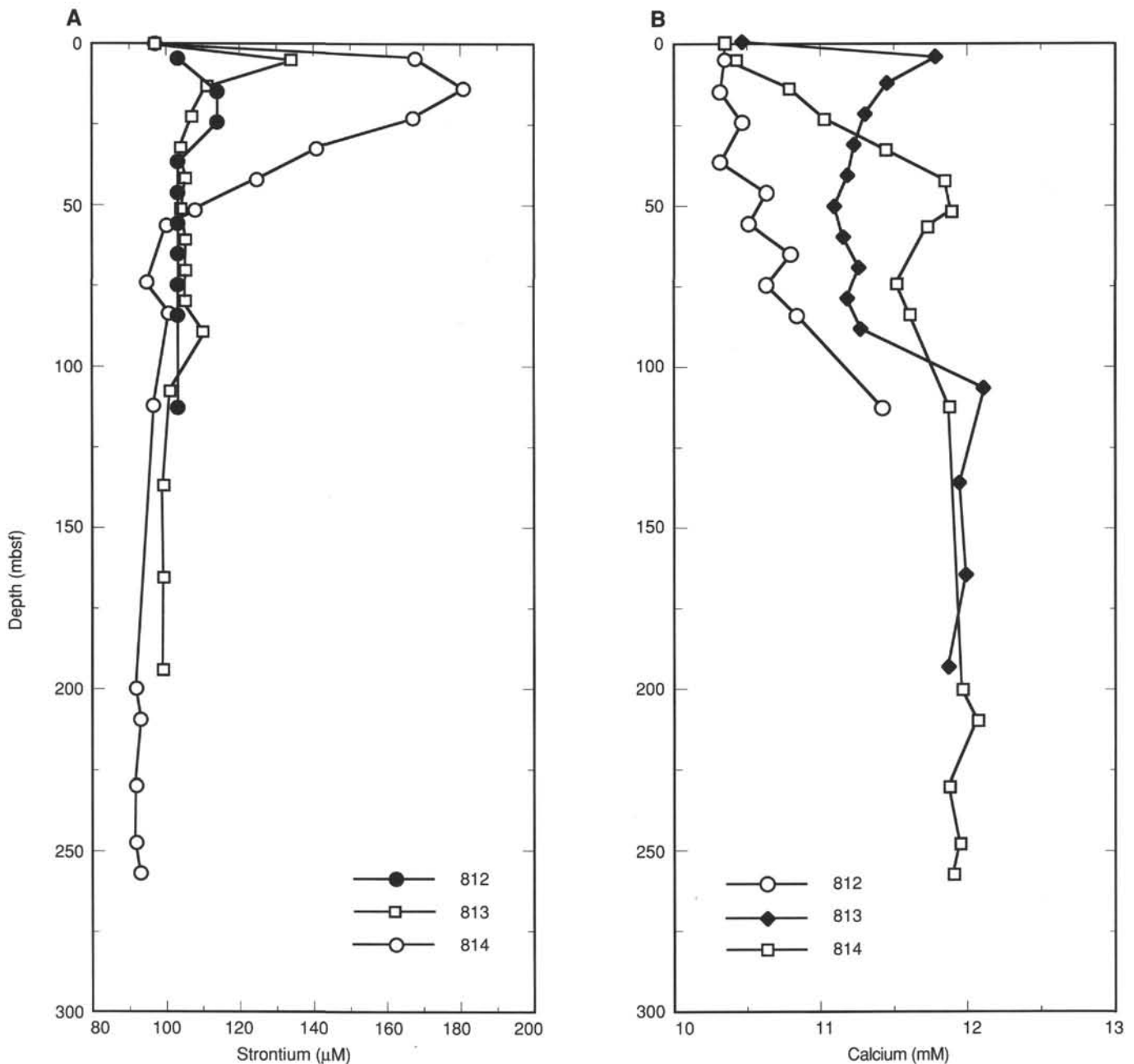


Figure 19. A. Summary of  $\text{Sr}^{2+}$  gradients at Sites 812, 813, and 814. B. Summary of  $\text{Ca}^{2+}$  gradients at Sites 812, 813, and 814.

other variations appear directly proportional to variations in carbonate. In Figure 24A, a plot of carbonate vs. porosity shows a linear relationship, but the fit of these data to a linear trend is by no means perfect.

The water content, derived from the same set of index property measurements, is plotted in Figure 21B. A plot of water content vs. porosity is depicted in Figure 24B. The low scatter of data in this figure, compared with Figure 21B, indicates a higher precision in the measurements at this site. Water content was calculated on the basis of measurements of mass for samples before and after drying. Porosity was similarly calculated using measurements of volume before and after drying. With good measurements, one should find a one-to-one correlation between water content and porosity in a fully saturated sediment.

### Electrical-Resistivity Formation Factor and Shear Strength

We measured the electrical-resistivity formation factor (FF) at three depths in each core section from Hole 814A (see Table 9). Although the data show a lot of scatter, two intervals are suggested as having high resistivity values—one between the seabed and about 50 mbsf and the other between about 75 and 140 mbsf (Fig. 21D). These intervals correspond roughly with those having high shear strength depicted in Figure 21E (see also Table 10). The regions of high shear strength shown in Figure 22 correspond with broader regions of high shear strength seen in Figure 21E. At Site 813, the interval having low shear strength between the

**Table 5. Volatile hydrocarbon data from headspace analysis at Site 814.**

Core, section, interval (cm)	Depth (mbsf)	Sample type	Volume (mL)	Gas chromatog.	C <sub>1</sub> (ppm)	C <sub>2+</sub> (ppm)
133-814A-						
1H-3, 145-146	4.45	HS	5	CAR132	2	0
2H-5, 145-146	13.35	HS	5	CAR132	2	0
3H-5, 145-146	22.85	HS	5	CAR132	2	0
4H-5, 145-146	32.35	HS	5	CAR132	2	0
5H-5, 145-146	41.85	HS	5	CAR132	2	0
6H-5, 145-146	51.35	HS	5	CAR132	2	0
7H-2, 145-146	55.48	HS	5	CAR132	2	0
9H-5, 145-146	73.95	HS	5	CAR132	2	0
10H-5, 145-146	83.45	HS	5	CAR132	2	0
11H-5, 149-150	92.99	HS	5	CAR132	2	0
12H-5, 149-150	102.49	HS	5	CAR132	2	0
13H-5, 145-146	111.95	HS	5	CAR132	2	0
14H-5, 149-150	121.49	HS	5	CAR132	2	0
15H-5, 149-150	130.99	HS	5	CAR132	2	0
16H-1, 0-2	133	HS	5	CAR132	2	0
17H-1, 0-2	136	HS	5	CAR132	2	0
24X-2, 149-150	209.79	HS	5	CAR132	2	0
26X-3, 149-150	230.19	HS	5	CAR132	2	0
27X-3, 149-150	239.79	HS	5	CAR132	2	0
28X-2, 149-150	247.59	HS	5	CAR132	2	0
29X-2, 149-150	257.19	HS	5	CAR132	2	0
33X-1, 49-50	293.39	HS	5	CAR132	2	0

HS = Headspace samples.

**Table 6. Concentrations of total organic carbon, inorganic carbon, carbon in sediments at Site 814.**

Core, section, interval (cm)	Depth (mbsf)	Sample type	Organic carbon (%)	Inorganic carbon (%)	Total carbon (%)
133-814A-					
1H-3, 145-146	4.45	HS	0.1	11.6	11.7
2H-5, 145-146	13.35	HS	0.1	11.5	11.6
3H-5, 145-146	22.85	HS	0.05	11.5	11.55
4H-5, 145-146	32.35	HS	0.05	11.6	11.65
5H-5, 145-146	41.85	HS	0	11.55	11.55
6H-5, 145-146	51.35	HS	0.2	11.6	11.8
7H-2, 145-146	55.48	HS	0.1	11.55	11.65
8X-1, 57-60	57.37	PP	0.1	12	12.1
9H-4, 93-94	71.93	JPC	0.25	11.8	12.05
9H-5, 145-146	73.95	HS	0.15	11.75	11.9
10H-5, 145-146	83.45	HS	0.25	11.8	12.05
11H-5, 149-150	92.99	HS	0.2	11.8	12
12H-5, 149-150	102.49	HS	0.15	11.85	12
13H-5, 145-146	111.95	HS	0.2	12	12.2
14H-5, 149-150	121.49	HS	0.1	11.8	11.9
15H-5, 149-150	130.99	HS	0	11.6	11.6
16H-1, 0-2	133	HS	0.15	11.7	11.85
17X-1, 0-2	136	HS	0.1	12.05	12.15
23X-1, 5-7	197.15	PP	0.1	12.8	12.9
24X-2, 149-150	209.79	HS	0.15	11.85	12
26X-3, 149-150	230.19	HS	0.05	11.8	11.85
27X-3, 149-150	239.79	HS	0.1	11.8	11.9
28X-2, 149-150	247.59	HS	0.1	11.9	12
29X-2, 149-150	257.19	HS	0.15	12.25	12.4
33X-1, 49-50	293.39	HS	0.25	12.55	12.8

HS = headspace sample; PP = physical properties; JPC = personal sample.

two highs is centered at 100 mbsf, instead of at roughly 50 mbsf, as at Site 814.

## DOWNHOLE MEASUREMENTS

### Reliability of Logs

Hole size is the most important control for accuracy of the logs from Hole 814A. Three caliper logs were obtained; in order of increasing reliability, these are (1) an apparent caliper calculated from the sonic log (see "Explanatory Notes"

chapter, this volume; Fig. 25), (2) the lithodensity tool caliper (Fig. 25), and (3) the two-axis caliper of the formation micro-scanner (FMS). The three are generally similar at Hole 814A, except that the FMS caliper saturates at a maximum opening of 15 in. (38.1 cm), while the lithodensity caliper saturates at 18 in. (45.7 cm). Both sonic and lithodensity calipers show broad swings in hole size with a period of about 30 m, presumably related to periodic changes in circulation pattern during drilling.

Except for the bottom 25 m of the hole, which is small, virtually the entire logged interval is greater than 14 in. (35.6 cm), which is significantly larger than bit diameter of 11.8 in. (30 cm). As a result, almost all of the FMS run achieved pad contact with only two of its four pads. Further, most of the lithodensity run obtained only marginal pad contact against the borehole wall. As a result, logs of density (Fig. 25) and photoelectric effect show swings to unreliably low values; the density compensation factor, which attempts to correct for inadequate pad contact, introduces corrections so large that the compensation is only approximate. Although the fully open caliper makes us dubious of the reliability of much of the density and photoelectric-effect logs, interlog relationships discussed in a following section permit a more accurate identification of unreliable intervals.

Most other logs do not require pad contact and thus are relatively insensitive to the changes in borehole size. Two minor exceptions are gamma-ray and resistivity logs, which probably will change slightly after post-cruise borehole correction. Pending this borehole correction, the 20- to 60-m cyclical changes in gamma-ray and uranium values should be treated with caution, as they are only roughly correlated with caliper values.

As is often the case with ODP holes, the initial sonic logs from Hole 814A exhibited several zones in which cycle skipping caused unreliable swings in apparent velocity. Re-processing (see "Explanatory Notes" chapter, this volume) seems to have removed all unreliable data, and we consider the reprocessed log of Figures 25 and 26 to be of good quality.

The spectral gamma-ray tool is the only tool in the seismic stratigraphic combination that can provide useful formation data even through pipe. At Hole 814A, through-pipe spectral gamma-ray logs were obtained for the interval from 7 to 58 mbsf. In this interval, values for uranium and potassium are just above the resolution of the tool, and values for thorium are below the resolution of the tool.

During most of the logging of Hole 814A, the base of drill pipe was kept at 87.9 mbsf. Just prior to the conclusion of each main open-hole upgoing log, pipe was raised 30 m to permit open-hole logging of the interval from 57.9 to 87.9 mbsf. Because of a small delay when pulling this pipe during logging with the seismic stratigraphic string, the spectral gamma-ray tool (the highest tool on the string) entered the pipe briefly. The low uranium and gamma-ray values for the interval from 82 to 87 mbsf (Fig. 27) are an artifact caused by this accidental through-pipe logging.

### Velocity, Resistivity, and Density

Velocity, resistivity, and density are strongly correlated throughout almost all of the logged interval at Hole 814A (Fig. 25). Because lithologic changes here are relatively minor and confined to variations in relative proportions of the geophysically similar minerals dolomite and calcite, log responses are controlled almost entirely by porosity.

The increases in velocity and density with depth (Fig. 25) generally follow a simple compaction profile, suggesting that mechanical compaction is dominant over diagenesis and grain-size fluctuations for controlling porosity at this site. This

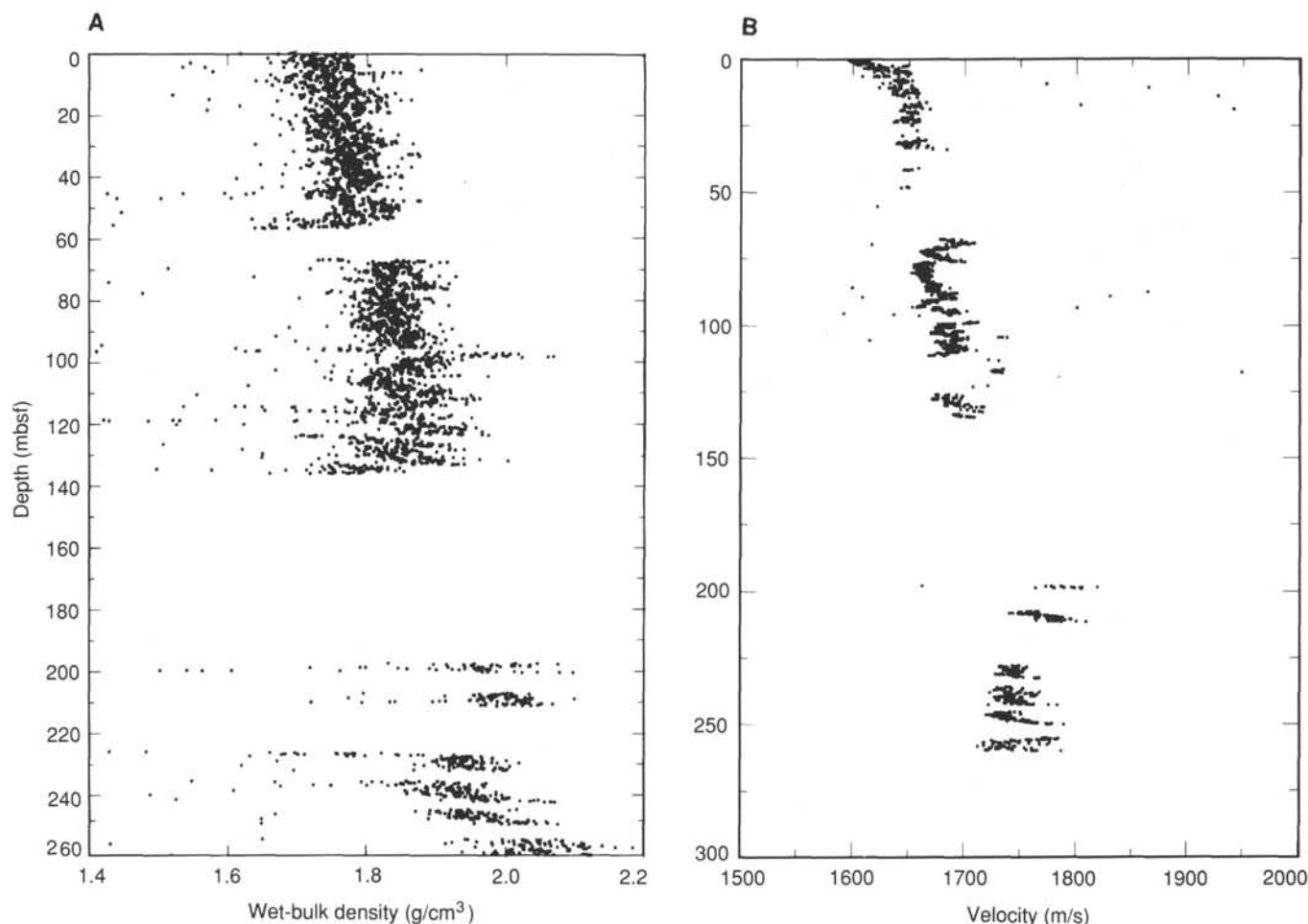


Figure 20. All data points displayed are averages of all data in 5-cm blocks along the core. **A.** Unfiltered GRAPE bulk density measurements for Hole 814A. Because of varying rate of motion of the core through the GRAPE system, multiple measurements often occur at the same position in the core. **B.** MST sonic velocity for whole-round cores from Site 814.

pattern is opposite that observed at Site 812, where diagenesis was an important control of velocity/depth and resistivity/depth patterns (see "Site 812" chapter, this volume). The velocity increase with depth is similar to that commonly observed in pelagic carbonates (Hamilton, 1979), but the expected corresponding density increase (Hamilton, 1976) is seen only above about 110 mbsf. The absence of any systematic increase in density log values below this depth may be an artifact attributable to poor pad contact.

The reprocessed sonic log was converted to an integrated traveltime log (Fig. 26) to facilitate depth-to-time conversion for comparing Site 814 data with seismic facies. For the unlogged interval between the seafloor and 57.5 mbsf, we used a simple linear interpolation between water velocity at the seafloor and the first log value at 57.5 mbsf. We subjectively estimate that an error of less than 5 ms is associated with any uncertainty in velocities of the top 57.5 mbsf. For the short interval from 277.5 to 294.3 mbsf at the bottom of the hole, resistivity logs (but not sonic logs) are available because the resistivity tool is much lower on the tool string. We did not generate a pseudosonic log from resistivity data for this interval as was done for the lowest interval at most logged sites (e.g., see "Site 812" chapter, this volume), because the relationship between resistivity and velocity is more complex in this portion of Site 814 than at Site 812.

Resistivity logs shown in Figure 25 indicate three distinct zones:

1. Above 134 mbsf, values are 0.6 to 1.0 ohm-m, with only slight variability.
2. Between 134 and 250 mbsf, values are 0.8 to 1.0 ohm-m, with only slight variability.
3. From 250 mbsf to the end of the logging run at 294 mbsf, resistivity varies rapidly, indicating alternating layers of high and low porosity.

Differences between the three resistivity log types are attributable to different responses of the three sondes. This effect is accentuated by a large hole diameter.

The general relative position of these three logs is similar to the situation at Hole 812B, where deep induction provided the highest resistivities and SFL the lowest, with a medium induction log providing intermediate values. The situation again suggests resistivity that increases with distance away from the borehole sondes as a result of the large diameter of the borehole. Thus, the deepest penetrating devices will provide the most reliable data where beds are thick, but all values probably have been degraded in the presence of thin beds. The situation at the top of Zone 2 illustrates this pattern by exhibiting a thin high-resistivity layer at 135 mbsf. This is

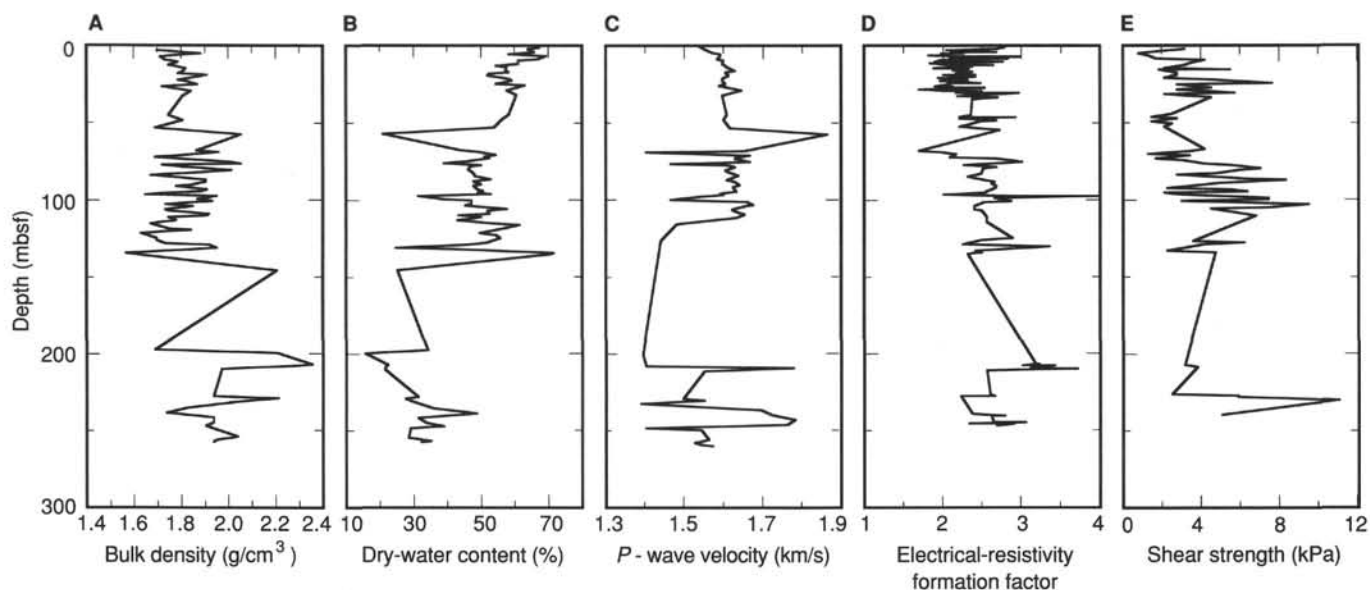


Figure 21. Physical properties data vs. depth, Site 814. **A.** Wet-bulk density derived from mass and volume measurements for discrete core samples (pycnometer). **B.** Dry-water content with water mass/dry sediment mass. Data were derived from mass measurements of discrete samples from cores before and after drying. **C.** *P*-wave velocity; data were derived from Hamilton Frame measurements of discrete samples from cores. Values of less than 1.5 km/s probably result from rapid draining of permeable sands. **D.** Electrical resistivity formation factor. **E.** Shear strength.

a single layer, unlike those at Hole 812B where many thin high-resistivity layers are interbedded with lower values. The FMS, which can delineate thin beds to a precision of 2 to 5 mm, indicates that this layer is 0.8 m thick. However, evidence from the velocity log and partial indications from the FMS record indicate that the subunit may extend down to 155 mbsf. If this is the case, we have an example of a lithologic unit that has widely varying physical properties, in this case, mainly cementation variations.

Further interpretation of the resistivity is shown in Figure 28, where the electrical-resistivity FF was plotted using the deep induction log and pore-water resistivities that decrease from 0.25 ohm-m (11.4°C) at the seafloor to 0.20 ohm-m (20°C) at 300 mbsf. The porosity values derived from the density log were used to calculate the component  $m$  in the Archie equation (1942) as follows:

$$FF = (\text{porosity})^{**}(-m), \quad (1)$$

which is probably the most applicable in the un lithified portion of the sediment column. The value of  $m$  is shown to be controlled by particle shape for unconsolidated marine sands and clays, while in turn the pore spaces are dependent on grain shape. Thus,  $m$  may be a useful indicator of changes in lithology, where such changes are accompanied by a change in grain morphology. Some of the density values were degraded by the large hole size, as this sonde required contact with the borehole wall for accurate measurements. The values of  $m$  tend to accentuate these situations, providing an indicator of exactly which portions of the density log are unreliable. Based on the log of  $m$ , a major change in pore/particle shape may have occurred at 211 mbsf, within the second resistivity zone identified above.

“Mirror” anomalies can be seen between the “porosity” and Archie  $m$  logs in Figure 28, which is caused by the large hole diameter’s degrading density measurements; a similar phenomenon was seen at Hole 812B (see “Site 812” chapter, this volume). These anomalies can be identified in Figure 28

using the additional log “Thin R,” which delineates thin resistive layers by taking a ratio of the shallow high-resolution SFL and the deeper-penetrating, but lower-resolution, induction log. This device is seen as insensitive to the degradation in porosity caused by hole enlargement.

Velocity and resistivity ratios were taken to display differences between these two porosity logs, which are usually assumed to move together (Fig. 29). Here, positive values will be formed when velocity is high and resistivity is low, as might be the case for a highly porous sediment in which grain contacts had been cemented; such a pattern may be present below 260 mbsf. Positive peaks can also be generated if velocity remains constant and resistivity declines, as might happen if the grains of an unconsolidated sediment became more rounded at a constant porosity. Only positive anomalies associated with increases in velocity have been highlighted in Figure 29.

### Log-Based Units

Lithologic Unit I (see “Lithostratigraphy” section, this chapter) was logged through pipe using the spectral gamma-ray tool. Pipe attenuation of about a factor of three, when combined with the already low proportions of uranium, potassium, and thorium, resulted in near-zero log responses for these three elements. However, a relatively high-potassium zone is evident at 38 to 43 mbsf, and a uranium-rich zone is evident at 35 to 38 mbsf (Fig. 27).

The Unit II/Unit III contact (at about 67 mbsf) is just barely in the open hole and can be detected on the velocity and resistivity logs (Fig. 25) as a downhole decrease in both properties, implying a porosity increase. A foraminiferal micritic limestone occupies approximately the lowest 10 m of Unit II (see “Lithostratigraphy” section, this chapter); its exact thickness is uncertain because its presence degraded core recovery, but logs suggest that it is at least 8 m thick and that it is only moderately more lithified than the underlying top of Unit III.

Log response to Unit III (67–136 mbsf) is consistent with a uniform high-porosity ooze. Thin low-porosity beds are evi-

Table 7. Index properties data from Site 814.

Core, section, interval (cm)	Depth (mbsf)	Bulk density (g/cm <sup>3</sup> )	Grain density (g/cm <sup>3</sup> )	Porosity (%)	Water content (%)	Void ratio
133-814A-						
1H-1, 80-83	0.80	1.71	2.71	67.3	67.8	2.05
1H-2, 80-83	2.30	1.70	2.55	65.1	64.5	1.86
1H-3, 80-83	3.80	1.88	2.70	73.0	66.3	2.70
1H-4, 80-83	5.30	1.77	2.77	64.0	58.8	1.77
2H-1, 70-73	6.60	1.71	2.78	68.5	69.5	2.18
2H-2, 70-73	8.10	1.73	2.72	67.9	67.1	2.11
2H-3, 70-73	9.60	1.79	2.68	66.4	61.4	1.98
2H-4, 70-73	11.10	1.75	2.67	64.8	61.3	1.84
2H-5, 70-73	12.60	1.78	2.87	61.4	54.8	1.59
2H-6, 71-74	14.11	1.82	2.66	65.2	58.1	1.88
2H-7, 71-74	15.61	1.81	2.82	64.6	57.5	1.83
3H-1, 100-103	16.40	1.79	2.62	64.5	58.4	1.82
3H-2, 100-103	17.90	1.91	2.62	64.7	53.0	1.83
3H-3, 100-104	19.40	1.87	2.56	62.9	52.4	1.70
3H-4, 100-104	20.90	1.79	2.76	64.7	58.7	1.83
3H-5, 100-104	22.40	1.82	2.63	66.3	59.7	1.97
3H-6, 100-104	23.90	1.87	2.69	64.6	54.6	1.82
4H-1, 96-100	25.86	1.72	2.60	65.2	63.4	1.87
4H-3, 96-100	28.86	1.84	2.59	65.9	57.9	1.93
4H-5, 96-100	31.86	1.81	2.65	66.8	60.9	2.01
6H-1, 96-100	44.86	1.75	2.68	63.0	58.6	1.70
6H-3, 96-100	47.86	1.81	2.63	64.0	56.7	1.78
6H-6, 96-100	52.36	1.69	2.62	58.2	54.4	1.39
8X-1, 57-60	57.37	2.05	2.75	35.0	21.2	0.54
9H-1, 81-84	67.31	1.86	2.66	56.2	44.9	1.28
9H-2, 74-77	68.74	1.96	2.64	63.1	49.2	1.71
9H-3, 101-104	70.51	1.81	2.66	62.7	54.9	1.68
9H-4, 56-59	71.56	1.69	2.58	56.0	51.4	1.27
9H-5, 63-66	73.13	1.77	2.59	59.8	52.8	1.49
9H-6, 101-104	75.01	2.00	2.80	61.5	46.1	1.60
9H-7, 43-46	75.93	2.05	2.65	56.7	39.5	1.31
10H-1, 101-104	77.01	1.72	2.52	56.4	50.6	1.29
10H-2, 101-104	78.51	1.81	2.54	56.7	47.3	1.31
10H-3, 81-84	79.81	2.01	2.71	62.4	46.6	1.66
10H-4, 81-84	81.31	1.90	2.47	60.1	47.8	1.51
10H-5, 101-104	83.01	1.67	2.88	53.2	48.5	1.14
10H-6, 101-104	84.51	1.75	2.52	55.7	48.6	1.26
11H-1, 101-104	86.51	1.90	2.69	64.5	53.4	1.82
11H-2, 101-104	88.01	1.90	2.67	60.2	48.2	1.52
11H-3, 101-104	89.51	1.84	2.52	60.2	50.5	1.51
11H-4, 101-104	91.01	1.78	2.45	56.4	48.2	1.29
11H-5, 101-104	92.51	1.91	2.76	61.5	49.3	1.60
11H-6, 101-104	94.01	1.88	2.51	61.8	51.0	1.62
11H-7, 51-54	95.01	1.76	2.60	56.7	49.3	1.31
12H-1, 101-104	96.01	1.65	2.52	55.8	53.3	1.26
12H-2, 101-104	97.51	1.95	2.75	45.9	31.7	0.85
12H-3, 101-104	99.01	1.87	2.58	51.6	39.4	1.07
12H-4, 101-104	100.51	1.93	2.52	60.5	47.4	1.53
12H-5, 101-104	102.01	1.73	2.48	54.3	47.4	1.19
12H-6, 101-104	103.51	1.85	2.74	56.8	45.9	1.31
13H-1, 76-79	105.26	1.73	2.66	61.9	58.0	1.62
13H-2, 101-104	107.01	1.75	2.59	58.9	52.6	1.44
13H-3, 101-104	108.51	1.92	2.52	65.0	52.9	1.86
13H-4, 101-103	110.01	1.90	2.68	56.5	43.8	1.30
13H-5, 71-74	111.21	1.75	2.46	57.3	50.7	1.34
13H-6, 101-103	113.01	1.78	2.44	52.4	43.1	1.10
14H-1, 101-103	115.01	1.67	2.49	57.5	54.4	1.36
14H-2, 101-103	116.51	1.70	2.80	63.7	62.1	1.75
14H-3, 101-103	118.01	1.75	2.41	62.6	57.8	1.67
14H-4, 101-103	119.51	1.84	2.48	63.5	54.7	1.74
14H-5, 101-103	121.01	1.63	2.60	52.9	50.0	1.12
14H-6, 101-103	122.51	1.66	2.65	57.3	54.7	1.34
15H-1, 101-103	124.51	1.70	2.51	59.7	56.3	1.48
15H-2, 61-64	125.61	1.70	2.48	58.9	54.8	1.43
15H-3, 101-103	127.51	1.73	2.54	57.8	52.0	1.37
15H-4, 101-103	129.01	1.92	2.73	59.7	46.7	1.48
15H-5, 101-103	130.51	1.95	2.58	38.3	25.3	0.62
15H-6, 101-103	132.01	1.82	2.45	52.9	42.3	1.13
16H-1, 101-103	134.01	1.57	2.52	63.9	71.7	1.77
16H-2, 101-103	135.51	1.61	2.80	65.0	70.9	1.86
18X-1, 5-7	145.75	2.20	2.70	43.6	25.5	0.77
23X-1, 90-94	198.00	1.69	2.56	42.9	35.0	0.75
23X-2, 90-94	199.50	2.20	2.50	29.6	16.0	0.42
24X-1, 20-24	207.00	2.35	2.80	42.9	23.0	0.75
24X-2, 20-24	208.50	2.29	2.52	41.1	22.5	0.70

Table 7 (continued).

Core, section, interval (cm)	Depth (mbsf)	Bulk density (g/cm <sup>3</sup> )	Grain density (g/cm <sup>3</sup> )	Porosity (%)	Water content (%)	Void ratio
24X-3, 20-24	210.00	1.97	2.64	34.2	21.7	0.52
26X-2, 80-84	228.00	1.94	2.50	45.8	32.0	0.85
26X-3, 80-84	229.50	2.21	2.77	47.1	27.9	0.89
26X-4, 80-84	231.00	2.05	2.63	46.9	30.7	0.89
27X-1, 70-74	236.00	1.83	2.87	47.2	36.0	0.89
27X-3, 70-74	239.00	1.74	2.64	55.8	49.0	1.26
27X-5, 70-74	242.00	1.94	2.60	45.9	32.0	0.85
28X-1, 70-73	245.30	1.94	2.68	48.2	34.1	0.93
28X-2, 70-73	246.80	1.90	2.62	52.7	39.6	1.12
28X-3, 70-73	248.30	1.92	2.49	43.0	29.7	0.75
29X-1, 70-73	254.90	2.04	2.73	44.8	29.1	0.81
29X-2, 70-73	256.40	1.95	2.87	50.0	32.7	1.00
29X-3, 70-73	257.90	1.94	2.68	46.5	32.7	0.87

dent on the resistivity, velocity, and FMS logs at 96 to 98 and 111 mbsf.

The Unit III/Unit IV contact (at 136 mbsf) was identified in the cores as the top of a possibly 15-m-thick dolomitized bioclastic packstone (see "Lithostratigraphy" section, this chapter). Resistivity and velocity logs show this bed, with a top at 135 mbsf, as the most cemented bed of the entire logged interval at Hole 814A. In these logs, the bed appears to have a layer of high resistivity and velocity of 1 m or less thick on its uppermost surface. The FMS imaging log confirmed this thin bed interpretation and showed it to be only 0.8 m thick (134.9-135.7 mbsf) and to have sharp upper and lower boundaries. The velocity log indicates an increase at 150 mbsf, which is consistent with an increase in cementation. These results support the findings (see "Lithostratigraphy" section, this chapter) of a more-lithified dolomitic packstone in the depth interval from 135 to 155 mbsf. Normally, this would be confirmed by the geochemical logs; however, they were not run because of a combination of operational constraints and because of poor hole conditions that were caused by the noncohesive sediments.

The underlying mudstones of Unit IV are consistently lower in porosity (i.e., higher in velocity and resistivity) than those of the overlying Unit III, with a baseline shift occurring at the dolomitized bed. In general, the mudstones of Unit IV (136-264 mbsf) are seen in logs as relatively uniform.

In contrast, the underlying Unit V has a markedly different log response. Variability is high, indicating many thin beds. Velocity is also high, but resistivity and density do not exhibit corresponding increases; this pattern implies increased rigidity and intergranular cementation without substantially higher porosity. Unit V is described as a dolomitized packstone (see "Lithostratigraphy" section, this chapter), and the increased, but presumably variable, diagenesis of this packstone is probably responsible for the interlog pattern. This type of high-porosity lithification is highlighted by the ratio plot in Figure 29 and is used as a means of easily identifying high-velocity, low-resistivity lithologies.

### Temperature

Heat flow was not measured at Site 814; thus, we do not know the thermal gradient at this site. The L-DGO temperature tool was run at the bottom of the seismic stratigraphic tool string. Because the hole temperatures had been reduced by circulation during coring and by hole conditioning immediately prior to logging, we were unable to infer an equilibrium thermal profile from a single temperature-logging run. Our recorded temperature of 19.5°C at 300 mbsf thus is a minimum estimate of equilibrium temperature.

Table 8. Compressional-wave velocity data from Site 814.

Core, section, interval (cm)	Depth (mbsf)	Direction	Distance (mm)	Traveltime ( $\mu$ s)	Velocity (m/s)
133-814A-					
1H-1, 8-8.3	0.08	a	28.29	20.87	1533
1H-2, 80-83	2.30	a	27.58	20.28	1545
1H-3, 80-83	3.80	a	27.48	20.00	1565
1H-4, 80-83	5.30	a	27.80	20.00	1584
2H-1, 70-73	6.60	a	27.63	19.87	1586
2H-2, 70-73	8.10	a	27.97	20.16	1579
2H-3, 70-73	9.60	a	26.44	19.05	1593
2H-4, 70-73	11.10	a	26.88	19.35	1590
2H-5, 70-73	12.60	a	28.11	20.04	1599
2H-6, 71-74	14.11	a	25.57	18.41	1602
2H-7, 71-74	15.61	a	27.85	19.65	1621
3H-1, 105-108	16.45	a	26.97	19.35	1596
3H-2, 100-104	17.90	a	29.70	20.99	1604
3H-3, 100-104	19.40	a	29.95	21.12	1606
3H-4, 100-104	20.90	a	28.45	20.35	1590
3H-5, 100-104	22.40	a	29.15	20.78	1591
3H-6, 100-104	23.90	a	29.15	20.69	1599
4H-1, 96-100	25.86	a	26.44	19.16	1581
4H-5, 96-100	31.86	a	28.46	20.38	1588
4H-3, 96-100	28.86	a	29.15	20.26	1640
6H-1, 96-100	44.86	a	26.11	18.76	1601
6H-3, 96-100	47.86	a	28.15	20.14	1592
6H-6, 96-100	52.36	a	28.76	20.31	1612
8X-1, 23-26	57.03	c	27.19	7.95	5075
8X-1, 23-26	57.03	a	38.32	12.86	3793
8X-1, 76-79	57.56	a	30.33	18.94	1854
8X-1, 76-79	57.56	c	25.23	16.71	1778
9H-1, 81-84	67.31	a	25.88	18.20	1645
9H-2, 74-77	68.74	a	25.49	20.56	1397
9H-3, 101-104	70.51	a	26.71	18.57	1660
9H-4, 56-59	71.56	a	25.71	18.27	1626
9H-5, 63-66	73.13	a	26.62	18.87	1623
9H-6, 101-104	75.01	a	26.49	18.44	1660
9H-7, 43-46	75.93	a	26.84	20.76	1459
10H-1, 101-104	77.01	a	25.23	18.19	1603
10H-2, 101-104	78.51	a	27.94	19.69	1623
10H-3, 81-84	79.81	a	27.19	19.46	1599
10H-4, 81-84	81.31	a	26.52	18.97	1606
10H-5, 101-104	83.01	a	25.66	18.21	1629
10H-6, 101-104	84.51	a	25.88	18.42	1622
11H-1, 101-104	86.51	a	27.10	19.39	1600
11H-2, 101-104	88.01	a	27.50	19.42	1622
11H-3, 101-104	89.51	a	27.46	19.27	1635
11H-4, 101-104	91.01	a	27.41	19.40	1619
11H-5, 101-104	92.51	a	26.58	18.83	1624
11H-6, 101-104	94.01	a	26.93	19.03	1626
11H-7, 51-54	95.01	a	25.23	18.37	1584
12H-1, 101-104	96.01	a	26.49	19.08	1593
12H-2, 101-104	97.51	a	27.41	20.30	1533
12H-3, 101-104	99.01	a	28.24	21.72	1459
12H-4, 101-104	100.51	a	28.66	19.85	1651
12H-5, 101-104	102.01	a	28.50	19.60	1666
12H-6, 101-104	103.51	a	29.68	20.53	1645
13H-1, 76-79	105.26	a	27.88	19.75	1613
13H-2, 101-104	107.01	a	28.93	20.31	1622
13H-3, 101-104	108.51	a	28.15	19.60	1645
13H-5, 71-74	111.21	a	27.81	19.59	1625
14H-1, 101-104	115.01	a	28.98	22.02	1475
15H-2, 97-100	125.97	a	28.58	22.26	1435
23X-2, 90-94	199.50	a	28.41	22.75	1389
24X-1, 20-24	207.00	a	28.54	22.74	1397
24X-2, 20-24	208.50	a	29.07	18.97	1770
24X-3, 20-24	210.00	a	30.55	22.21	1545
26X-2, 80-84	228.00	a	30.33	22.74	1491
26X-3, 80-84	229.50	a	30.03	21.89	1543
26X-4, 80-84	231.00	a	29.72	23.74	1386
27X-1, 70-74	236.00	a	29.76	20.15	1687
27X-3, 70-74	239.00	a	30.23	20.16	1715
27X-5, 70-74	242.00	a	30.11	19.54	1772
28X-1, 70-73	245.30	a	28.88	19.00	1754
28X-2, 70-73	246.80	a	28.24	22.53	1396
28X-3, 70-73	248.30	a	29.37	21.54	1536
29X-1, 50-53	254.70	a	29.76	21.56	1556
29X-2, 50-53	256.20	a	29.02	21.50	1520
29X-3, 50-53	257.70	a	28.36	20.88	1536
29X-4, 50-53	259.20	a	28.88	20.89	1565

The temperature tool was run to determine whether fluid flow was present. In Figure 30, a plot of measured temperature as a function of pressure was recorded simultaneously by the tool. Depths shown are approximate and may be revised by up to 5 m during post-cruise merging of the Schlumberger time/depth data with the temperature-tool time/pressure data.

The temperature pattern in Figure 30 is approximately linear between the bottom of the hole and the interval at 0 to 25 mbsf, but then declines rapidly to bottom-water temperatures of 10° to 12°C. Between the conclusion of the first run (evident as the path reversal at 62 bars and 18.4°C in Fig. 30) and the start of the second run, mud was circulated for about 30 min with the pipe at 88 mbsf. However, this circulation seems to have had almost no effect on the thermal gradient.

One possible explanation for these observations is that water flows up out of the lowest penetrated portion of the formation. Such a flow should be fast enough to erase any effect of shallow pumping between runs, but not fast enough to create a constant-temperature profile with depth. One presumes that most of the outflow would be to the seafloor, but we also noted some backflow through the pipe. An alternative explanation is that there is no fluid flow effect on borehole temperatures. Instead, annual variations in bottom-water temperatures might be so large that these formation fluids are not in thermal equilibrium with the current bottom-water temperature.

### SEISMIC STRATIGRAPHY

Site 814 was located approximately 0.07 nmi southwest of its proposed position. Thus, the lithologic and seismic ties are not as good as hoped. However, they are good enough to allow one to make a reasonable comparison between seismic and drilling data.

Outlined below is a seismic stratigraphic interpretation of Site 814 that compares stratigraphic and sedimentological data. The time-vs.-depth velocity plot shown in Figure 5 was calculated during the cruise to compare seismic data with drilling results and to predict lithologies ahead of drilling.

An interpretation of seismic stratigraphy at Site 814 is shown in Figure 31. These data form part of the site-survey data set generated by BMR before Leg 133. Figure 31 also connects Sites 813 and 814 and is used for both site descriptions.

At Site 814, five seismic sequences were recognized between the seafloor and the bottom of the hole (300 mbsf). As most of these also were recognized at Site 813, the same reflector numbers have been used (Fig. 31).

Sequence 1 occurs between the seafloor and reflector 1, which is overlapped by reflectors within sequence 1. It is essentially transparent with few prominent reflectors and equates to lithologic Unit I, which has been defined as a nannofossil foraminifer ooze of Pleistocene age. At Sites 814 and 813, the base of this unit was dated at around 2.5 Ma. This sequence was deposited in a bathyal environment.

Sequence 2 can be seen between reflectors 2 and 3 and is thinner than its corresponding thickness at Site 813. This sequence equates with the basal part of Unit I, defined as foraminifer bioclastic packstones. The hardground drilled between 55 and 66 mbsf probably forms the base of sequence 2 and is responsible for the prominence of reflector 2. This reflector was dated at Sites 813 and 814 as near 3.4 Ma. The lower Pliocene and upper Miocene sections (sequences 3 and 4 in Site 813) either were not condensed or have been eroded.

Sequence 5 lies between the merged reflectors R2/3/4 and reflector 5. This sequence appears as an aggrading unit with onlap on reflector 5 to the east. At Site 814, the sequence below the composite reflector 2/3/4 is dated as middle Mi-

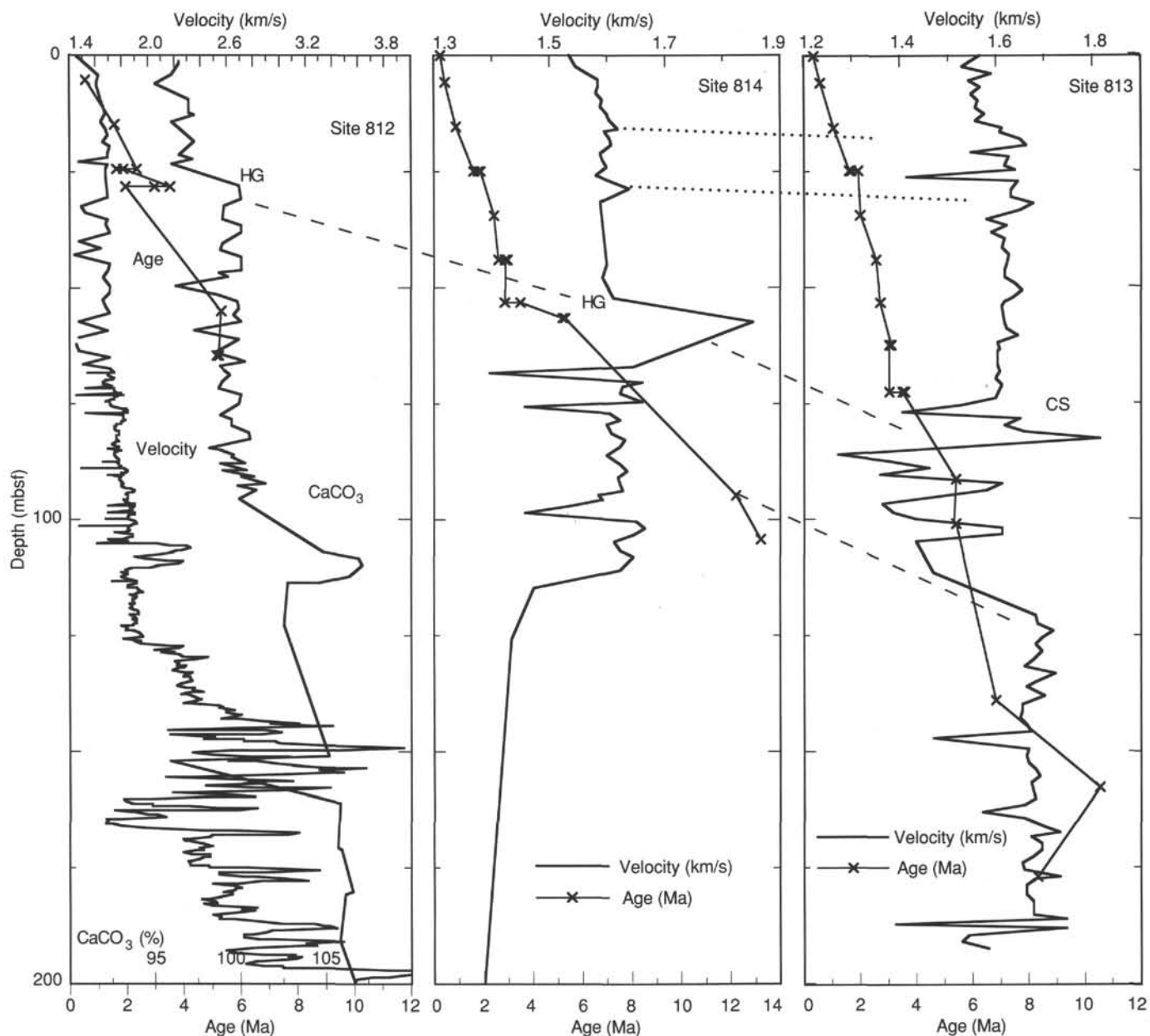


Figure 22. Comparison of velocity vs. depth curves for Sites 812, 813, and 814. Overlain on the plots are age-vs.-depth curves derived from paleontological dating of core-catcher samples. Depths for age plotted here are depths to upper boundary for estimated depth of sample. For Site 812, we also plotted  $\text{CaCO}_3$  content. Note that weight percentage of  $\text{CaCO}_3$  increases downward parallel with increase in acoustic velocity. At Sites 812 and 814, hardgrounds found at about 26 and 55 m, respectively, are denoted by HG. A possible time-correlative condensed section encountered at Site 813 is denoted as CS. Dashed line emphasizes correlation between hardgrounds and condensed section, which correspond approximately to velocity peaks at Sites 813 and 814 and a step in the velocity function at Site 812. Dotted lines connecting points along velocity profiles for Sites 813 and 814 suggest points of similar character in velocity curves. These may indicate horizons of similar acoustic velocity that can be traced from Sites 813 to 814.

ocene, as at Site 813. Thus, sequence 5 correlates with Unit II, which is 65 m thick and shows an upward-finishing, energy-related sequence from shallow-water bioclastic packstones at its base to bathyal micritic ooze at its top. Paleontologic dates within the sequence indicate that it is 12.2 to 13.2 Ma old in the middle of the sequence.

Sequence 6 occurs between reflectors 5 and 6. These boundaries have been delineated to correspond with Unit III. However, sequence 6 is a mega-sequence comprising at least four sequences. These are defined as follows:

1. Sequence 6-1 forms the lower half of sequence 6 and is made up of reflectors that are discontinuous. It is approximately 62 ms thick at the drill site, but expands to 100 ms farther west. At the base, reflector 6 is onlapped, and thus sequence 6-1 has been interpreted as a transgressive and high-sea-level sequence. The onlap barely reaches Site 814, but may be defined at the drill site by coarse lithified sands and rudstones at the base of Unit III. These thus would represent the transgressive deposits. The upper surface of sequence 6-1 has been eroded.

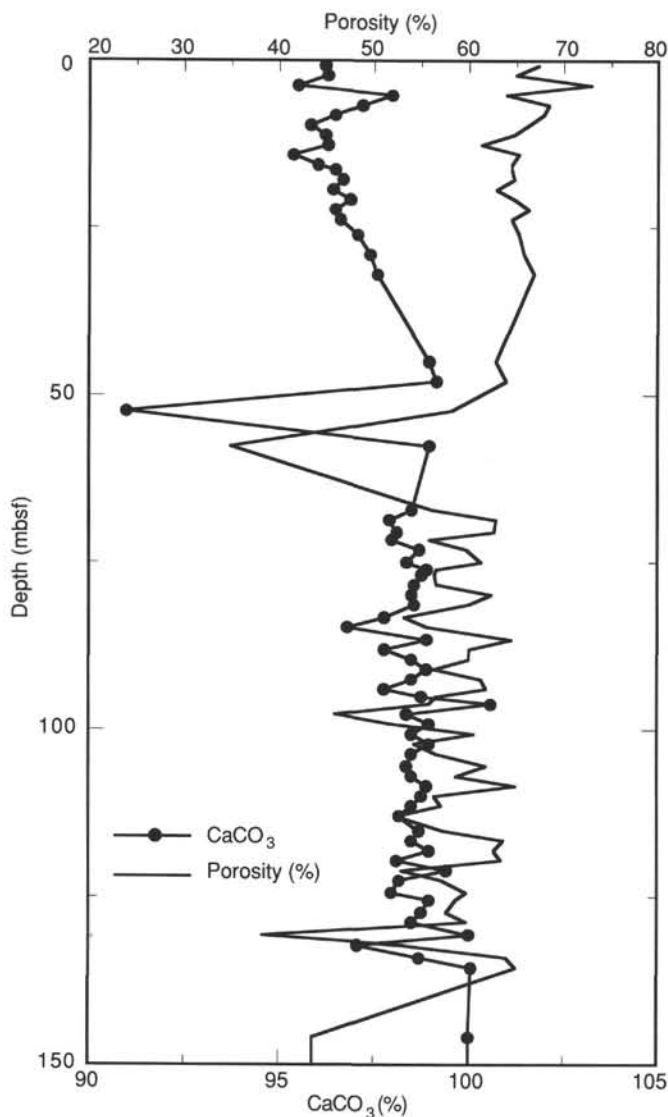


Figure 23. Porosity and weight percent  $\text{CaCO}_3$  vs. depth at Site 814. Note general tendency for porosity to decrease as carbonate increases in abundance. However, a one-to-one inverse correlation does not occur.

2. Sequence 6-2 is a bedded unit, which to the west of the drill site includes a small build-up. It is 25 ms thick at the drill site, but is 30 ms thick at the build-up to the west. The upper surface has been eroded.

3. Sequence 6-3 is a thin-bedded unit, 12 ms thick at the drillsite but 25 ms thick farther west, where onlap can be seen within. Its upper surface has been eroded.

4. Sequence 6-4 is approximately 25 ms thick at the drill site, but expands westward to approximately 40 ms. Reflectors indicate that the upper part of the sequence may be prograding.

5. Sequences 6-2 and 6-3 correlate with the calcareous ooze and mudstones that make up most of lithologic Subunit IIIB.

6. Sequence 6-4 correlates with Subunit IIIA, which is composed of dolomitized, highly porous, lithified bioclastic packstones. The unit also contains coralline algal fragments and is almost certainly shallow water in origin.

7. Sequence 7 occurs below 910 ms at the drill site and is characterized by strong, but discontinuous reflectors. It correlates with Unit IV, which is composed of dolomitized lithified packstones and thought to have a shallow water origin. That reflector 6 is an unconformity is corroborated by the interpretation of exposure and subaerial diagenesis in the dolomitized packstones that comprise sequence 7. The age of this unconformity is unknown, but it may represent any lowstand of sea level between 20 and 15 Ma. The dates of 13.2 to 17.1 Ma in Unit III suggest that it may represent a major lowstand at 20 Ma.

#### REFERENCES

- Andrews, J. E., 1973. Correlation of seismic reflectors. In Burns, R. E., Andrews, J. E., et al., *Init. Repts. DSDP*, 21: Washington (U.S. Govt. Printing Office), 459-479.
- Archie, G. E., 1942. The electrical resistivity log as an aid in determining some reservoir characteristics. *J. Pet. Tech.*, 5:1-8.
- Davies, P. J., Symonds, P. A., Feary, D. A., and Pigram, C. J., 1989. The evolution of the carbonate platforms of northeast Australia. *Soc. Econ. Palentol. Mineral. Spec. Publ.*, 44:233-258.
- Falvey, D. A., and Mutter, J. C., 1981. Regional plate tectonics and the evolution of Australia's passive continental margins. *BMR J. Aust. Geol. Geophys.*, 6:1-29.
- Feary, D. A., Pigram, C. J., Davies, P. J., Symonds, P. A., Droxler, A. W., and Peerdeman, F., 1990. Ocean Drilling Program—Leg 133 safety package. *Bur. Miner. Res. Aust. Rec.*, 1990/6.
- Hamilton, E. L., 1976. Variations in density and porosity with depth in deep-sea sediments. *J. Sediment. Petrol.*, 46:280-300.
- , 1979. Sound velocity gradients in marine sediments. *J. Acoust. Soc. Am.*, 65:909-922.
- Mullins, H. T., Heath, K. C., Van Buren, M., and Newton K., 1984. Anatomy of a modern open-oceanic carbonate slope: northern Little Bahama Bank. *Sedimentology*, 31:141-168.
- Simms, M., 1984. Dolomitization by groundwater systems in carbonate platforms. *Trans. Gulf Coast Assoc. Geol. Soc.*, 34:411-420.
- Swart, P. K., and Burns, S. J., 1990. Pore-water chemistry and carbonate diagenesis in sediments from Leg 115: Indian Ocean. In Duncan, R. A., Backman, J., Peterson, L. C., et al., *Proc. ODP, Sci. Results*, 115: College Station, TX (Ocean Drilling Program), 629-645.
- Swart, P. K., and Guzikowski, M., 1988. Interstitial-water chemistry and diagenesis of periplatform sediments from the Bahamas, ODP Leg 101. In Austin, J. A., Jr., Schlager, W., et al., *Proc. ODP, Sci. Results*, 101: College Station, TX (Ocean Drilling Program), 363-380.
- Symonds, P. A., Fritsch, J., and Scluter, J. U., 1984. Continental margin around the the western Coral Sea Basin: structural elements, seismic sequences and petroleum geological aspects. In Watson, S. T. (Ed.), *Trans. 3rd Circ. Pac. Energ. Min. Res. Conf.*, Hawaii, AAPG, 143-152.
- van Morkhoven, F.P.C.M., Berggren, W. A., and Edwards, A. S., et al., 1986. Cenozoic cosmopolitan deep-water benthic foraminifera. *Bull. Cent. Rech. Explor.-Prod. Elf-Aquitaine*, Mem. 11.

Ms 133-107

**NOTE:** All core description forms ("barrel sheets") and core photographs have been printed on coated paper and bound separately as Part 2 of this volume, beginning on page 813.

Formation microscanner images for this site are presented on microfiche in the back of Part 2.

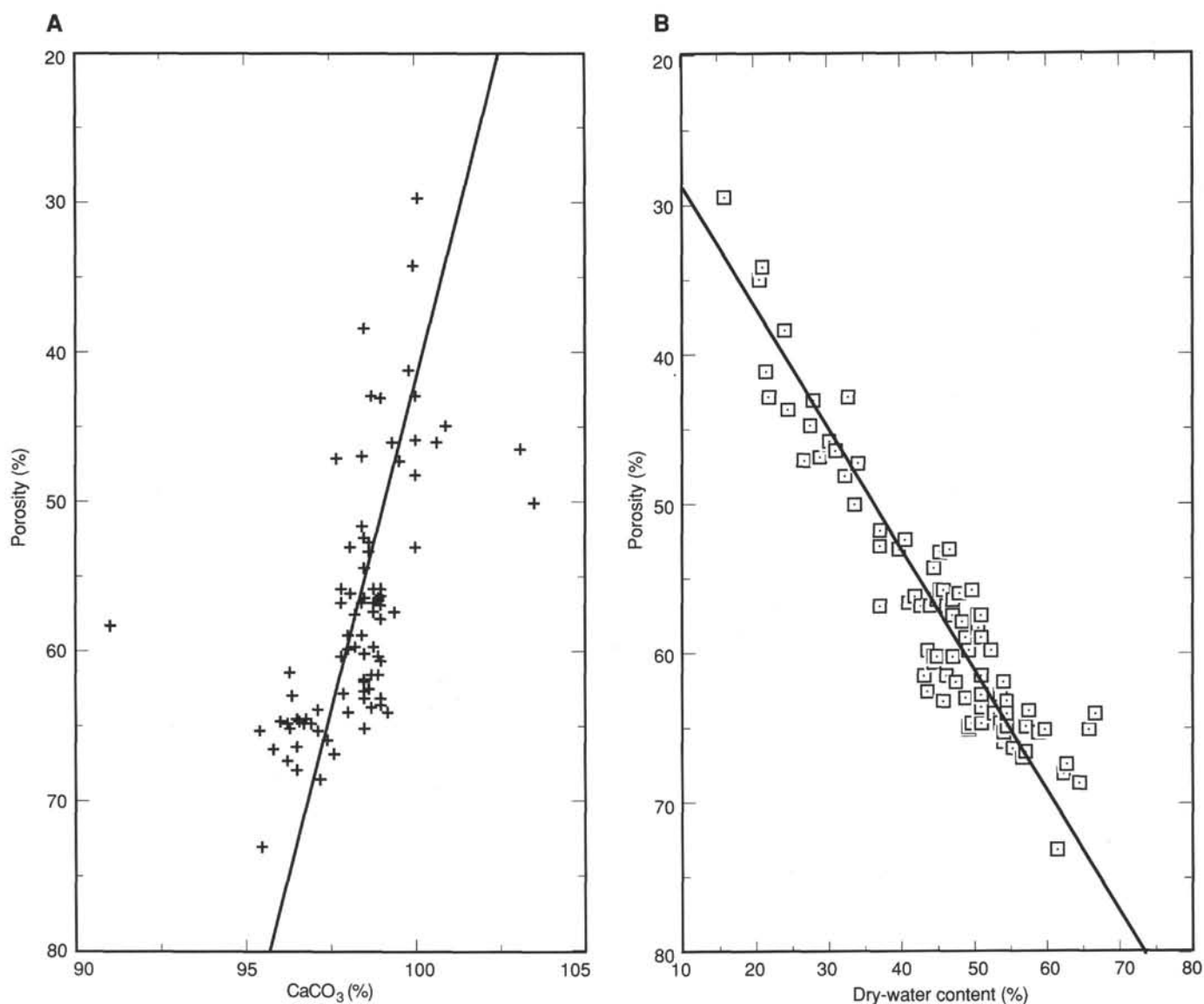


Figure 24. **A.** Porosity vs. wt% carbonate at Site 814. Porosity tends to decrease as carbonate content of sediments increases. Carbonate values in excess of 100% are an artifact of neglecting magnesium when calculating  $\text{CaCO}_3$  content. The best least-squares linear fit to the data is  $Y = 104.74 - 0.11303 X$ , where  $Y = \text{CaCO}_3$  content,  $X = \text{porosity}$ , and regression coefficient  $R = 0.583$ . **B.** Dry-water content vs. porosity at Site 814. Data were derived from mass and pycnometer volume measurements for discrete samples from cores. A least-squares linear regression was calculated for dry-water content as a function of porosity. This yielded dry-water content = 1.3506; porosity = 28.7, with regression coefficient = 0.877. The tighter clustering of values compared to Figure 22 indicates greater precision in measurement of wet-bulk volume compared to Site 812. This increase in precision is attributed, at least in part, to our measuring sample volumes soon after removing them from the core.

**Table 9. Electrical-resistivity formation factor data from Hole 814A.**

Core, section, interval (cm)	Depth (mbsf)	Seawater (ohms)	Sample (ohms)	Formation factor
133-814A-				
1H-1, 20-20	0.20	3.3	9.2	2.79
1H-1, 70-70	0.70	3.3	8.9	2.70
1H-1, 120-120	1.20	3.3	8.7	2.64
1H-2, 20-20	1.70	3.6	7.4	2.06
1H-2, 70-70	2.20	3.5	7.8	2.23
1H-2, 120-120	2.70	3.5	9.4	2.69
1H-3, 20-20	3.20	3.4	7.2	2.12
1H-3, 70-70	3.70	3.5	8.0	2.29
1H-3, 120-120	4.20	3.5	7.0	2.00
1H-4, 20-20	4.70	3.6	7.7	2.14
1H-4, 70-70	5.20	3.6	7.1	1.97
1H-4, 116-116	5.66	3.7	6.8	1.84
2H-1, 20-20	6.10	3.5	7.9	2.26
2H-1, 70-70	6.60	3.1	9.3	3.00
2H-1, 120-120	7.10	3.1	6.5	2.10
2H-2, 20-20	7.60	3.2	9.1	2.84
2H-2, 70-70	8.10	3.3	7.1	2.15
2H-2, 120-120	8.60	3.4	6.9	2.03
2H-3, 20-20	9.10	3.5	6.7	1.91
2H-3, 70-70	9.60	3.5	9.7	2.77
2H-3, 120-120	10.10	3.5	6.9	1.97
2H-4, 20-20	10.60	3.6	6.7	1.86
2H-4, 70-70	11.10	3.7	7.8	2.11
2H-4, 120-120	11.60	3.4	9.0	2.65
2H-5, 20-20	12.10	3.6	7.9	2.19
2H-5, 70-70	12.60	3.7	8.7	2.35
2H-5, 120-120	13.10	3.6	8.6	2.39
2H-6, 20-20	13.60	3.7	7.0	1.89
2H-6, 70-70	14.10	3.8	8.9	2.34
2H-6, 120-120	14.60	3.6	7.7	2.14
3H-1, 20-20	15.60	3.3	7.8	2.36
3H-1, 70-70	16.10	3.2	7.6	2.38
3H-1, 120-120	16.60	3.3	7.3	2.21
3H-2, 20-20	17.10	3.3	7.2	2.18
3H-2, 70-70	17.60	3.5	8.5	2.43
3H-2, 120-120	18.10	3.6	7.3	2.03
3H-3, 20-20	18.60	3.7	8.7	2.35
3H-3, 70-70	19.10	3.6	8.7	2.42
3H-3, 120-120	19.60	3.5	7.4	2.11
3H-4, 20-20	20.10	3.8	7.4	1.95
3H-4, 70-70	20.60	3.6	8.4	2.33
3H-4, 120-120	21.10	3.4	7.5	2.21
3H-5, 20-20	21.60	3.4	7.4	2.18
3H-5, 70-70	22.10	3.7	7.3	1.97
3H-5, 120-120	22.60	3.6	7.4	2.06
3H-6, 20-20	23.10	3.3	8.2	2.48
3H-6, 70-70	23.60	3.6	7.5	2.08
3H-6, 120-120	24.10	3.7	7.8	2.11
4H-1, 20-20	25.10	3.7	7.1	1.92
4H-1, 70-70	25.60	3.5	7.5	2.14
4H-1, 120-120	26.10	3.7	7.4	2.00
4H-2, 20-20	26.60	3.3	8.4	2.55
4H-2, 70-70	27.10	3.9	6.7	1.72
4H-2, 120-120	27.60	3.9	7.2	1.85
4H-3, 20-20	28.10	3.6	7.3	2.03
4H-3, 70-70	28.60	3.4	8.5	2.50
4H-3, 120-120	29.10	3.7	8.1	2.19
4H-4, 20-20	29.60	3.5	8.0	2.29
4H-4, 70-70	30.10	3.5	10.4	2.97
4H-4, 120-120	30.60	3.2	8.6	2.69
4H-5, 20-20	31.10	3.2	7.3	2.28
4H-5, 70-70	31.60	3.2	8.3	2.59
4H-5, 120-120	32.10	3.4	7.5	2.21
4H-6, 20-20	32.60	3.4	9.2	2.71
4H-6, 70-70	33.10	3.4	9.2	2.71
4H-6, 120-120	33.60	3.3	7.9	2.39
6H-1, 70-70	44.60	3.5	8.3	2.37

**Table 9 (continued).**

Core, section, interval (cm)	Depth (mbsf)	Seawater (ohms)	Sample (ohms)	Formation factor
6H-1, 120-120	45.10	3.5	7.8	2.23
6H-2, 20-20	45.60	3.5	10.3	2.94
6H-2, 70-70	46.10	3.5	7.8	2.23
6H-3, 70-70	47.60	3.6	9.7	2.69
6H-4, 70-70	49.10	3.7	9.1	2.46
6H-5, 70-70	50.60	3.7	8.6	2.32
6H-6, 70-70	52.10	3.6	8.0	2.22
7H-1, 50-50	53.90	3.7	10.1	2.73
9H-1, 100-100	67.50	4.1	7.0	1.71
9H-2, 60-60	68.60	4.2	8.3	1.98
9H-3, 70-70	70.20	4.0	8.7	2.18
9H-4, 70-70	71.70	4.1	8.6	2.10
9H-5, 60-60	73.10	3.1	8.4	2.71
9H-6, 60-60	74.60	3.1	9.4	3.03
10H-1, 60-60	76.60	3.6	8.2	2.28
10H-2, 60-60	78.10	3.0	8.1	2.70
10H-3, 70-70	79.70	3.0	7.6	2.53
10H-4, 70-70	81.20	3.0	7.5	2.50
10H-5, 70-70	82.70	3.0	7.5	2.50
10H-6, 70-70	84.20	3.0	7.0	2.33
11H-1, 70-70	86.20	3.0	7.6	2.53
11H-2, 70-70	87.70	3.0	8.0	2.67
11H-3, 70-70	89.20	3.0	7.9	2.63
11H-4, 70-70	90.70	3.0	8.1	2.70
11H-5, 70-70	92.20	3.0	8.0	2.67
11H-6, 70-70	93.70	3.1	8.0	2.58
11H-7, 30-30	94.80	3.1	7.9	2.55
12H-1, 70-70	95.70	3.0	6.1	2.03
12H-2, 30-30	96.80	3.0	8.6	2.87
12H-2, 80-80	97.30	3.0	8.1	2.70
12H-2, 110-110	97.60	3.0	11.9	3.97
12H-3, 70-70	98.70	3.0	8.0	2.67
12H-4, 70-70	100.20	3.0	8.6	2.87
12H-5, 70-70	101.70	3.0	7.6	2.53
12H-6, 70-70	103.20	3.0	7.2	2.40
13H-1, 70-70	105.20	3.0	7.2	2.40
13H-2, 70-70	106.70	3.0	7.5	2.50
13H-5, 70-70	111.20	3.0	7.7	2.57
14H-1, 46-46	114.46	3.0	7.7	2.57
15H-1, 72-72	124.22	3.0	8.7	2.90
15H-2, 60-60	125.60	3.0	7.5	2.50
15H-4, 50-50	128.50	3.0	6.8	2.27
15H-5, 85-85	130.35	3.0	10.1	3.37
16H-1, 25-25	133.25	3.0	7.3	2.43
16H-1, 70-70	133.70	3.0	7.5	2.50
16H-1, 110-110	134.10	3.0	7.3	2.43
16H-2, 20-20	134.70	3.0	7.0	2.33
16H-2, 80-80	135.30	3.0	7.0	2.33
24X-1, 20-20	207.00	3.3	10.5	3.18
24X-1, 70-70	207.50	3.1	10.0	3.23
24X-1, 120-120	208.00	3.3	10.0	3.03
24X-2, 20-20	208.50	3.5	12.0	3.43
24X-2, 70-70	209.00	3.2	10.5	3.28
24X-2, 120-120	209.50	3.2	10.0	3.13
24X-3, 20-20	210.00	3.4	10.6	3.12
24X-3, 70-70	210.50	3.5	13.0	3.71
24X-3, 115-115	210.95	3.5	9.0	2.57
26X-2, 20-20	227.40	3.3	8.6	2.61
26X-2, 70-70	227.90	3.3	8.8	2.67
26X-2, 120-120	228.40	3.3	7.4	2.24
27X-4, 20-20	240.00	3.4	8.1	2.38
27X-4, 70-70	240.50	3.3	9.2	2.79
27X-4, 120-120	241.00	3.2	8.4	2.63
28X-1, 20-20	244.80	3.4	9.0	2.65
28X-1, 70-70	245.30	3.3	10.1	3.06
28X-1, 120-120	245.80	3.4	8.0	2.35
28X-2, 20-20	246.30	3.3	9.6	2.91
28X-2, 70-70	246.80	3.3	9.0	2.73
28X-2, 120-120	247.30	3.3	8.9	2.70

Table 10. Vane shear strength data from Hole 814A.

Core, section, interval (cm)	Depth (mbst)	Torque (degrees)	Strain (degrees)	Shear strength (kPa)
133-814A-				
1H-1, 9-9.1	0.09	16	24	3.4
1H-2, 90-91	2.40	15	15	3.2
1H-3, 90-91	3.90	6	10	1.3
1H-4, 90-91	5.40	4	2	0.8
2H-1, 90-91	6.80	6	4	1.3
2H-2, 90-91	8.30	8	6	1.7
2H-3, 90-91	9.80	20	16	4.2
2H-4, 90-91	11.30	16	14	3.4
2H-5, 91-92	12.81	15	6	3.2
2H-6, 91-92	14.31	10	6	2.1
2H-7, 66-67	15.56	26	15	5.5
3H-1, 92-93	16.32	9	18	1.9
3H-2, 91-92	17.81	13	14	2.8
3H-3, 89-90	19.29	13	11	2.8
3H-4, 91-92	20.81	10	6	2.1
3H-5, 91-92	22.31	22	15	4.7
3H-6, 91-92	23.81	36	18	7.6
4H-1, 92-93	25.82	13	13	2.8
4H-2, 91-92	27.31	21	16	4.5
4H-3, 91-92	28.81	13	7	2.8
4H-4, 91-92	30.31	27	13	5.7
4H-5, 91-92	31.81	10	12	2.1
4H-6, 91-92	33.31	21	16	4.5
6H-1, 91-92	44.81	12	13	2.5
6H-2, 91-92	46.31	7	3	1.5
6H-3, 84-85	47.74	13	6	2.8
6H-4, 84-85	49.24	7	4	1.5
6H-5, 84-85	50.74	12	13	2.5
6H-6, 91-92	52.31	10	6	2.1
9H-1, 93-94	67.43	20	15	4.2
9H-2, 82-83	68.82	17	13	3.6
9H-3, 92-93	70.42	6	3	1.3
9H-4, 72-73	71.72	16	9	3.4
9H-5, 92-93	73.42	8	3	1.7
9H-6, 92-93	74.92	15	15	3.2
10H-1, 86-87	76.86	20	16	4.2
10H-2, 86-87	78.36	26	15	5.5
10H-3, 94-95	79.94	33	18	7.0
10H-4, 94-95	81.44	28	18	5.9
10H-5, 94-95	82.94	22	14	4.7
10H-6, 94-95	84.44	13	14	2.8
11H-1, 94-95	86.44	29	16	6.2
11H-2, 94-95	87.94	39	16	8.3
11H-3, 94-95	89.44	23	16	4.9
11H-4, 94-95	90.94	19	16	4.0
11H-5, 94-95	92.44	11	15	2.3
11H-6, 94-95	93.94	26	17	5.5
11H-7, 44-45	94.94	30	18	6.4
12H-1, 94-95	95.94	10	8	2.1
12H-2, 90-91	97.40	14	10	3.0
12H-3, 93-94	98.93	35	22	7.4
12H-4, 93-94	100.43	35	18	7.4
12H-5, 93-94	101.93	14	15	3.0
12H-6, 93-94	103.43	45	19	9.5
13H-1, 93-94	105.43	35	15	7.4
13H-2, 93-94	106.93	21	13	4.5
13H-5, 93-94	111.43	32	14	6.8
15H-2, 93-94	125.93	102	46	21.6
15H-3, 90-91	127.40	17	20	3.6
15H-4, 73-74	128.73	29	25	6.2
15H-5, 91-92	130.41	20	17	4.2
16H-1, 91-92	133.91	11	18	2.3
16H-2, 90-91	135.40	22	14	4.7
24X-2, 91-92	209.21	15	11	3.2
24X-3, 91-92	210.71	18	11	3.8
26X-2, 91-92	228.11	12	11	2.5
26X-3, 91-92	229.61	28	21	5.9
26X-4, 91-92	231.11	52	23	11.0
27X-4, 91-92	240.71	24	6	5.1

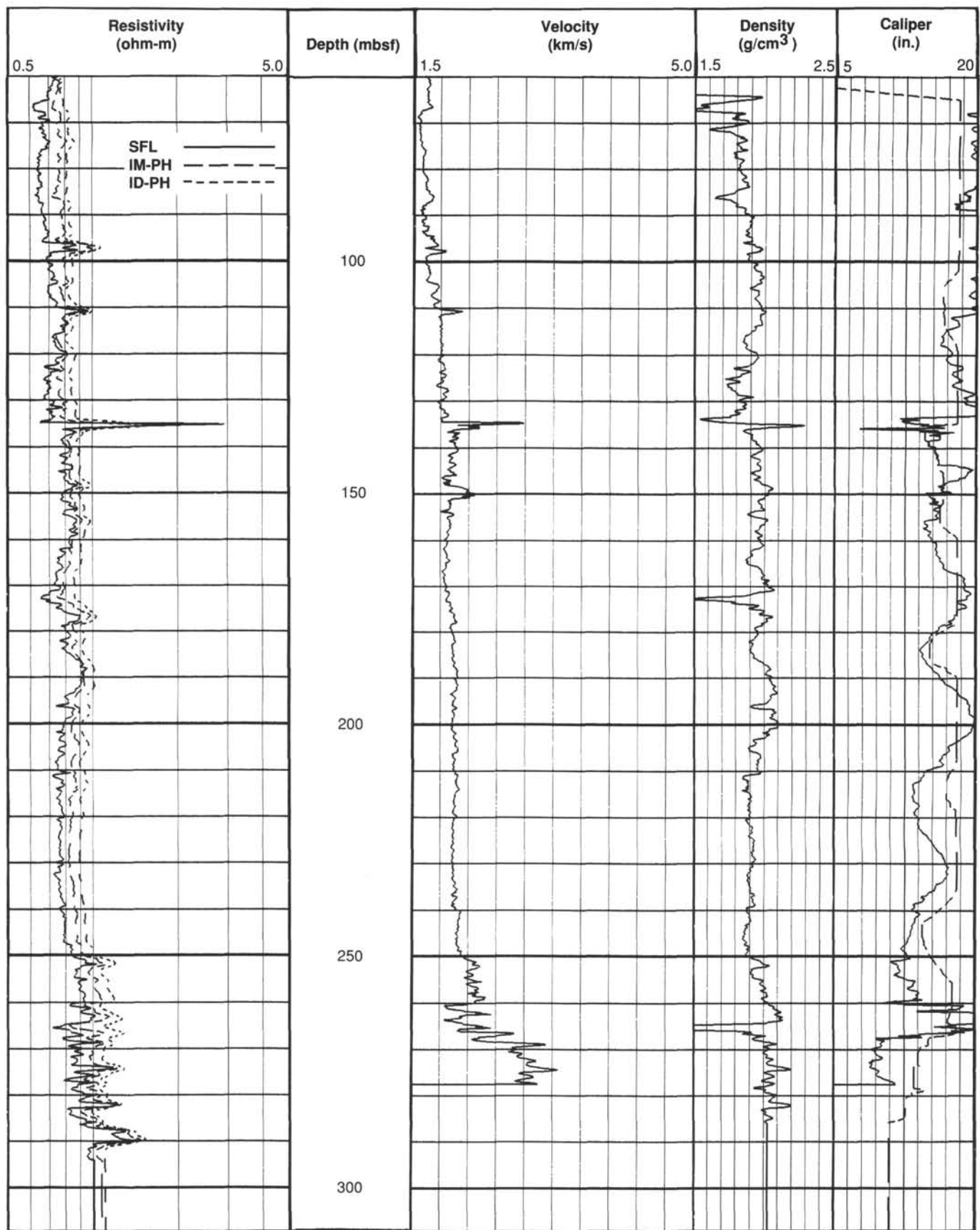


Figure 25. Primary porosity logs obtained by seismic stratigraphic tool string, used for differentiating lithologies at Site 814.

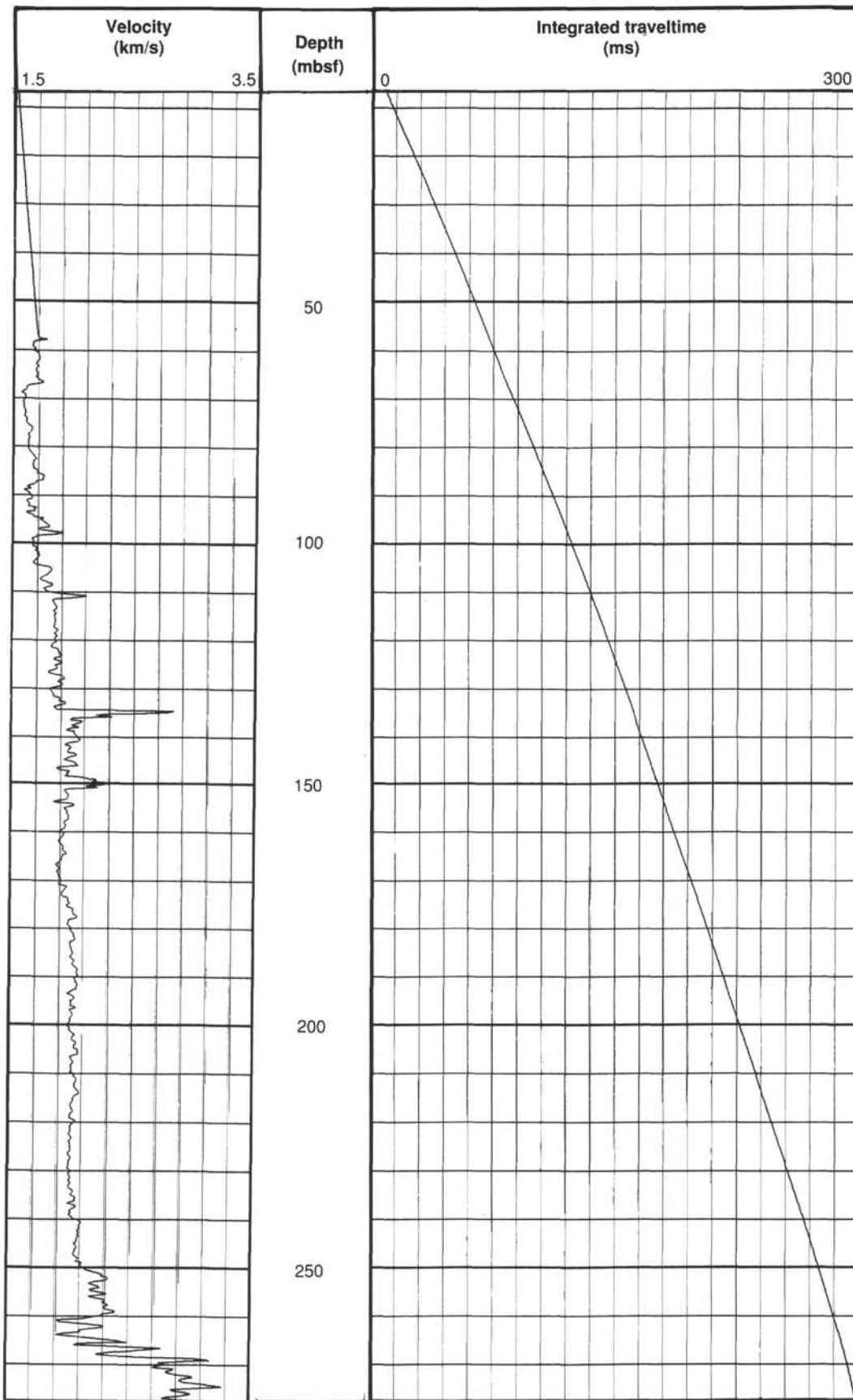


Figure 26. Velocity log (and TWT function it implies) for matching core-derived information from Site 814 with seismic sections across the site.

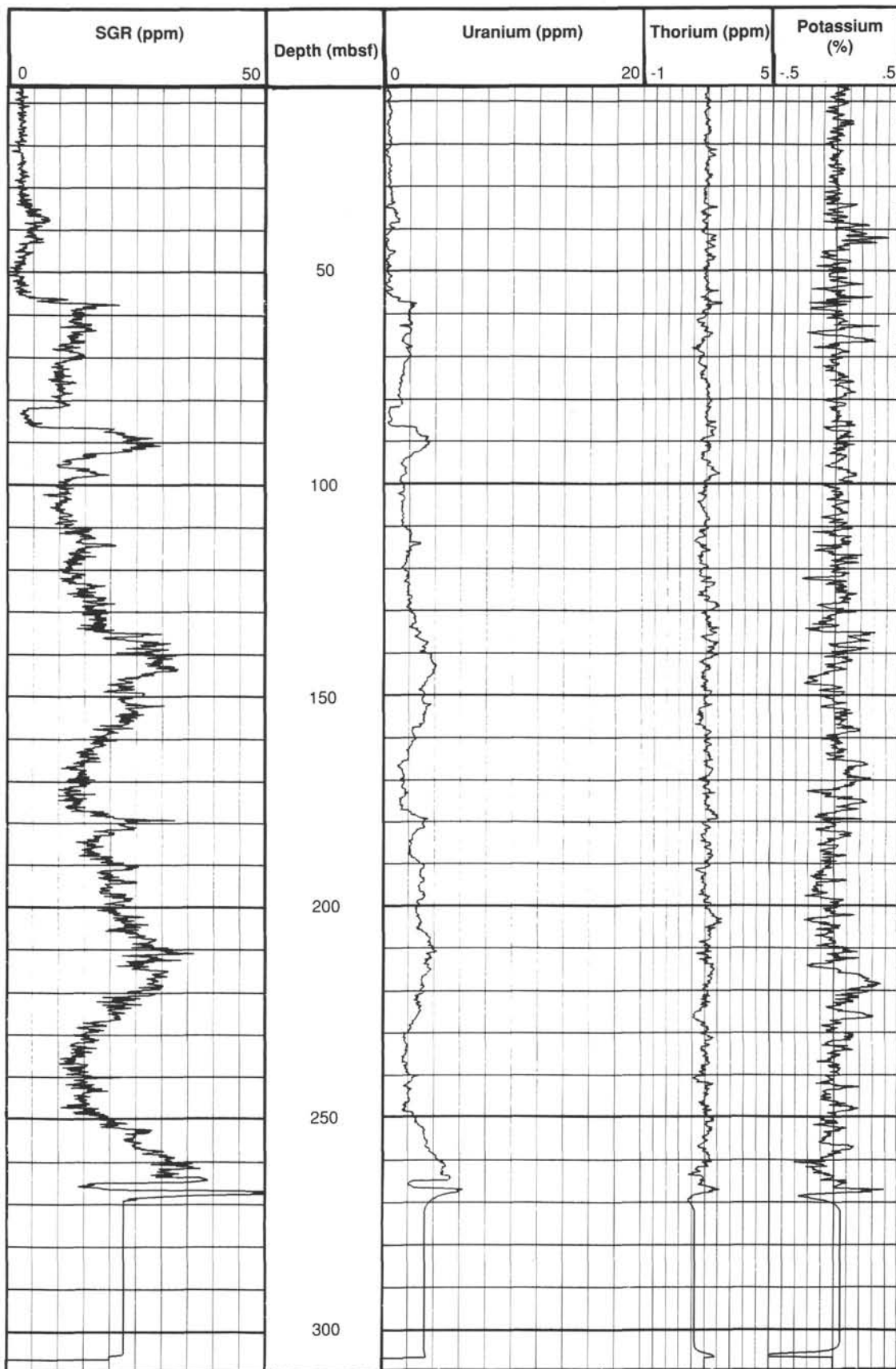


Figure 27. Spectral gamma-ray logs for Site 814, showing the effect of pipe at 85 to 95 mbsf and of large hole size.

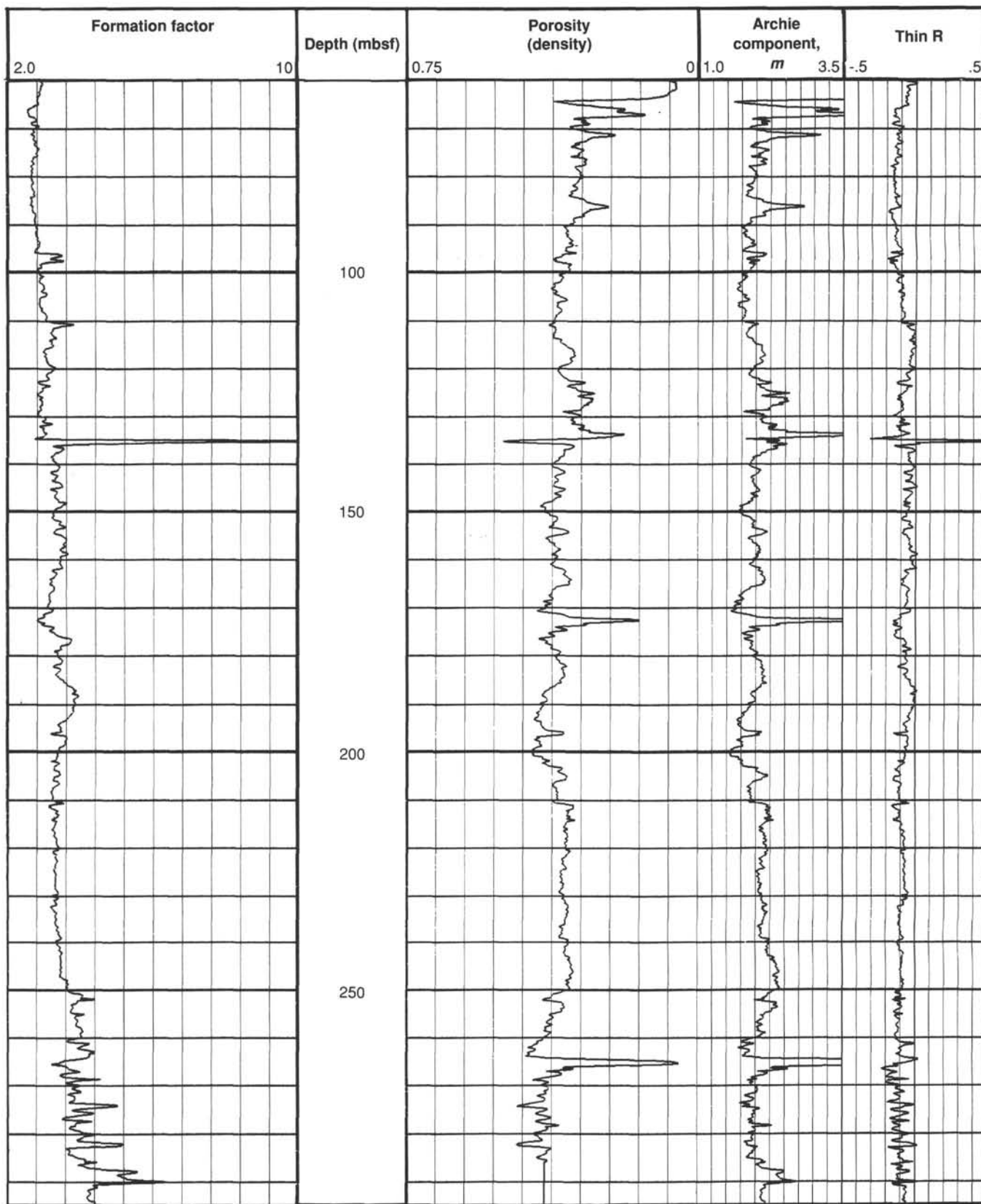


Figure 28. Site 814 logs of formation factor (from the ratio of formation resistivity to fluid resistivity), porosity (from density), and the Archie (1942) component  $m$  that relates formation factor to porosity.

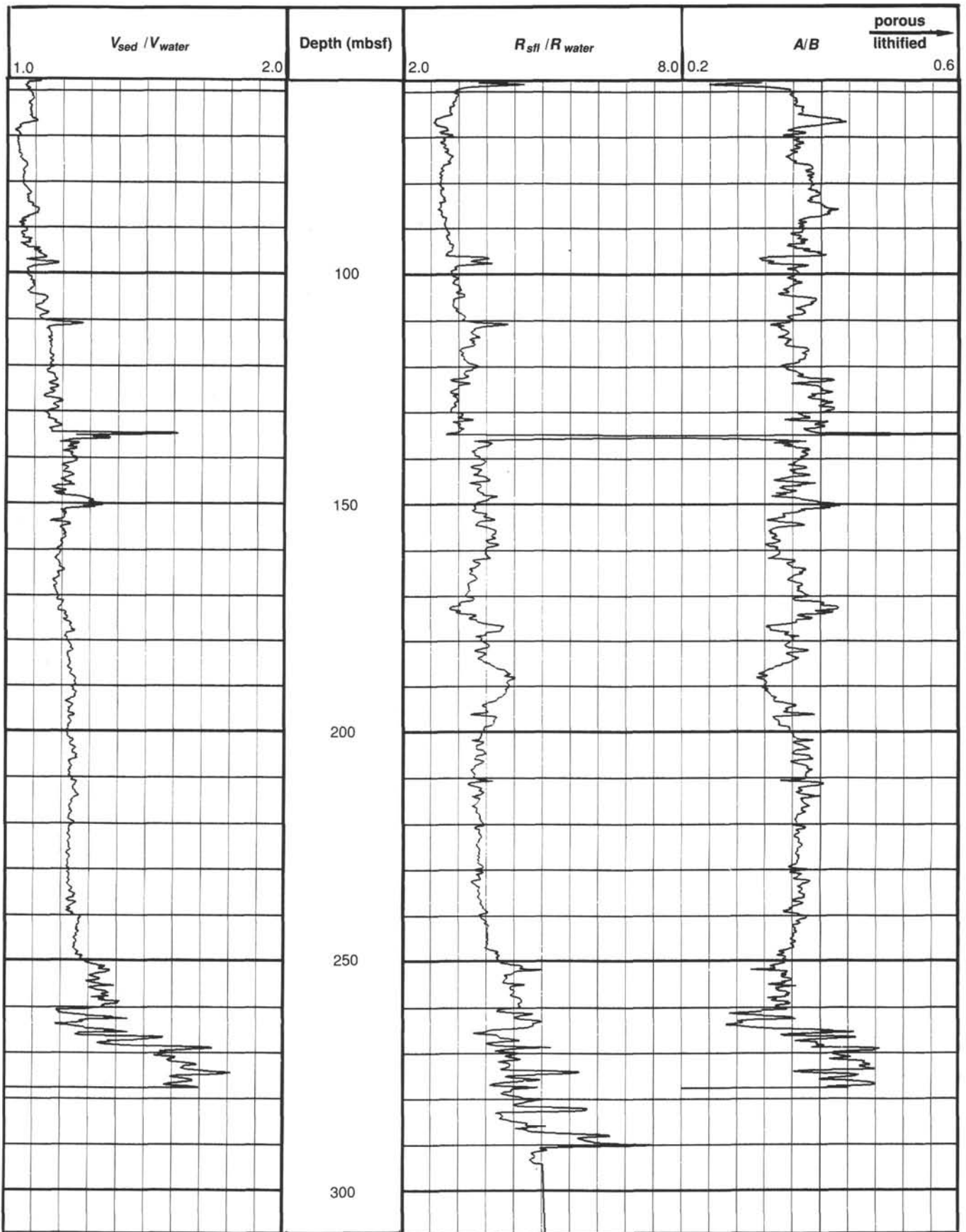


Figure 29. Velocity and resistivity logs for Site 814, plotted as ratios to each other or to water, used to highlight porous lithified facies that exhibit high velocities and correspondingly low resistivities.

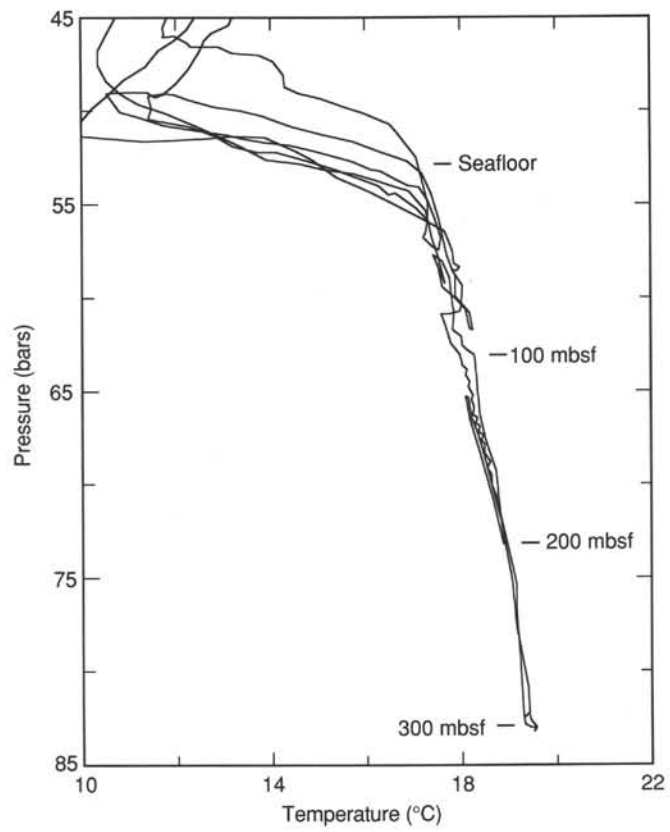


Figure 30. Temperature log for Site 814 as a function of pressure (or depth).

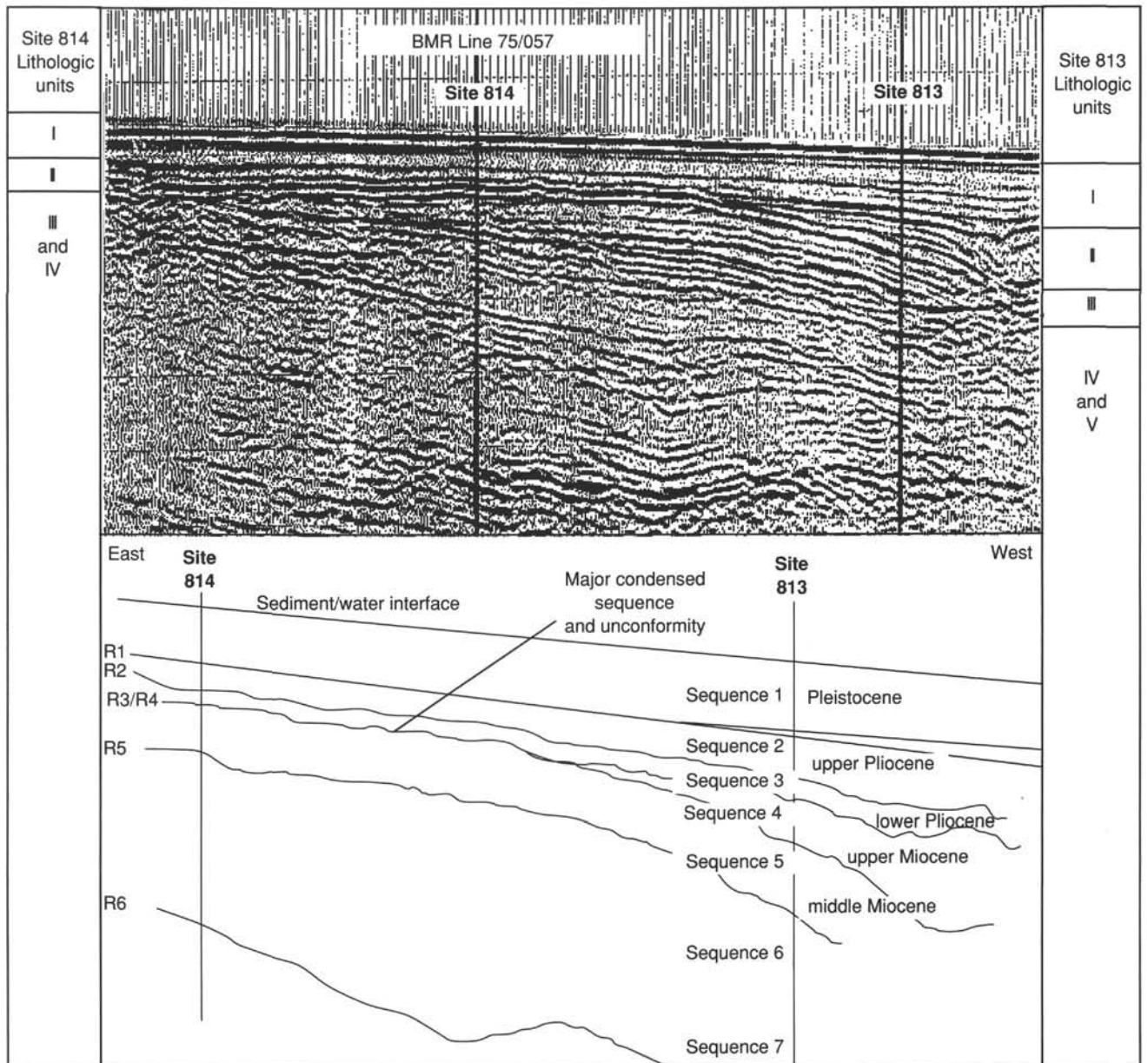
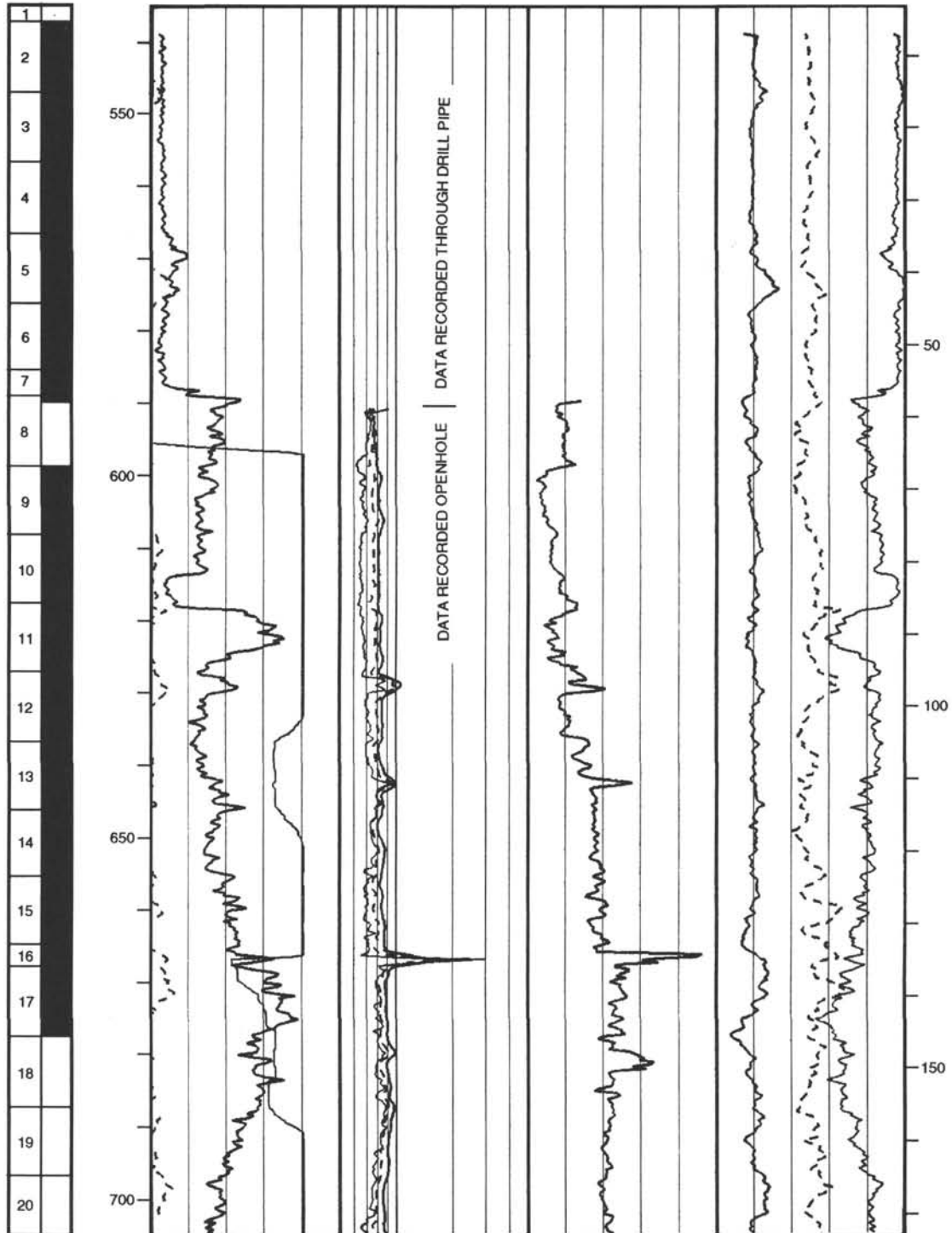


Figure 31. Seismic section connecting Sites 813 and 814 and interpreted seismic stratigraphy and lithologic correlations.

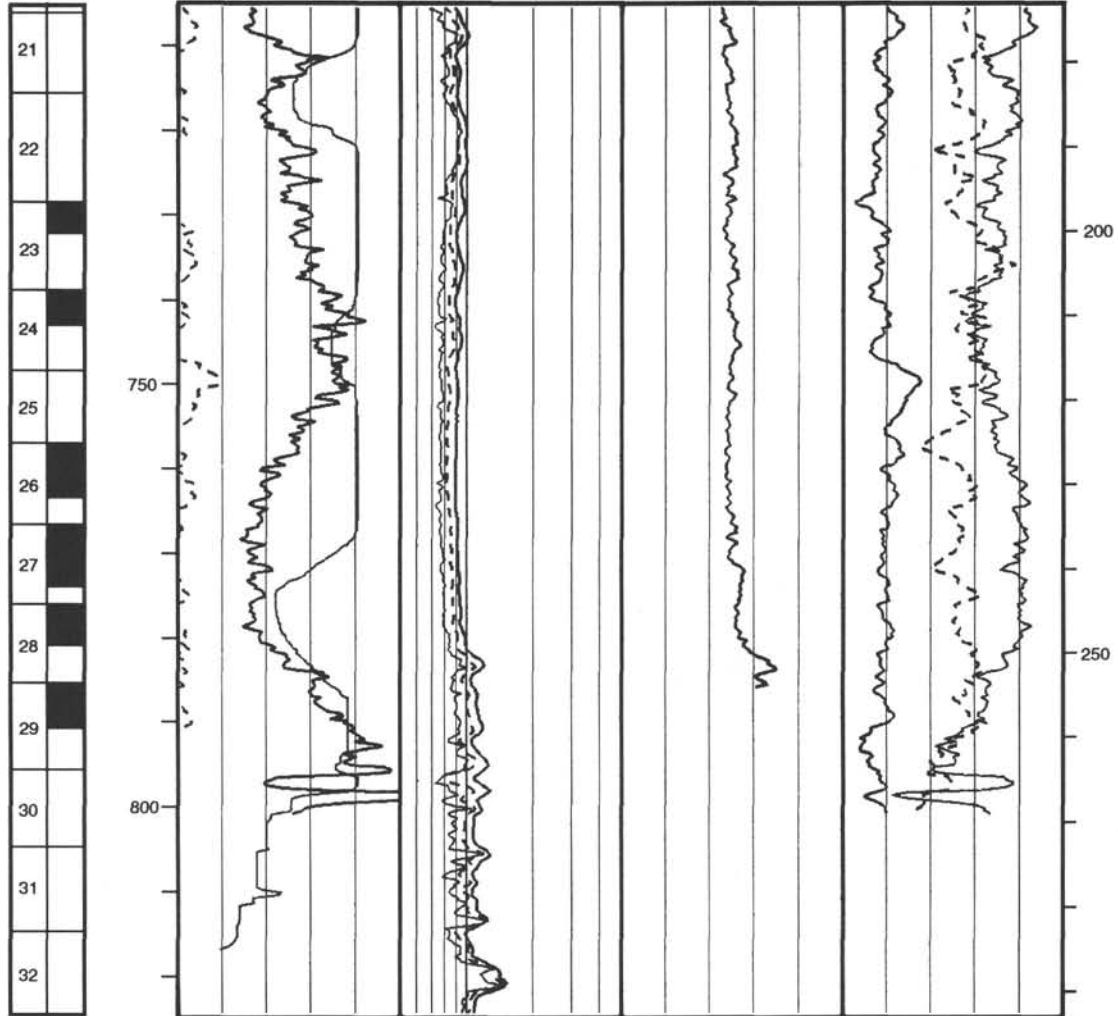
Hole 814A: Resistivity-Sonic-Natural Gamma Ray Log Summary

CORE RECOVERY	DEPTH BELOW RIG FLOOR (m)	SPECTRAL GAMMA RAY			RESISTIVITY			TRANSIT TIME			POTASSIUM			DEPTH BELOW SEA FLOOR (m)
		TOTAL		FOCUSED		URANIUM		SHALLOW		DEEP		THORIUM		
		0	50	0.5	5	10	0	0	3	200	100	-0.5	2	
		API units		ohm-m		ppm		ohm-m		μs/ft		ppm		
		COMPUTED		SHALLOW		THORIUM								
		0	50	0.5	5	-3	3							
		CALIPER		DEEP		POTASSIUM								
		10	20	0.5	5	-0.5	2							
		in.		ohm-m		ppm								

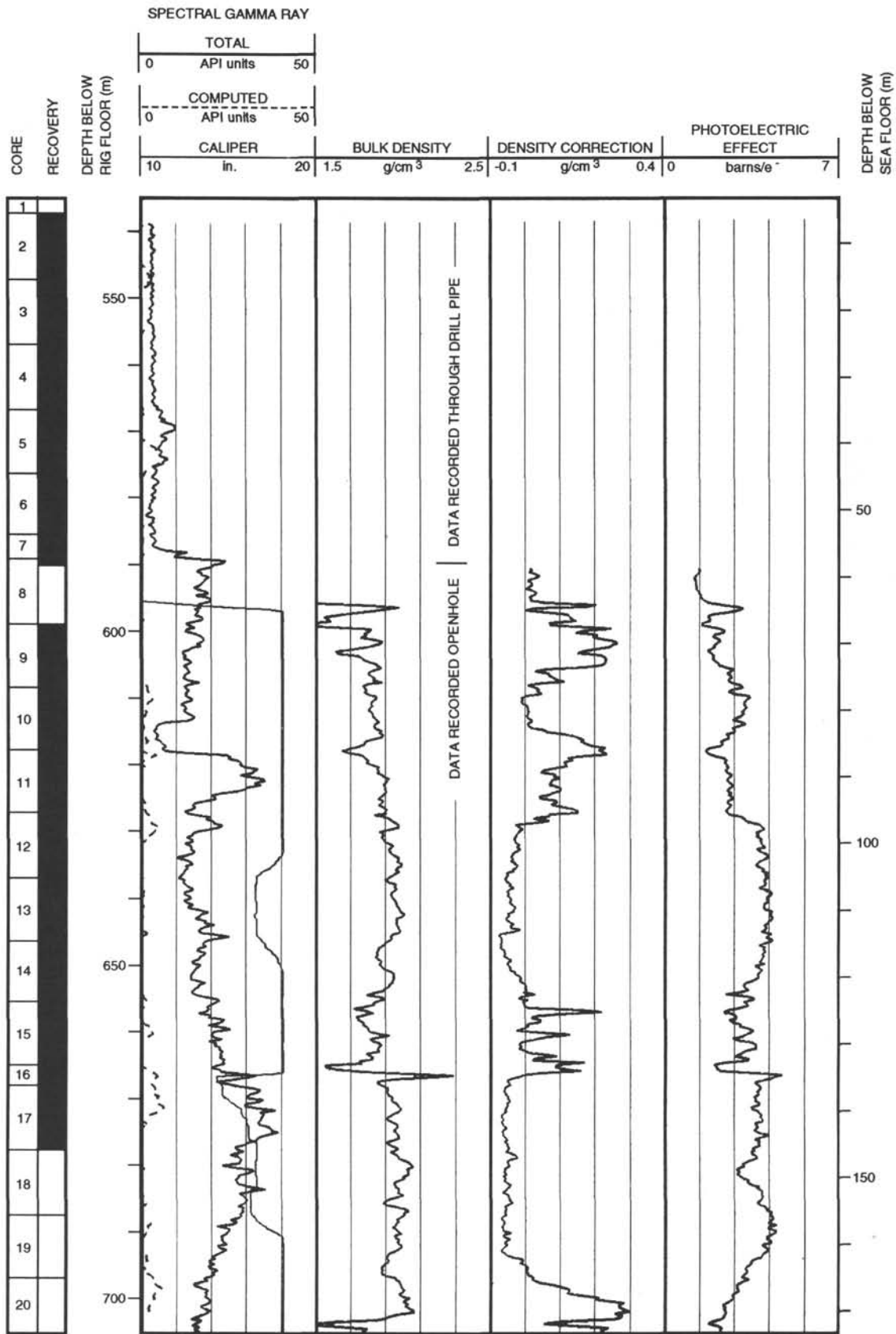


Hole 814A: Resistivity-Sonic-Natural Gamma Ray Log Summary (continued)

CORE RECOVERY	DEPTH BELOW RIG FLOOR (m)	SPECTRAL GAMMA RAY			RESISTIVITY			TRANSIT TIME			POTASSIUM			DEPTH BELOW SEA FLOOR (m)
		TOTAL		0.5	FOCUSED		5	URANIUM			THORIUM			
		API units	50		ohm-m	5		10	ppm	0	-3	ppm	3	
	0	API units	50	0.5	ohm-m	5								
	0	COMPUTED	50	0.5	SHALLOW	5								
	10	CALIPER	20	0.5	DEEP	5	200	$\mu$ s/ft	100	-0.5	ppm	2		



Hole 814-A: Density-Natural Gamma Ray Log Summary



Hole 814-A: Density-Natural Gamma Ray Log Summary (continued)

